อนุพันธ์พอร์ไฟรินที่มีกรดลิโปอิกเพื่อการประยุกต์สู่เป้าหมายไมโทคอนเดรีย

นางสาวดวงกมล แก้ววิชิต

วิทยานิพนธ์นี้เป็นส่วนหนึ่งของการศึกษาตามหลักสูตรปริญญาวิทยาศาสตรมหาบัณฑิต
สาขาวิชาเคมี ภาควิชาเคมี
คณะวิทยาศาสตร์ จุฬาลงกรณ์มหาวิทยาลัย
ปีการศึกษา 2559

LIPOIC ACID-CONTAINING PORPHYRINIC DERIVATIVES FOR MITOCHONDRIA TARGETING APPLICATIONS

Miss Duangkamon Kaewwichit

A Thesis Submitted in Partial Fulfillment of the Requirements
for the Degree of Master of Science Program in Chemistry
Department of Chemistry
Faculty of Science
Chulalongkorn University
Academic Year 2016

Thesis Title	LIPOIC ACID- CONTAINING PORPHYRINIC DERIVATIVES FOR MITOCHONDRIA TARGETING APPLICATIONS
By	Miss Duangkamon Kaewwichit
Field of Study	Chemistry
Thesis Advisor	Associate Professor Patchanita Thamyongkit, Dr.rer.nat.

Accepted by the Faculty of Science, Chulalongkorn University in Partial Fulfillment of the Requirements for the Master's Degree

.....Dean of the Faculty of Science
(Associate Professor Polkit Sangvanich, Ph.D.)

THESIS COMMITTEE

.....Chairman
(Associate Professor Vudhichai Parasuk, Ph.D.)

.....Thesis Advisor
(Associate Professor Patchanita Thamyongkit, Dr.rer.nat.)

.....Examiner
(Assistant Professor Puttaruksa Varanusupakul, Ph.D.)

.....External Examiner
(Assistant Professor Amornpun Sereemaspun, M.D.)

.....External Examiner
(Assistant Professor Vachiraporn Ajavakom, Ph.D.)

ดวงกมล แก้ววิชิต : อนุพันธ์พอร์ไฟรินที่มีกรดลิโปอิกเพื่อการประยุกต์สู่เป้าหมายไมโทคอนเดรีย (LIPOIC ACID-CONTAINING PORPHYRINIC DERIVATIVES FOR MITOCHONDRIA TARGETING APPLICATIONS) อ.ที่ปรึกษาวิทยานิพนธ์หลัก: รศ. ดร. พัชณิตา ธรรมยงค์กิจ, 85 หน้า.

งานวิจัยนี้สังเคราะห์พอร์ไฟรินที่ละลายน้ำได้ที่มีไพริดีเนียมและกรดลิโปอิกแทนที่ที่ตำแหน่งเมโซได้สำเร็จ สารประกอบชนิดใหม่ทั้งหมดได้รับการพิสูจน์เอกลักษณ์ด้วยเทคนิค NMR-สเปกโทรสโคปี และแมสสเปกโทรเมทรี สมบัติทางกายภาพเชิงแสงของสารประกอบได้รับการตรวจสอบด้วยเทคนิคยูวี-วิสิเบิล และฟลูออเรสเซนส์สเปกโทรโฟโตเมทรี สำหรับการศึกษาฤทธิ์ทางชีวภาพ สารประกอบนี้แสดงค่าความเป็นพิษต่ำ (IC_{50} = 25–150 μg/mL) ในเซลล์ HaCaT และ HDFa อย่างไรก็ตาม จากการทดสอบด้วยวิธี ROS generation สารประกอบนี้ไม่แสดงฤทธิ์ต้านอนุมูลอิสระในเซลล์ทั้งสองชนิด นอกเหนือจากนั้น การประเมินผลในไมโทคอนเดรียเป้าหมายของสารประกอบที่สังเคราะห์แสดงให้เห็นว่าสารประกอบนี้สามารถถูกสะสมในในไมโทคอนเดรียของเซลล์ HaCaT ได้

ภาควิชา เคมี ลายมือชื่อนิสิต .....

สาขาวิชา เคมี ลายมือชื่อ อ.ที่ปรึกษาหลัก .....

ปีการศึกษา 2559

5671962323 : MAJOR CHEMISTRY

KEYWORDS: CYTOTOXICITY / ANTIOXIDATIVE ACTIVITY

DUANGKAMON KAEWWICHIT: LIPOIC ACID- CONTAINING PORPHYRINIC DERIVATIVES FOR MITOCHONDRIA TARGETING APPLICATIONS. ADVISOR: ASSOC. PROF. PATCHANITA THAMYONGKIT, Dr.rer.nat., 85 pp.

In this research, an asymmetric water-soluble porphyrin having pyridinium and lipoic acid- based *meso*- substituents was successfully synthesized. All new compounds were characterized by NMR spectroscopy and mass spectrophotometry. Their optical properties were also investigated by UV-visible and fluorescence spectrophotometry. For the biological studies, low cytotoxicity (IC_{50} = 25–150 μg/mL) of these compounds in HaCaT and HDFa cells was observed. However, based on ROS generation assay, these compounds did not exhibit antioxidative activity in both kinds of cells. Moreover, mitochondria-targeting evaluation of the synthesized compounds showed that these compounds can be accumulated in the mitochondria of the HaCaT cells.

Department: Chemistry Student's Signature .....

Field of Study: Chemistry Advisor's Signature .....

Academic Year: 2016

ACKNOWLEDGEMENTS

Firstly, the author gratefully acknowledge the support by Chulalongkorn University graduate scholarship to commemorate to 72nd anniversary of his majesty King Bhumibol Adulyadaj. Corrsesponding author of this research is Associate Professor Dr. Patchanita Thamyomgkit.

The author would like to express her deepest gratitude to Associate Professor Dr. Patchanita Thamyomgkit for extensive support, enthusiastic guidance, valuable advices and kindness in this research, and Assistant Professor Dr. Amornpun Sereemaspun, M.D., for his guidance and suggestions in medical data analysis and serving as one of the member of this thesis committee.

The author also wish to express appreciation to Associate Professor Dr. Vudhichai Parasuk, for serving as the chairman, Assistant Professor Dr. Puttaruksa Varanusupakul and Assistant Professor Dr. Vachiraporn Ajavakom for serving as the members of this thesis committee, and for all of their valuable suggestions in this research

Finally, the author would like to thank her family for their fully support, care and encouragement for an entire of this course.

CONTENTS

Page

Page

LIST OF FIGURES

Page

LIST OF SCHEMES

Page

LIST OF ABBREVIATIONS

°C	: degree Celcius
calcd	: calculated
$CDCl_3$	: deuterated chloroform
CO_2	: carbondioxide
^{13}C-NMR	: carbon nuclear magnetic resonance spectroscopy
DMF	: *N,N'*-dimethylformamide
DMSO-d_6	: deuterated dimethyl sulfoxide
DMSO	: dimethylsulfoxide
DMEM	: dulbecco's Modified Eagle Medium
DNA	: deoxyribonucleic acid
D_2O	: deuterium oxide
d	: doublet (NMR)
ESI-HRMS	: electrospray ionization-high resolution mass spectrometry
EtOH	: ethanol
g	: gram(s)
HDFa	: human dermal fibroblast, adult
HaCaT	: human keratinocyte
h	: hour(s)
^{1}H-NMR	: proton nuclear magnetic resonance spectroscopy
Hz	: hertz
H_2O_2	: hydrogen peroxide
IC_{50}	: the half maximal inhibitory concentration
J	: coupling constant
m/z	: mass to charge ratio
MALDI-TOF-MS	: matrix-assisted laser desorption ionization-time of flight-mass spectrometry
MeOH	: methanol
CH_2Cl_2	: methylene chloride

MHz	: megahertz
min	: minute(s)
ε	: molar absorptivity
m	: multiplet (NMR)
mmol	: millimole(s)
mg	: milligram(s)
mL	: milliliter(s)
nm	: nanometer(s)
N_2	: nitrogen
O_2	: oxygen
obsd	: observed
rt	: room temperature
ROS	: reactive oxygen species
s	: singlet (NMR)
t	: triplet (NMR)
TEA	: triethylamine
UV-Vis	: ultraviolet and visible spectroscopy
λ	: wavelength
λ_{ex}	: excitation wavelength
λ_{abs}	: absorption wavelength
λ_{em}	: emission wavelength
µL	: microliter(s)
µM	: micromolar(s)
δ	: chemical shift
% yield	: percentage yield

CHAPTER I
INTRODUCTION

Mitochondria are organelle which have important role in metabolism in the body and control of cell equilibrium. Cycle of cell division, growth, decline and death is controlled by mitochondrial function, called intrinsic pathway,[1] which keeps the body balance all the time. In mitochondria, the important mechanism is oxidative phosphorylation[2] which is metabolic pathway of ATP synthesis for using in the body activity. For mechanism of oxidative phosphorylation, electrons are transferred to oxygen molecules through electron transport chain in mitochondria. During oxidative phosphorylation, reactive oxygen species (ROS) are generated.[3] Normally, the presence of ROS in each part of body is not equal. ROS generation mostly occurs in the mitochondria because this organelle involves a respiratory chain. However, the ROS generation in the body is balanced by the presence of molecules in the body called antioxidants. The antioxidant molecules can change ROS to neutral molecules, and, therefore, control the amount of ROS. However, the ROS in the body do not come from only the metabolism, but also from the external sources, such as air pollution, ultraviolet and radiation chemistry, resulting in loss of oxidation-antioxidation equilibrium[4] in case the antioxidants in the body cannot handle the excessive ROS. Due to their high reactivity, ROS can destroy various membranes and cells *via* an oxidative damage process.[5] As the metabolism center, mitochondria is affected the most by this process[6] and, therefore, its DNA (mitochondrial DNA, mtDNA) become a major target of the oxidative damage. The first expression of the body, when damaged mtDNA has occurred, is cellular aging[7] which associated with many diseases.

Recently, porphyrin compounds are of great interest as an antioxidant for biomedical applications,[8] such as emerging applications,[9] photodynamic therapy[10] and mitochondria-targeting applications.[11] Several kinds of porphyrin are known to localize and be accumulated in mitochondria without distributing to other cells.[12] Some porphyrin derivatives were used in mitochondria-targeting applications, such as *meso*-

tetraphenyl porphyrin derivatives[13] which showed effective photodynamic activity to MCF-7 human breast cancer cell line (**Figure 1–1**).

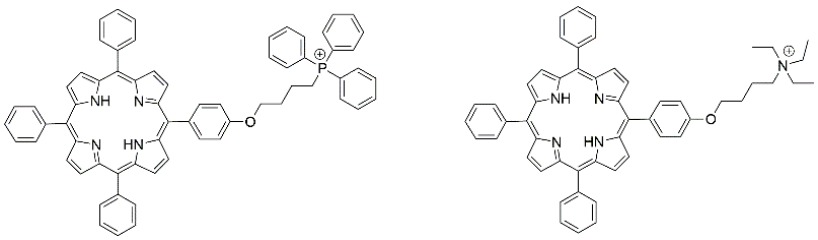

Figure 1–1: Some *meso*-tetraphenyl porphyrin derivatives used in mitochondria-targeting applications.

α-Lipoic acid (ALA) is one of biomedically active compounds acting as an antioxidant.[14] ALA is naturally occurring compound synthesized by plants and animals, including mitochondria in humans. Basically, ALA is both water- and fat-soluble, and thus, is widely distributed in both cellular membranes and the cytosol of eukaryotic and prokaryotic cells.[15] An important property of ALA is prevention of mitochondrial dysfunction from oxidative stress. ALA alone is an effective antioxidant, but, in some cases, it also can combine with other antioxidants, *e. g*. glutathione, vitamin C, coenzyme Q10, to become a high potential antioxidant.[16]

According to above-mentioned properties of porphyrin and ALA, in this research, we aim to synthesize asymmetric porphyrin having three water-solubilizing pyridinium *meso*-groups and a biomedically active unit derived from ALA at the remaining *meso* position. Both of ALA and pyridinium-substituted porphyrin are well-known water-soluble and biocompatible compounds that can pass through cell membranes.[17] The target molecule is expected to exhibit antioxidative properties with low cytotoxicity and high specificity to mitochondria.

1.1 objective of this research

To synthesize lipoic acid-containing porphyrinic derivatives and investigate for their potential applications as antioxidants and mitochondria-targeting applications.

1.2 Scope of this research

This research covers the synthesis of asymmetric water-soluble porphyrin having pyridinium and lipoic acid-bared *meso*-substituents. New compounds will be fully characterized by spectroscopic techniques, *i.e.* proton-nuclear magnetic resonance (^{1}H-NMR) and carbon-nuclear magnetic resonance (^{13}C-NMR) spectroscopy, mass spectrometry. Photophysical properties will be investigated by ultraviolet-visible and fluorescence spectrophotometry. Medical evaluation includes the studies of cytotoxicity, reactive oxygen species (ROS) generation and specificity to mitochondria.

CHAPTER II

THEORY AND LITERATURE REVIEWS

THEORY

2.1 Mitochondrial Structure

In 1890, mitochondria (singular, mitochondrion) were first described by Richard Altmann.[18] Mitochondria are double-membraned organelles which found in cytoplasm. Mitochondria have diameter and length of 0.1–0.5 micron and 1–2 micron respectively.[14b] In cytoplasm, they are composed of outer and inner membranes as shown in **Figure 2–1**.[19] The outer membrane fully covers the inner membrane organelle with an intermembrane space in between. The outer membrane contains many types of protein-based pored that called "porins"[20] and allows diffusion of large molecules and ions to the cell. The inner membrane is highly complex structure[21] that relates with electron transport system, transport proteins and ATP synthetase. The boundary inner membrane is folded into layers, called cristae, which can increase the inner membrane area. Furthermore, this membrane encompasses mitochondrial matrix which contains enzymes for citric acid cycle reactions. The matrix also contains mitochondrial DNA (mtDNA),[22] called a nucleoid, and contains dissolved oxygen, carbon dioxide and water that play important role for metabolism.[23] For this reason, permeability of the inner membrane is different from the outer one in that it only allows oxygen, carbon dioxide and water to pass through.

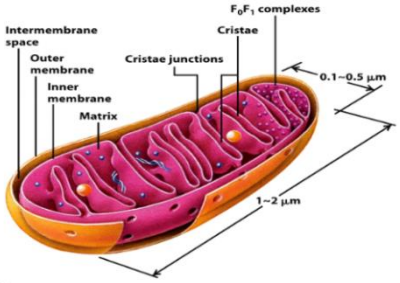

Figure 2–1: General structure of mitochondria.

2.2 Detection of mitochondrial imaging with fluorescent probe

Mitochondrial transmembrane potential ($\Delta\psi$m)[24] is an important parameter of mitochondrial function and has been used as an indicator of healthy cells. High $\Delta\psi$m indicates healthy cell, while low $\Delta\psi$m indicates unhealthy one. $\Delta\psi$m changes can be observed from a fluorescent probe.

5,5',6,6'-tetrachloro-1,1',3,3'tetraethylbenzimi-dazolylcarbocyanine iodide (JC-1) is one of the fluorescent probe used to detect mitochondrial imaging.[25] JC-1 is a novel cationic carbocyanine dye that accumulates in mitochondria. In healthy cells with high mitochondrial $\Delta\psi$m, JC-1 spontaneously forms complexes known as J-aggregates with intense red fluorescence. On the other hand, in unhealthy cells with low $\Delta\psi$m, JC-1 remains in the monomeric form, which shows only green fluorescence.

An example of the treatment of hepatocyte cells with JC-1 is shown in **Figure 2–2**.[26]

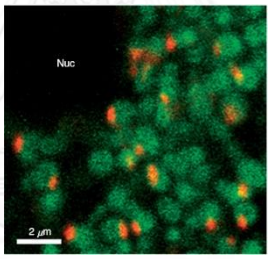

Figure 2–2: Red and green mitochondrial fluorescence after treating hepatocyte with JC-1. Nuc stands for nucleus.

2.3 Detection of cell viability

PrestoBlue (PB) is one of commercial reagents[27] used for detection of cell viability. PB has been developed for detecting cell-mediated cytotoxicity *in vitro*. The reagent exhibits change in a color, as well as a shift in its fluorescence, and thus can be quantified using either fluorometric or spectrophotometric approach. Similarly, PB is commercially prepared as a non-toxic, ready-to-use solution. According to the manufacturer, PB is the fastest live assay for assessing cell viability with an incubation step as short as 10 min. It is also a very sensitive assay, which can detect as few as 12 cells per well. So far, the PB assay has been used to establish the biological activity.

This reagent has also been reported to be useful to evaluate the growth of *cell* and to visualize microorganisms in environment.

2.4 Reactive Oxygen Species (ROS) generation

2.4.1 Overview

Free radical can be defined as reactive chemical species having a single unpaired electron in an outer orbit.[28] The major kind of the free radical that damages the biological systems is oxygen free radical which is generally known as a reactive oxygen species (ROS).[29] In ROS, an atomic oxygen has two unpaired electrons in separate orbits in its outer electron shell. In general, ROS can be

(1) generated during UV light irradiation and by X-ray or gamma ray
(2) present in the atmosphere as pollutant
(3) caused by metal-catalyzed reactions
(4) caused by neutrophils and macrophages during inflammation.[30]

ROS are known as factor of mitochondrial damage and cell deterioration. Appearance of oxygen free radical has harmful to health and lifespan in human.[31] However, oxygen free radical is not only harmful effect to cells, but also has important role for metabolic pathway and mitochondrial electron transport chain which is related to many activities in the body.

2.4.2 Detection of ROS generation

2',7'–Dichlorofluoreceine-diacetate (H_2DCF-DA) is one of the molecular probes used as indicators for ROS. It is often called a "hydrogen peroxide-detecting probe" as it measures a H_2O_2 level in intact cells.[32] Oxidation of these probes can be detected by monitoring the increase in fluorescence with a flow cytometer, fluorometer, microplate reader, or fluorescence microscope, using excitation sources and filters appropriate for fluorescein, which is maximally excited at 495 nm and emits at 520 nm. The oxidation of dichlorodihydro-fluorescein (H_2DCF) to 2',7'–dichlorofluoreceine (DCF) is a two-step process[33] as shown in **Scheme 2–1**.

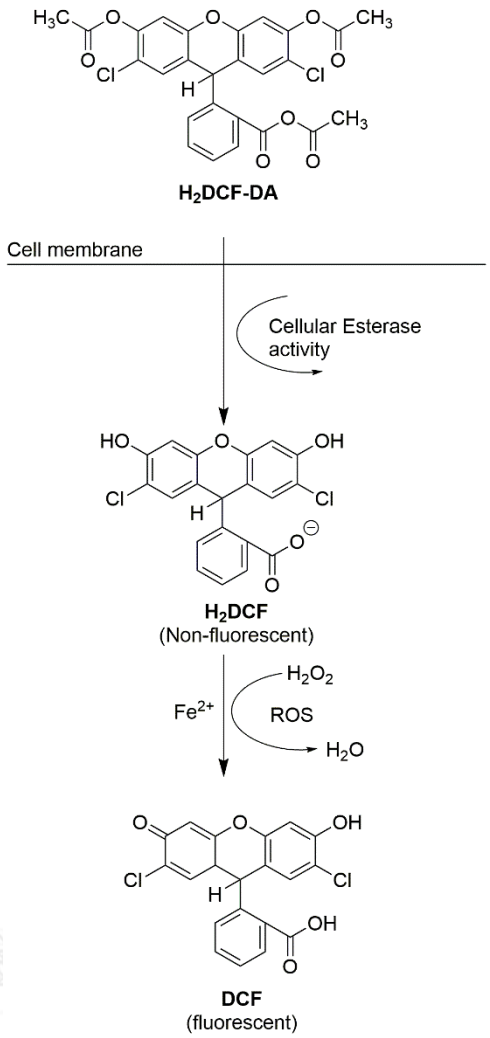

Scheme 2–1: Mechanism of the oxidation of H_2DCF-DA.

First, the DCF radical is formed, and then further oxidized to DCF by a reaction with molecular oxygen. The first step of H_2DCF oxidation can be mediated by different radical species, such as hydroxyl radical, carbonate radical, and nitrogen dioxide. H_2O_2 does not react with H_2DCF directly but requires the presence of peroxidases or other enzymes containing transition metals. Moreover, an alteration of the signal can be caused by antioxidant enzymes or superoxide that react with the probe, resulting in the appearance of the fluorescent signal. The superoxide radical is formed in the second step of probe oxidation and can then be dismutated to H_2O_2 and cause self-amplification of the signal.

2.5 Lipoic acid (ALA)

2.5.1 Structure

ALA is a disulfide derivative of octanic acid.[34] It appears as yellow solid. Its chemical structure, shown in **Figure 2–3**, contains two sulfer atoms at C6 and C8 which are linked by a disulfide bond, forming a dithiolane ring. At C6, an C5-alkyl chain with a terminal carboxyl group is attached. Since C6 is chiral, the molecule exists as two enantiomers, *i.e*. (*R*)-(+)-lipoic acid and (*S*)-(-)-lipoic acid, or as a racemic mixture, (*RS*)-lipoic acid.

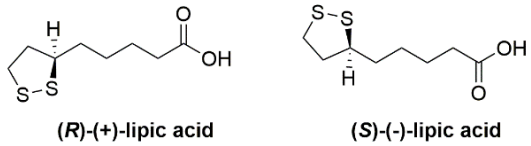

Figure 2–3: Enantiomers of ALA.

Naturally, ALA appears in two forms, *i.e*. oxidized and reduced forms.[35] The oxidized form is called ALA and the reduced form is called α-dihydrolipoic acid (DHLA). Their structures are shown in **Figure 2–4**.

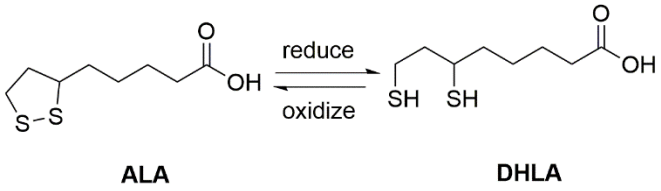

Figure 2–4: Chemical structures of ALA and DHLA.

2.5.2 Antioxidative activities of ALA

ALA occurring in the nature is *R*-enantiomer form (*R*-ALA).[36] It is an essential cofactor in an α-ketoacid dehydrogenase complex and a glycine cleavage system. In plants and animal tissues, it contains low amounts of *R*-ALA and is detected in the form of lipoyllysine. However, the highest concentration of lipoyllysine in animal tissues was found in kidney, heart, and liver.

ALA is generally non-toxic to normal cells. In the cells, ALA has been suggested as an essential mitochondrial co-factor and help regenerating other antioxidants to

make them active again.[37] Furthermore, it has direct scavenging activity towards ROS. ALA and DHLA are found to be highly reactive against a variety of ROS *in vitro*, hydroxyl radical, hypochlorous acid, and singlet oxygen.[38]

In medical applications, ALA can combine with other antioxidant molecules to improve the antioxidative properties, leading to more effective cognitive function and increased antioxidant capacity in biomembranes.[39]

2.5.3 Uses and applications of lipoic acid

Lipoic acid is generally used for medical therapy such as

(1) cosmetic industrial applications,

(2) treatment of many diseases, such as diabetes and nerve-related symtoms of diabetes, cancer liver diseases, diseases of the heart and blood vesels, and

(3) supplement food and antioxidant application.[40]

2.6 Porphyrin

2.6.1 Overview

In 1841, porphyrins were discovered by Scherer.[41] The name of porphyrin derived from "porphyra" (Greek language) meaning reddish-purple.[42] Porphyrins are highly conjugated macrocyclic organic compounds consisting of tetra pyrrole rings linked by four methane (—CH═) bridges. Porphyrin molecules are highly stable because of conjugated system and due to its conjugated 18 π-e^- system. It conforms to Huckel (4n+2) rule for aromaticity. The Porphyrin having no any substituent is called "porphine".[43] The structure of porphine is shown in **Figure 2–5**.

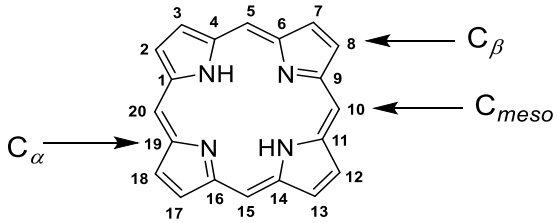

Figure 2–5: Structure of porphine.

In the porphyrin ring, C_5, C_{10}, C_{15} and C_{20} are in *meso*-positions, and C_2, C_3, C_7, C_8, C_{12}, C_{13}, C_{17} and C_{18} are in β-positons. The porphyrins can have various substituents at these positions. The porphyrin core is a tetradentate ligand having four nitrogen atoms available for coordination with any metal to form an organometallic complex. When the porphyrin core coordinates with a metal, the two inner protons are removed from the pyrrole ring providing a very stable complex and displays aromatic character.[44] Normally, porphyrins exhibit characteristic absorption properties in a visible region with four Q bands and one B band (also called Soret band) present between 500 to 700 and around 400 nm, respectively.[45]

Porphyrin complexes play an important role in biological system. For example, magnesium complexes in the chlorophyll, iron complexes in the hemoproteins (heme, cytochrome C), and cobalt complexes in vitamin B_{12}.[46] The structure of some natural porphyrin complexes are shown in **Figure 2–6.**

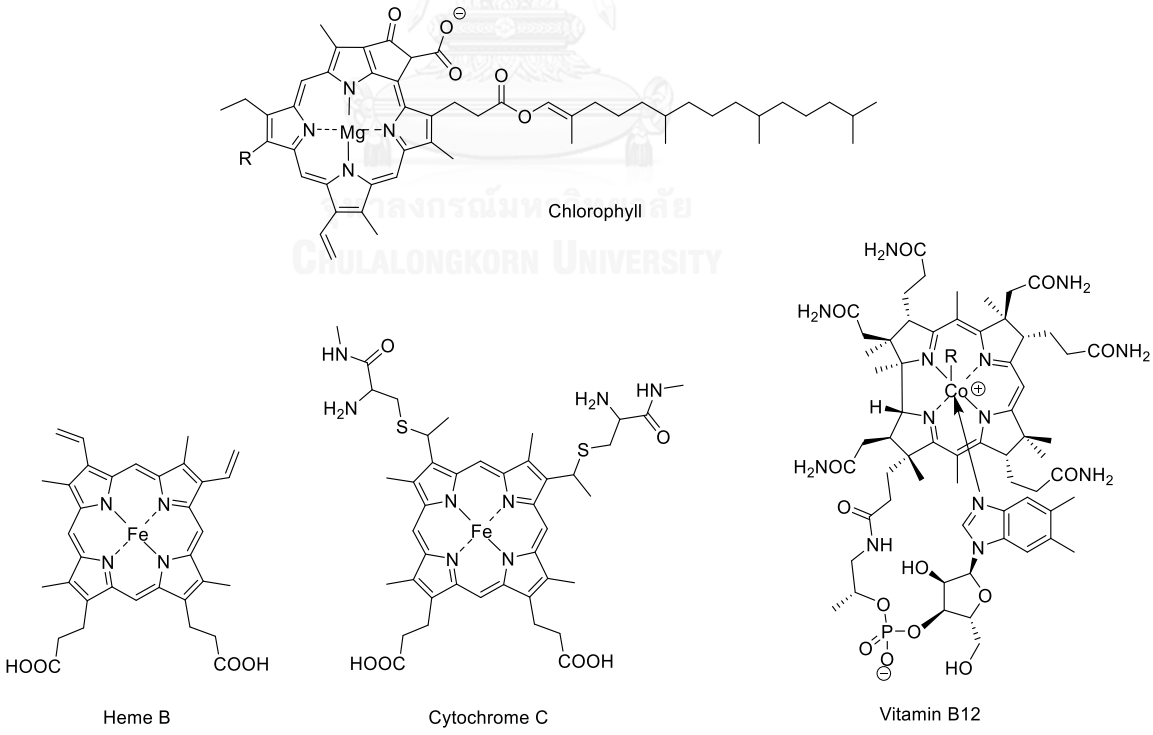

Figure 2–6: Structures of some natural porphyrin complexes.

2.6.2 Porphyrin synthesis

Porphyrin and their derivatives can be synthesized by condensation reaction between pyrrole and aldehyde. *Meso*-substituents (R in **Figure 2–7**) can be varied by the type of aldehydes.

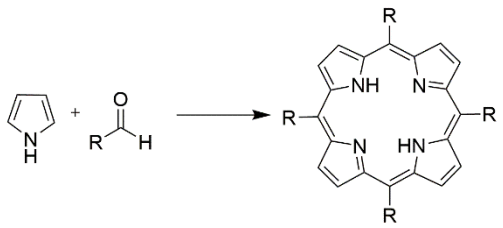

Figure 2–7: Synthesis of *meso*-substituted porphyrins.

One of the simplest porphyrins derivative is tetraphenylporphyrin (**TPP**). Synthesis of TPP was firstly synthesized by Adler *et al.,*[47] as shown in **Scheme 2–2**, from a condensation of pyrrole and benzaldehyde in the presence of propionic acid.

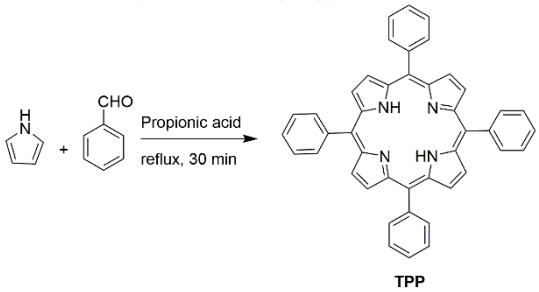

Scheme 2–2: Synthesis of **TPP** by Adler *et al*.

The development for the synthesis of **TPP** was then introduced by Lindsey *at al*..[48] Firstly, tetraarylporphyrinogen is formed by a condensation between appropriate aldehyde and pyrrole in the presence of a mild acid, usually $BF_3{\cdot}OEt_2$ or TFA, at room temperature following by the irreversibly oxidation with a quinone derivatives in the second step (**Scheme 2–3**).

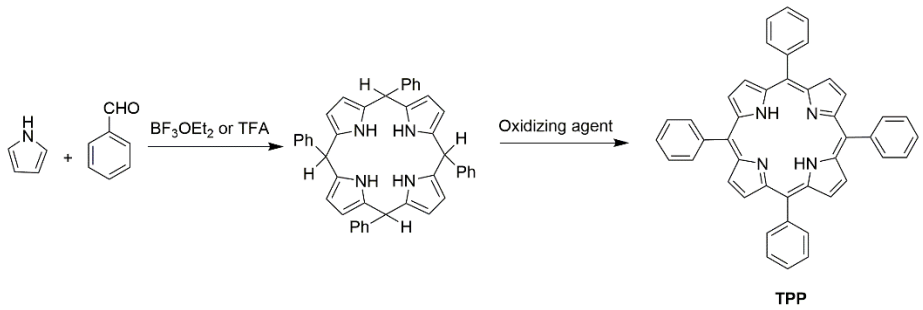

Scheme 2–3: Synthesis of **TPP** by Lindsey *et al.*

LITERATUE REVIEWS

In 1993, Meunier, B. *et al.*[49] reported synthesis of water-soluble cationic metal-chelated tris(methylpyridiniumly)porphyrin containing a hydroxy and amino tethers for using as DNA cleavers in the tumor cells as shown in **Scheme 2–4**. The studies indicated that the porphyrin derivatives exhibited antitumoral activity.

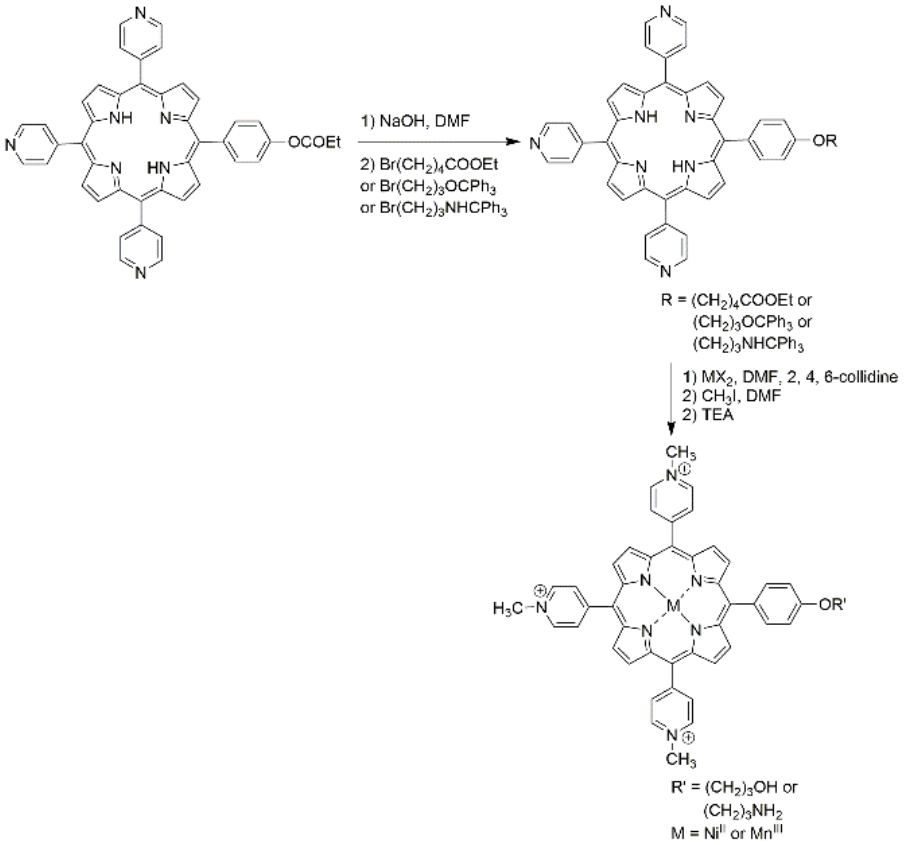

Scheme 2–4: Preparation of asymmeteric water soluble cationic porphyrins by Meunier, B. *et al.*

In 2006, Benfi, S. *et al*.[50] reported design and synthesis of 5,10,15,20-tetraarryl-, 5,10-diaryl- and 5-monoarylporphyrins for using as photosensitizers in HCT116 human colon adenocarcinoma cells as shown in **Figure 2–8**. The studies indicated that the difference of aryl *meso*-substitution patterns affected hydrophobic/hydrophilic character of the resulting photosensitizers. This is an essential feature for both cell penetration and subcellular localization. Compounds with the tetraarryl and diaryl substituents were more effective in term of photodynamic activity than the monoaryl

substituents. However, the hydroxyl-substituted diaryl derivatives were more photodynamic active than the corresponding methoxy-substituented ones. Moreover, the monoaryl porphyrins which are byproducts from the synthesis of diarylporphyrin was found to be particularly effective photosensitizers and selectively targeted to HCT116 human colon adenocarcinoma cells.

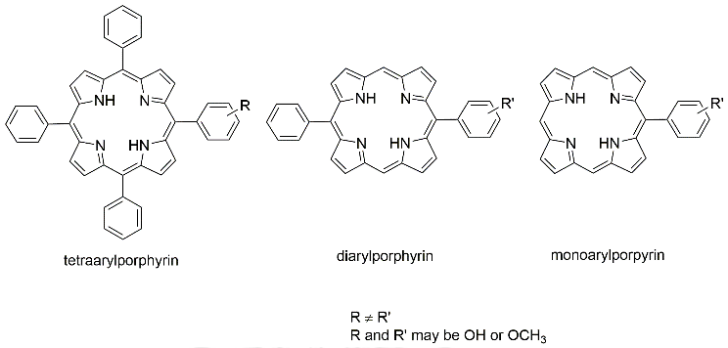

Figure 2–8: General structures of tetraarylporphyrin, diarylporphyrin, and monoaryporphyrins studied by Benfi, S. *et al.*

In 2008, Pujic, M. G. *et al.*[51] reported the synthesis of new antioxidative resveratrol-lipoic acid (**A**) and resveratrol-vitamin E (**B**) conjugates and their in vitro hydrolysis with Stratum corneum enzymes (Schemes **2–5** and **2–6**).

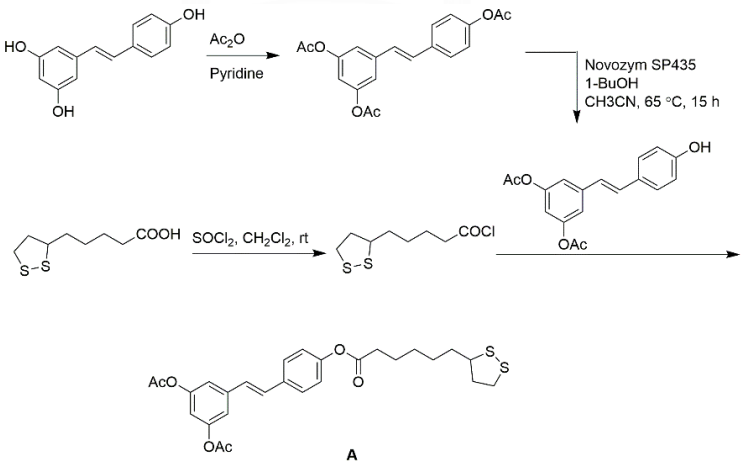

Scheme 2–5: Preparation of resveratrol-lipoic acid and conjugates studied by Pujic, M. G. *et al*.

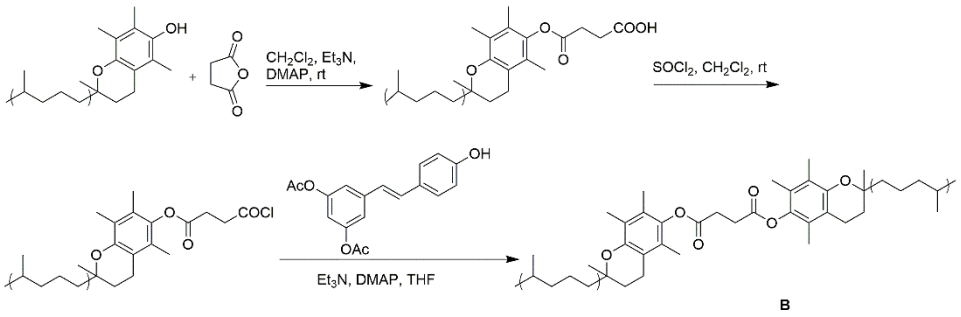

Scheme 2–6: Preparation of resveratrol-lipoic acid and conjugates studied by Pujic, M. G. *et al.*

Both new antioxidants showed beneficial antioxidative effect that can efficiently protect skin cells from sun light.

In 2009, You, Y. *et al.*[52] described evolution of delocalized lipophilic cationic dyes as delivery vehicles for photosensitizers to mitochondria. A porphyrin-rhodamine B conjugate (**TPP-Rh**) and a porphyrin-acridine orange conjugate (**TPP-AO**) were synthesized by coupling a monohydroxy porphyrin (**TPP-OH**) to rhodamine B (**Rh B**) and acridine orange base (**AO**), respectively, *via* a saturated hydrocarbon linker. The synthesis of both molecules were shown in **Schemes 2–7** and **2–8**.

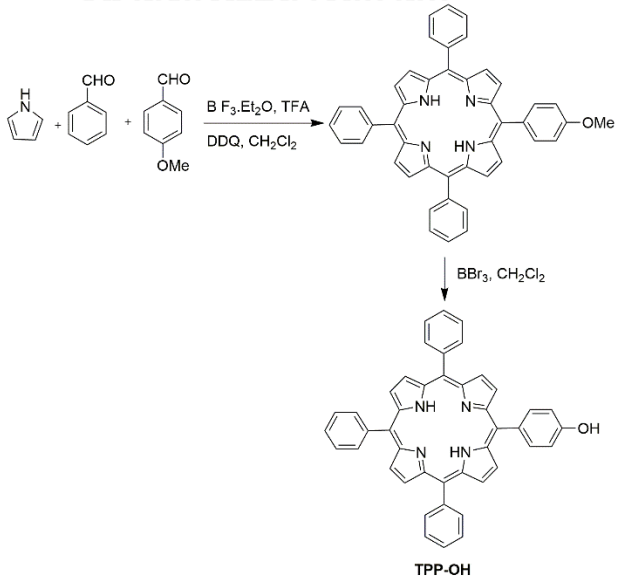

Scheme 2–7: Synthesis of **TPP-OH** by You, Y. *et al.*

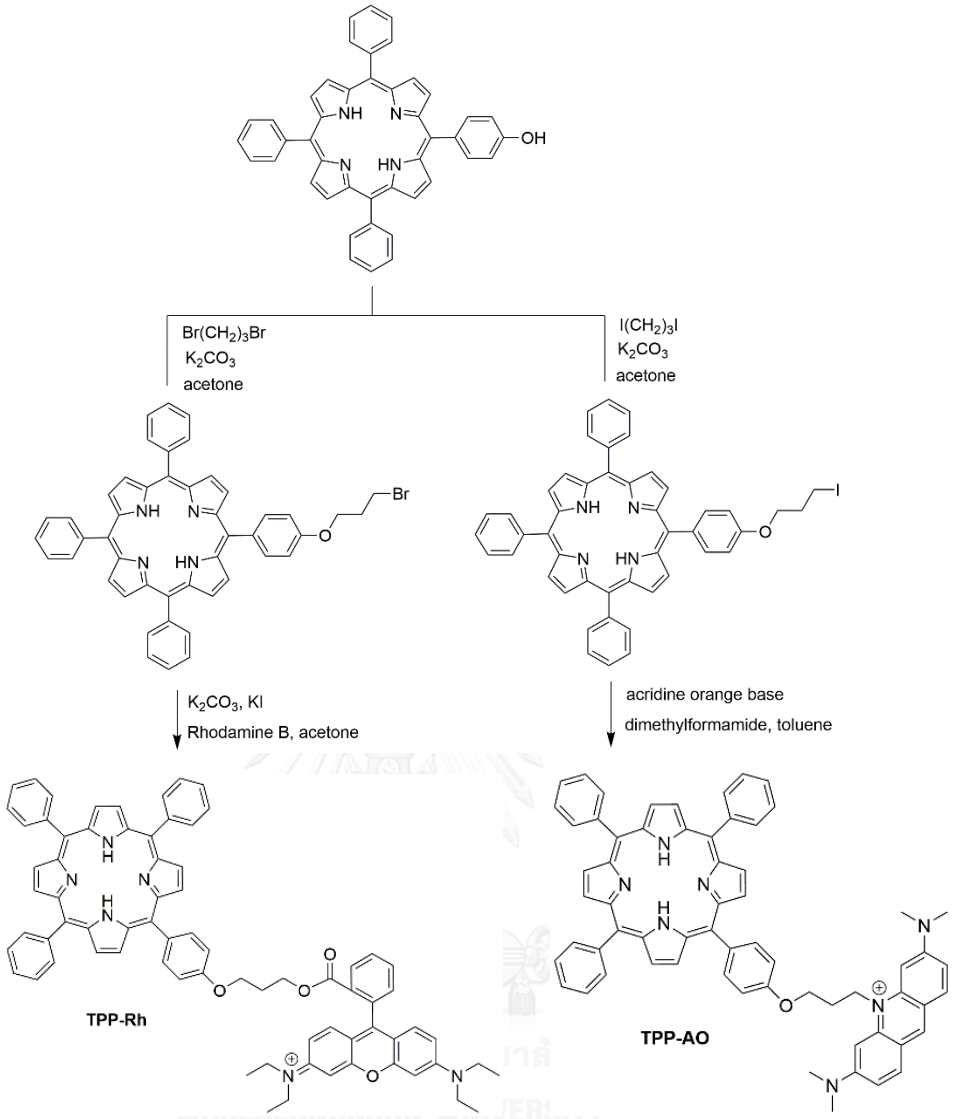

Scheme 2–8: Synthesis of **TPP-Rh** and **TPP-AO** by You, Y. *et al.*

Their mitochondria-targeting ability was confirmed by fluorescence imaging. The mitochondrial localization of **TPP-Rh** and **TPP-AO** was obtained by staining each dye (red region) with Mitotracker green (MG). The green and red images were superimposed, and the region of colocalization appeared as yellow as shown in **Figure 2–9**.

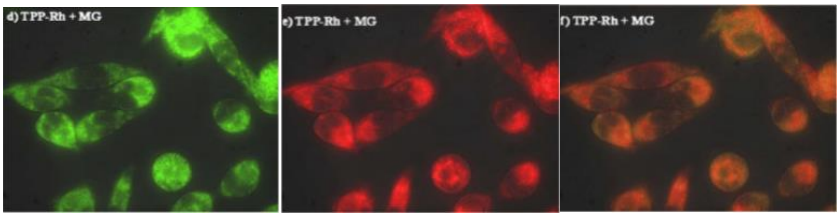

Figure 2–9: Fluorescence images from staining experiment by You, Y. *et al.*

In 2011, Lu, C. *et al.*[53] reported design, synthesis and evaluation of PEGylated lipoic acid derivatives as potent anti-melanogenic agent. The novel PEGylated lipoic acid ester derivatives were synthesized by simple routes and also studied for their anti-melanogenic property on B16F10 melanoma cell. This molecule can inhibit melanin formation better than lipoic acid and thus the lipoic acid derivatives act as active anti-melanogenic and anti-aging agent. The synthetic pathway and inhibitory effect of the PEGylated lipoic acid ester derivatives were described in **Scheme 2–9** and **Figure 2–10**, respectively.

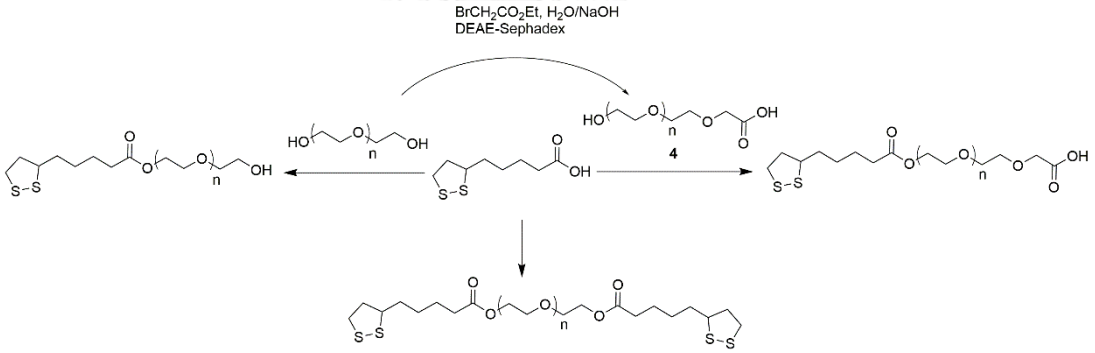

Scheme 2–9: Synthetic route to novel water-soluble PEGylated lipoic acid ester derivatives by Lu, C. *et al.*

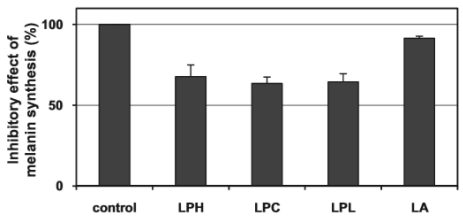

Figure 2–10: Inhibitory effects of PEGylated lipoic acid ester derivatives on melanin synthesis.

In the same year, Bernini, R. *et al*.[54] reported the synthesis of a novel ester of hydroxytyrosol and α-lipoic acid exhibiting an antiproliferative effect on human colon cancer HT-29 cells. The molecule was synthesized by general esterification reaction to provide lipoic acid derivatives (**Scheme 2–10**).

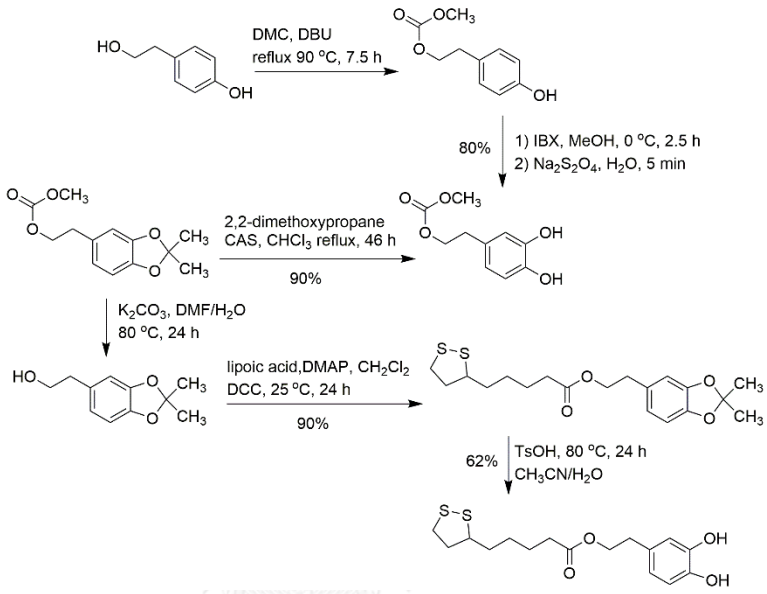

Scheme 2–10: A synthetic pathway of lipoic acid derivatives described by Bernini, R. *et al*.

The target product presented a cell growth inhibitory activity expressively more potent than that of the corresponding parent compounds.

CHAPTER III

EXPERIMENTS

3.1 Chemicals

All chemical are purchased from commercial sources and used as received without further purification.

1. 4-pyridine carboxzaldehyde : Sigma-Aldrich
2. 4-ntrobenzaldehyde : Sigma-Aldrich
3. pyrrole : Sigma-Aldrich
4. propionic acid : Merck
5. sodium hydroxide (NaOH) : Merck
6. tin(II) chloride dihydrate ($SnCl_2 \cdot 2H_2O$) : Merck
7. hydrochloric acid (HCl) : Lab-scan
8. α-Lipoic acid : Sigma-Aldrich
9. *N,N'*-dicyclohexylcarbodiimide (DCC) : Sigma-Aldrich
10. Iodomethane (CH_3I) : Merck
11. dimethylformamide (DMF) : Lab-scan
12. manganese (II) chloride tetradydrate ($MnCl_2 \cdot 4H_2O$) : Fluka
13. methylene chloride (CH_2Cl_2) : Lab-scan
14. methanol (MeOH) : Merck
15. ethanol (EtOH) : Merck
16. triethylamine (Et_3N) : Lab-scan
17. dethyl ether : Merck

18. acetone : Lab-scan

19. sodium sulfate (Na_2SO_4) : Merck

20. silica gel : Merck

21. deuterated chloroform ($CDCl_3$) : Merck

22. deuterated dimethy sulfoxide

(DMSO-d_6) : Merck

23. dulbecco's modified eagle's medium (DMEM) : Gibco

24. fetal bovine serum (FBS) : Gibco

25. antimycotic : Gibco

26. trypsin/Ethylenediaminetetraacetic acid

(trypsin/EDTA) : Gibco

27. 5,5',6,6'-tetrachloro-1,1',3,3'tetraethylbenzimi-

dazolylcarbocyanine iodide (JC-1) : MERK, Calbiochem

3.2 Analytical instruments

^{1}H-NMR and ^{13}C-NMR spectra were obtained in deuterated chloroform ($CDCl_3$) using an NMR spectrometer operated at 400 MHz. Chemical shifts (δ) are reported in part per million (ppm) relative to the residual $CHCl_3$ peak at 7.26 ppm for ^{1}H-NMR spectroscopy and 77.0 ppm for ^{13}C-NMR spectroscopy. Coupling constants (*J*) are reported in Hertz (Hz).

Mass spectra were obtained using high resolution electrospray ionization (HRESI), and matrix-assisted laser desorption ionization (MALDI) mass spectrometry with α-cyano-4-hydroxy cinamic acid (α-CCA) as a matrix.

Absorption and emission spectra of the solution were measured in dimethyl formamide and H_2O and absorption extinction coefficient (ε) were reported in

L/mol·cm. Fluorescence spectra were measured in dimethyl formamide and H_2O. Absorption and emission were measured in dimethyl formamide and H_2O at room temperature.

3.3 Experimental section

3.3.1 Synthesis

3.3.1.1 5-*p*-nitrophenyl-10–15–20-(tripyridin-4-yl)porphyrin (**1**)

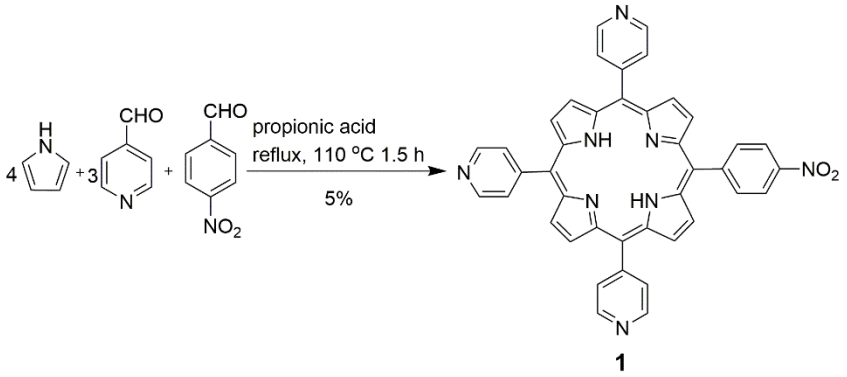

1

Following a previous report,[55] a mixture of 4-pyridine carboxaldehyde (2.73 g, 25.5 mmol) and 4-nitrobenzaldehyde (1.28 g, 8.50 mmol) in propionic acid (200 mL) was stirred at 110 °C for an hour. Then, pyrrole (2.27 g, 38.9 mmol) was added and the reaction mixture was refluxed for additional 1 h. Afterwards, the mixture was cooled and neutralized with a 1 M aqueous solution of NaOH until pH was 8. The solution was filtered and washed with a 1 M aqueous solution of NaOH. The filtrate was dissolved in H_2O (2 L) and filtered again. The resulting purple solid was purified by column chromatography (silica gel, 6% EtOH in CH_2Cl_2), affording **1** as purple solid (0.286 g, 5%). ^{1}H-NMR δ –2.89 (s, 2H), 8.17 (d, J = 4.0 Hz, 6H), 8.38 (d, J = 8.0 Hz, 2H), 8.65 (d, J = 8.0 Hz, 2H), 8.82–8.88 (m, 8H), 9.07 (d, J = 4.0 Hz, 6H) (**Figure A-1**); MALDI-TOF-MS *m/z* obsd 662.447 (M^+), calcd avg mass 662.218 (M^+, M = $C_{41}H_{26}N_8O_2$) (**Figure A-2**); λ_{abs} 417, 513, 546, 587, 642 nm (**Figure A-3**); λ_{em} (λ_{ex} = 417 nm) 652, 715 nm (**Figure A-4**). The spectral data are consistent with those described in the literature.

3.3.1.2 5-*p*-aminophenyl-10-15-20-(tripyridin-4-yl)porphyrin (**2**)

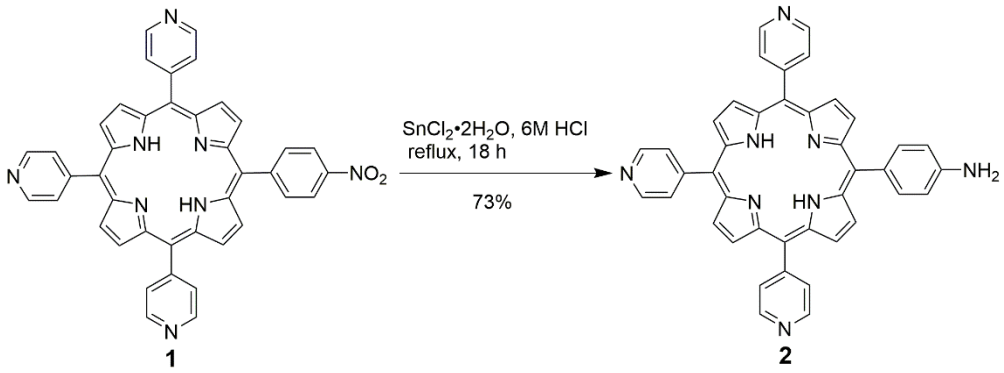

Following a previous reported,[56] a solution of **1** (53 mg, 0.084 mmol) in a 6 M aqueous solution of HCl (8 mL) was reacted with $SnCl_2 \cdot 2H_2O$ (90 mg, 0.40 mmol) under reflux for 18 h. After cooling down to room temperature, the mixture was neutralized with a 1 M aqueous solution of NaOH until pH was 8 and the aqueous phase was extracted with CH_2Cl_2. The organic phase was washed with H_2O, dried over $MgSO_4$ and concentrated to dryness. The purple crude product was purified by column chromatography (silica gel, 6% EtOH in CH_2Cl_2), affording **2** as purple solid (37 mg, 73%). ^{1}H-NMR δ –2.84 (s, 2H), 7.09 (d, J = 8.0 Hz, 2H), 7.99 (d, J = 8.0 Hz, 2H), 8.16 (d, J = 4.0 Hz, 6H); 8.78–8.87 (m, 6H), 9.00–9.07 (m, 8H) (**Figure A-5**); MALDI-TOF-MS *m/z* obsd 633.785 ($[M+H]^+$), calcd avg mass 632.244 ($[M+H]^+$, M = $C_{41}H_{28}N_8$) (**Figure A-6**); λ_{abs} 418, 517, 551, 595, 652 nm (**Figure A-7**); λ_{em} (λ_{ex} = 418 nm) 647, 713 nm (**Figure A-8**). The spectral data are consistent with those described in the literature.

3.3.1.3 5-*p*-nitrophenyl-10-15-20-tri(4-*N*-methylpyridinium)porphyrin (**TMNPyP**)

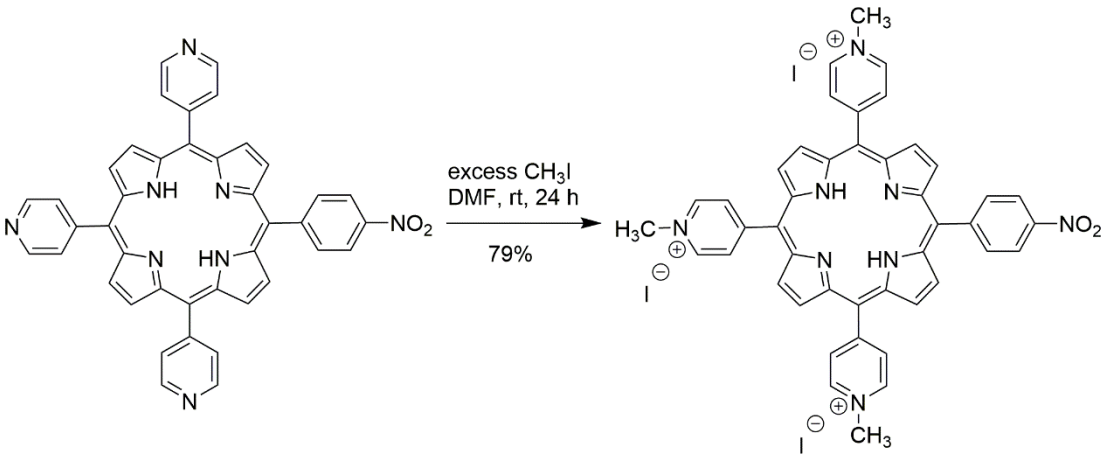

1 **TMNPyP**

Following a previous report,[57] a solution of **1** (23 mg, 0.035 mmol) in DMF (10.0 mL) was reacted with iodomethane (1.0 mL) at room temperature for 24 h. After that, the resulting mixture was precipitated with diethyl ether and the precipitate was washed with hexane and acetone, leading to **TMNPyP** as brownish purple solid (20 mg, 79%). ^{1}H-NMR (DMSO-d_6) δ –3.05 (s, 2H), 4.72 (s, 9H), 8.52 (d, J = 8.0 Hz, 2H), 8.74 (d, J = 8.0 Hz, 2H), 8.87–9.29 (m, 14H), 9.48 (d, J = 4.0 Hz, 6H) (**Figure A-9**); MALDI-TOF-MS m/z obsd 707.108 (M^+); calcd avg mass 707.800 ([M]$^+$, M = $C_{44}H_{35}I_3N_8O_2$) (**Figure A-10**); λ_{abs} 425, 517, 551, 590, 646 nm (**Figure A-11**); λ_{em} (λ_{ex} = 425 nm) 652, 716 nm. (**Figure A-12**).

3.3.1.4 Compound **3**

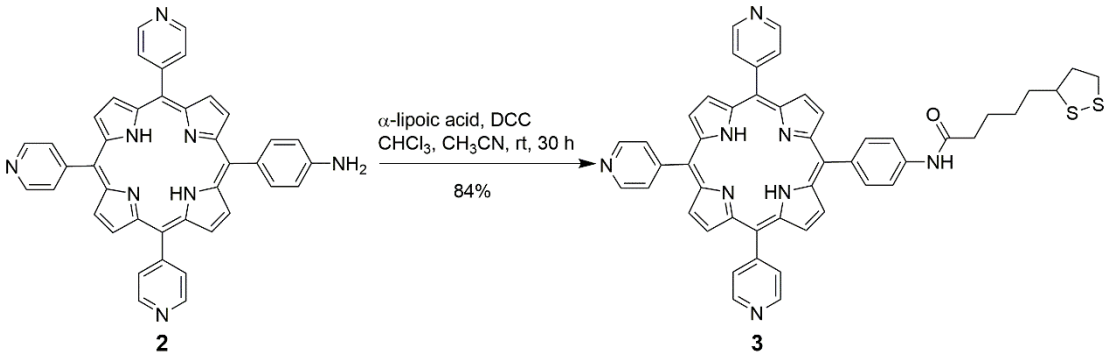

2 **3**

Following a published procedure,[58] α-lipoic acid (0.418 g, 2.03 mmol) was reacted with dicyclohexyl carbodiimide (DCC, 0.230 g, 0.280 mmol) in acetonitrile (10.0 mL) at room temperature for 10 h. After that, the solution was filtered to remove dicyclohexylurea. Lipoic anhydride was obtained as filtrate and directly treated with **2** (0.031 g, 0.045 mmol) in $CHCl_3$ (10.0 mL). The resulting mixture was stirred at room temperature for 20 h and then precipitated with hexane, affording compound **3** as air-sensitive purple solid (0.034 g, 84%). ^{1}H-NMR δ –2.89 (s, 2H), 1.78–1.86 (m, 4H), 1.88–2.04 (m, 2H), 2.47–2.65 (m, 4H), 3.18–3.32 (m, 2H), 3.61–3.76 (m, 1H), 7.61 (s, 1H), 7.96 (d, *J* = 8.0 Hz, 2H), 8.16 (s, 8H), 8.78–8.88 (m, 6H), 8.94 (d, *J* = 4.0 Hz, 2H), 9.04 (s, 6H) (**Figure A-13**);.^{13}C-NMR δ 25.3, 29.0, 34.7, 37.7, 38.5, 40.3, 56.5, 117.0, 117.4, 118.1, 121.2, 129.4, 135.1, 138.1, 148.3, 150.1, 171.4 (**Figure A-14**); HR-ESI-MS *m/z* obsd 821.2817 ($[M+H]^+$); calcd 821.2845 ($[M+H]^+$, M = $C_{49}H_{40}N_8OS_2$) (**Figure A-15**); λ_{abs} 419, 514, 549, 567, 646 nm. (**Figure A-16**); λ_{em} (λ_{ex} = 419 nm) 650, 720 nm (**Figure A-17**).

3.3.1.5 Compound **P-Lp**

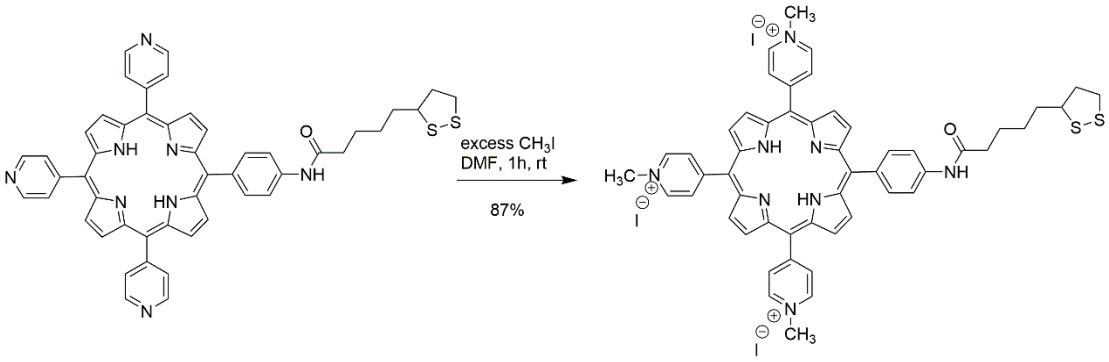

3 **P-Lp**

Following Tome *et al*.,[59] compound **3** (12 mg, 0.013 mmol) in DMF (2.0 mL) was reacted with iodomethane (1.0 mL) at room temperature for 1 h. After that, the resulting mixture was precipitated with diethyl ether and the precipitate was washed with EtOH, leading to **P-Lp** as brownish purple solid (10 mg, 87%). ^{1}H-NMR: δ –3.88 (s, 2H), 0.59–1.41 (m, 10H), 2.02–2.21 (m, 3H), 3.84 (s, 9H), 7.26 (d, *J* = 4.0 Hz, 4H), 8.08–8.34 (m, 14H), 8.60 (d, *J* = 4.0 Hz, 4H), 9.48–9.60 (m. 1H) (**Figure A-18**); ^{13}C-NMR: δ 25.0, 28.4, 34.2, 34.4, 36.5, 38.2, 47.9, 56.2, 114.4, 115.2, 117.6, 122.9, 132.1, 134.8, 139.7, 144.1, 156.6, 171.7 (**Figure A-19**); HR-ESI-MS *m/z* obsd 865.3463 (M^+), calcd 865.3454 (M^+, M = $C_{52}H_{49}I_3N_8OS_2$) (**Figure A-20**); λ_{abs} (ε) 428 (8.1×10^4), 519, 555, 648 nm (**Figures A-21** and **A-22**); λ_{em}(λ_{ex}= 428 nm) 658, 719 nm (**Figure A-23**).

3.3.1.6 Compound **Mn-P-Lp**

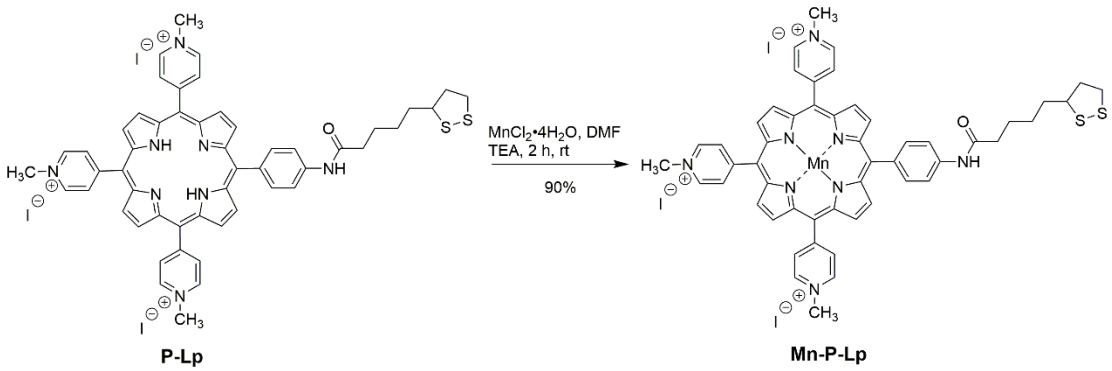

Following a published method,[60] **P-Lp** (10 mg, 0.011 mmol) in DMF (2.00 mL) was reacted with $MnCl_2 \cdot 4H_2O$ (45 mg, 0.23 mmol) at room temperature for 4 h. The mixture was washed with diethyl ether to obtain brownish purple solid (9 mg, 90%). MALDI-TOF-MS *m/z* obsd 918.405 ($[M+H]^+$), 1062.458 ($[M+\alpha\text{-CCA}]^+$); calcd avg mass 919.060 ($[M^+]$, M = $C_{52}H_{47}I_3MnN_8OS_2$) (**Figure A-24**); λ_{abs} (ε) 373, 398, 469 (6.5×10^4), 673 nm (**Figures A-25** and **A-26**). No emission peak was observed (**Figure A-25**).

3.3.2 Biological studies

3.3.2.1 Cell culture

Human dermal fibroblasts, adult (HDFa) and Human keratinocyte (HaCaT) cell lines[61] were cultured in Dulbecco's modified eagle's medium (DMEM) supplemented with 10% (v/v) fetal bovine serum (FBS) 1% (v/v) antibiotic and antimycotic at 37 °C in a humidified atmosphere containing 5% CO_2. Cell at early passages (below 30 passages) were used in cell experiments to avoid complications of replicative senescence. After HFDa and HeaCaT cell lines approximately reached 90% confluence, cell were sub-cultured using 0.25% (v/v) trypsin / EDTA.

3.3.2.2 Cytotoxicity

Cell viability was assessed using Prestoblue™ reagent.[62] HFDa and HaCaT cell lines were seeded into 96-well plates at density of $5x10^3$ cells/well under 5% CO_2 atmosphere for 12 h. Cells were washed by phosphate buffered saline (PBS) twice and treated with various concentrations of lipoic acid, **TMNPyP**, **P-Lp** or **Mn-P-Lp** (90 µL) for 24 h. Then, PrestoBlue™ solution (10 µL) was added and the cells were incubated at 37 ℃ for 30 min. Finally, absorbance was measured on a microplate reader at 560 and 590 nm to obtain the percentage of the viable cells which was calculated by comparison with that of the control group (DMEM).

3.3.2.3 Reactive oxygen species (ROS) generation

Intracellular reactive oxygen species (ROS)[63] production was confirmed by 2',7'-dichlorofluoreceine-diacetate (H_2DCF-DA) assay. Briefly, HFDa and HaCaT cell lines were seeded into 96-black well plates at density of $5x10^3$ cells/well (100 µL) of complete medium and incubated at 37 ℃ under 5% CO_2 atmosphere for 12 h. The cells were washed by PBS twice. After that, various concentrations of lipoic acid, **TMNPyP**, **P-Lp** or **Mn-P-Lp** (100 µL) were added into the cells for pre-treatment and incubated for 24 h. After that, the solution was discarded, and the cell were added with H_2DCFDA and then incubated for 30 min at 37 ℃ in dark place. The cells were washed by PBS twice and treated with 10% H_2O_2 (100 µL). Fluorescence was measured using a microplate reader at 485 nm and 528 nm every 10 min for 1 h.

3.3.2.4 Mitochondria-targeting evaluation

Mitochondria-targeting activity was determined by LSM 800 confocal microscope. From previous report,[64] HaCaT cells were seeded in 24 wells corning-plate at density 1×10^5 cells/well. Then cells were incubated at 37 ℃ under 5% CO_2 atmosphere for 12 h. After that, the cells were treated with 50 ppm lipoic acid, **P-Lp** or **Mn-P-Lp**, and the resulting mixtures were incubated at 37 ℃ under 5% CO_2

atmosphere for 6 h. Protocol of JC-1 staining was applied from Chazotte, B..[65] The cells were washed with PBS. JC-1 dye and Hoechst 33342 (10 μg·mL^{-1}) in DMSO were loaded in each well and incubated for 15 min, the cells were then washed with PBS and imaged by a LSM 800 confocal microscope using lens 40X with excitation wavelength of 488 and 561 nm using emission filters at 505–550 nm for a green channel, and 575–630 nm for a red channel. The pictures were collected and analysed by ZEN software version 2.1.

3.3.2.5 Statistical analysis

Statistical analysis of the data was determined with a one-way randomized ANOVA design by GraphPad Prism 5.0 software. When the overall test of significance ($p < 0.05$, p-value is probability of the randomness in sampling) led to a rejection of the null hypothesis, post-hoc comparison (Tukey) were performed.

CHAPTER IV

RESULTS AND DISCUSSION

4.1 Synthesis and characterization of target asymmetric porphyrin

The synthesis of the target asymmetric porphyrin started with a condensation of 4-nitrobenzaldehyde, pyrrole and 4-pyridinecarboxaldehyde in propionic acid to give **1**[56] in 5% yield as shown in **Schemes 4–1** and **4–2**.

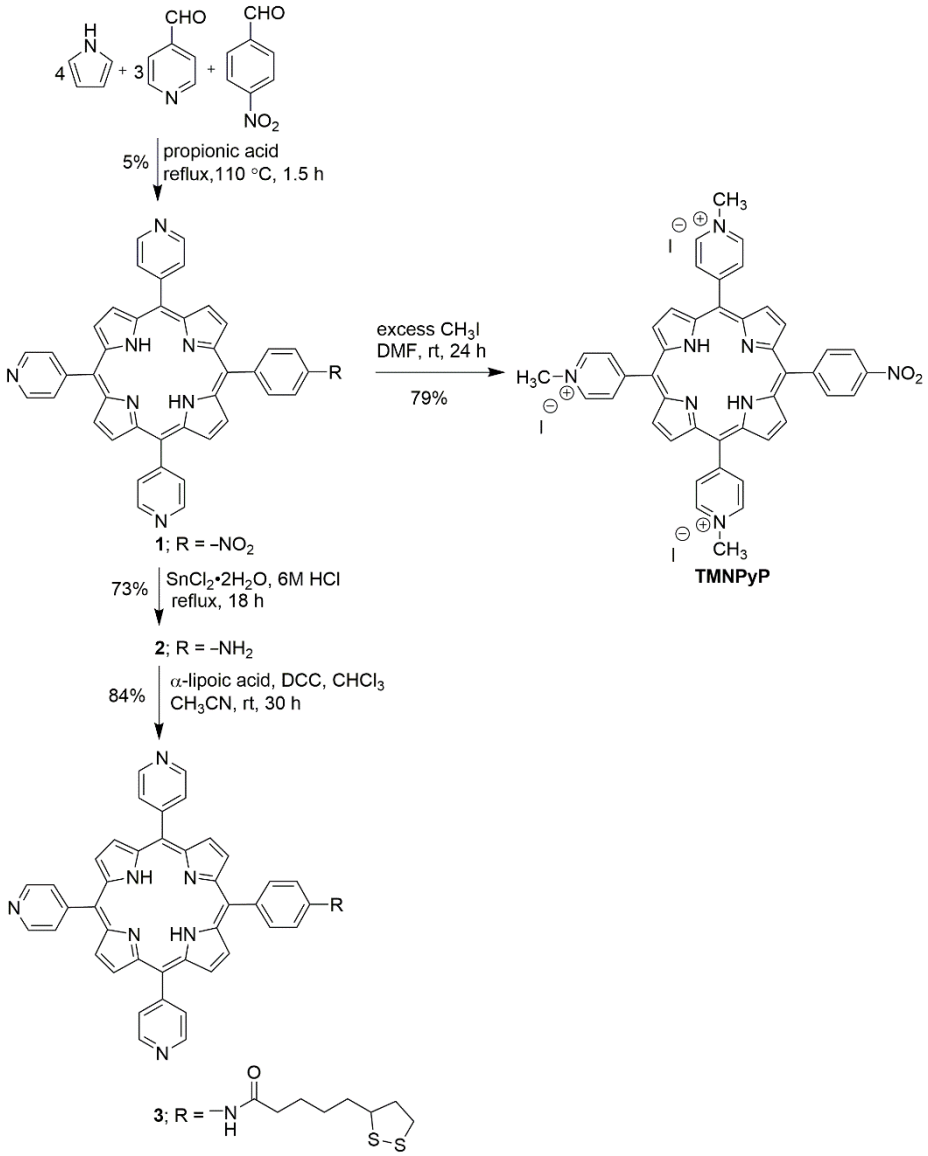

Scheme 4–1: A synthetic route of the lipoic acid-containing porphyrinic precursor.

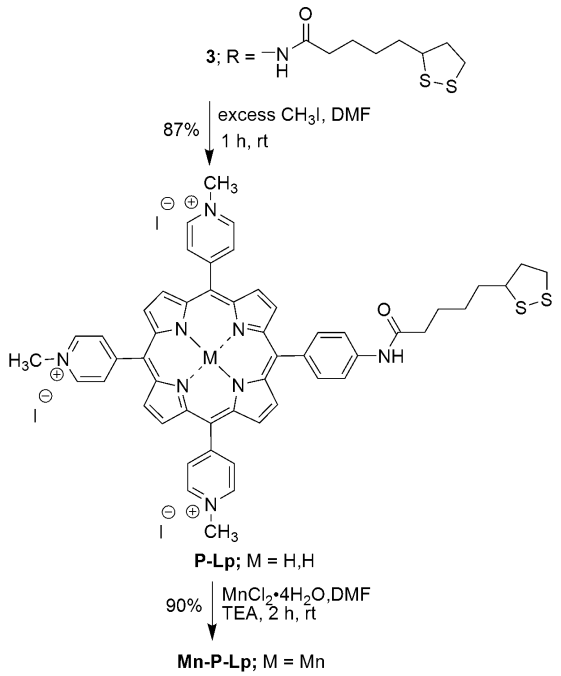

Scheme 4–2: A synthetic route of the target lipoic acid-containing porphyrinic derivative.

Low yield of **1** is attributed to the formation of other statistically possible porphyrinic byproducts. After that, **1** was reduced with $SnCl_2 \cdot 2H_2O$ in a 6 M aqueous solution of HCl under reflux for 18 h, affording **2**[66] in 73% yield. To obtain benchmark compound **TMNPyP**, used to compare biological activities with **P-Lp**, compound **1** was methylated with an excess amount of iodomethane at room temperature for 24 h. Then, **2** was condensed with lipoic anhydride[67] *via* amidation reaction in the presence of DCC in a mixture of $CHCl_3$ and CH_3CN with a ratio of 1:1 at room temperature for 30 h, leading to **3** in 84% yield. Mechanism of these steps are shown in **schemes 4–3** and **4–4**.

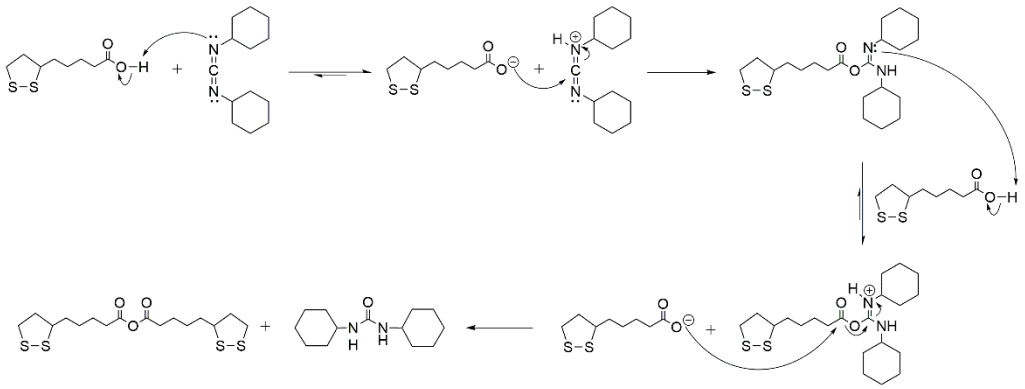

Scheme 4–3: Mechanism of preparation of lipoic anhydride using DCC.

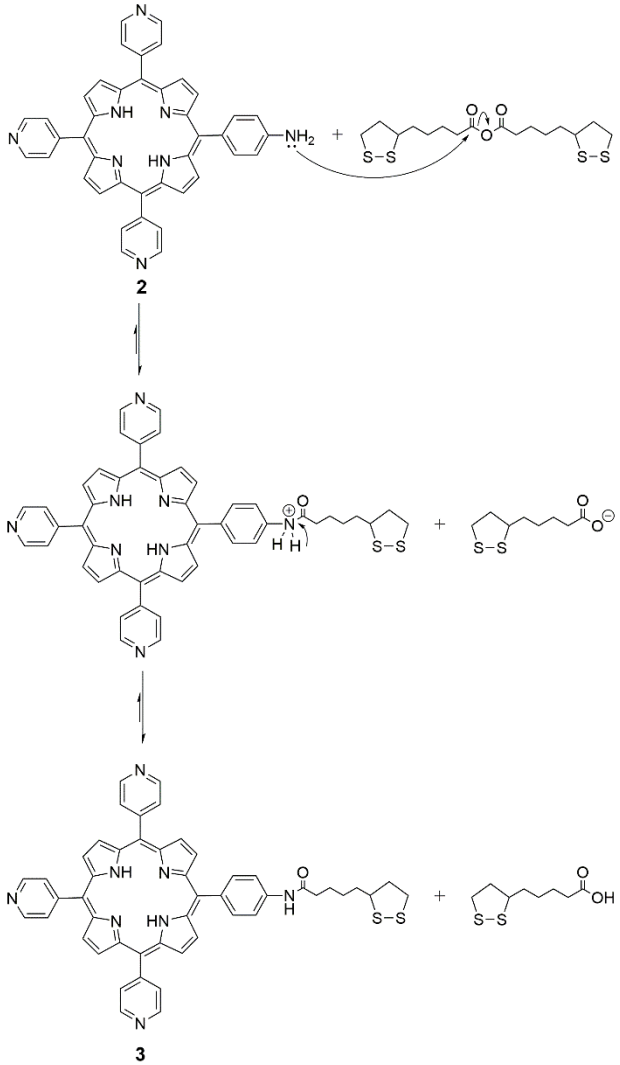

Scheme 4–4: Mechanism of amidation of compound **2** with activated lipoic anhydride.

Subsequently, compound **3** was alkylated with an excess amount of CH_3I in DMF at room temperature for an hour, resulting in **P-Lp** in 87% yield. **P-Lp** was then metalated with $MnCl_2 \cdot 4H_2O$ in DMF in the presence of TEA at room temperature for 4 h, affording **Mn-P-Lp** in 90%.

MALDI-TOF mass spectra of compounds **1** and **2** exhibited their molecular ion peaks at *m/z* 662.218 and 633.785, respectively. ^{1}H-NMR Spectra of these free base porphyrins showed characteristic peaks of their inner protons at δ –2.84 to –2.89 ppm with multiplet signals of the protons on pyrrole, pyridine and phenyl rings at δ 7.07–9.07 ppm. A signal of the phenyl protons of **2** slightly shifted from 8.37–8.66 ppm to 7.08–7.98 ppm, when compared with those of **1**, possibly because of mesomeric effect from an amino to the phenyl ring in **2**. However, no clear signal of amino protons of compound **2** was observed. Then, compound **1** was alkylated with iodomethane to get **TMNPyP**. MALDI-TOF mass spectrum of **TMNPyP** exhibited its molecular ion peaks at *m/z* 707.287. According to its ^{1}H-NMR spectrum, **TMNPyP** exhibited a characteristic singlet signal of methyl protons at δ 4.72 ppm. Multiplet protons signals of the pyrrole, pyridine and phenyl rings slightly shifted from 8.17–9.07 ppm to 8.52–9.48 ppm, compared with those of compound **1**, because of inductive effect from the pyridinium rings.

Formation of the compound **3** was confirmed by the presence of a molecular ion peak in its HR-ESI mass spectrum at *m/z* 821.2817. According to its ^{1}H-NMR spectrum, compound **3** exhibited a characteristic singlet signal of an amide proton at δ 7.61 ppm. Multiplet protons signals of the pyrrole, pyridine and phenyl rings slightly shifted from 7.08–9.05 ppm to 7.96–9.04 ppm, compared with compound **2**, because of inductive and mesomeric effects from the amide group. Aromatic protons exhibited δ at 7.61–9.04 ppm. Moreover, multiplet signals indicating aliphatic protons of the lipoyl group were observed at δ 1.78–3.76 ppm. Based on ^{13}C-NMR, aromatic carbons exhibited signals at δ 117.04–150.10 ppm. A peak of carbonyl carbon of the amide group was found at δ 171.39 ppm, while those of the lipoyl group appeared at δ 25.3–56.5 ppm.

Then, the resulting compound **3** was alkylated with iodomethane, followed by metallation of the resulting **P-Lp** with $MnCl_2 \cdot 4H_2O$ to get **Mn-P-Lp**. Formation of **P-Lp** was confirmed by ^{1}H-NMR and ^{13}C-NMR spectra, MALDI-TOF mass spectrum, UV-visible and fluorescent spectra. A methyl groups on the pyridinium rings gave a singlet peak at δ 3.84 ppm, while multiplet protons signals of the pyrrole, pyridine and phenyl rings were found at 7.26–8.60 ppm. A singlet signal indicating the amide proton was obviously shifted from 7.61 to 9.53 ppm because of inductive effect from the pyridinium rings. Based on ^{13}C-NMR, aromatic carbons exhibited signals at δ 114.38–156.61 ppm. A peak of carbonyl carbon of the amide group was found at δ 171.72 ppm, while those of the lipoyl group appeared at δ 25.01 –56.19 ppm and methyl carbons was found at δ 47.94 ppm. A molecular ion peak of **P-Lp** in a MALDI-TOF mass spectrum was found at *m/z* 866.170. Absorbtion peaks of **P-Lp** were observed at 428, 519, 555, 648 nm, while the emission ones were observed at 657, 719 nm. Successful formation of **Mn-P-Lp** was confirmed by MALDI-TOF mass spectrum, UV-visible and fluorescent spectra. Maximum absorbtion of **Mn-P-Lp** was shifted from 428 to 469 nm, compared with that of **P-Lp** and a molecular ion peak of **Mn-P-Lp** in its MALDI-TOF mass spectrum was found at *m/z* 918.405. Moreover, another ion peak of **Mn-P-Lp** was found at *m/z* 1082.458, corresponding to $[(M+\alpha\text{-CCA})^+]$ ion.

4.2 Biological studies

4.2.1 Cytotoxicity

Cytotoxicity of **P-Lp**, **Mn-P-Lp** and **TMNPyP** was determined by cell viability assay.[68] These porphyrins were evaluated for its effect on the viability of HDFa and HaCaT cells compared to a control group, Dulbecco's modified eagle's medium (DMEM), and a parent natural compound, lipoic acid. For this purpose, HDFa and HaCaT cells were incubated in 96-well plates in solutions of these compounds at concentration of 25, 50, 100 and 150 $\mu g \cdot mL^{-1}$ for 24 h. PrestoBlue™ solutions was then added and the cells were incubated for additional 30 min. Finally, absorbance of the compounds of interest were measured on a microplate reader at 560 and 590 nm to

obtain percentage of viable cells in each treatment group which was calculated by comparison to that of the control group as shown in **Figure 4–1**.

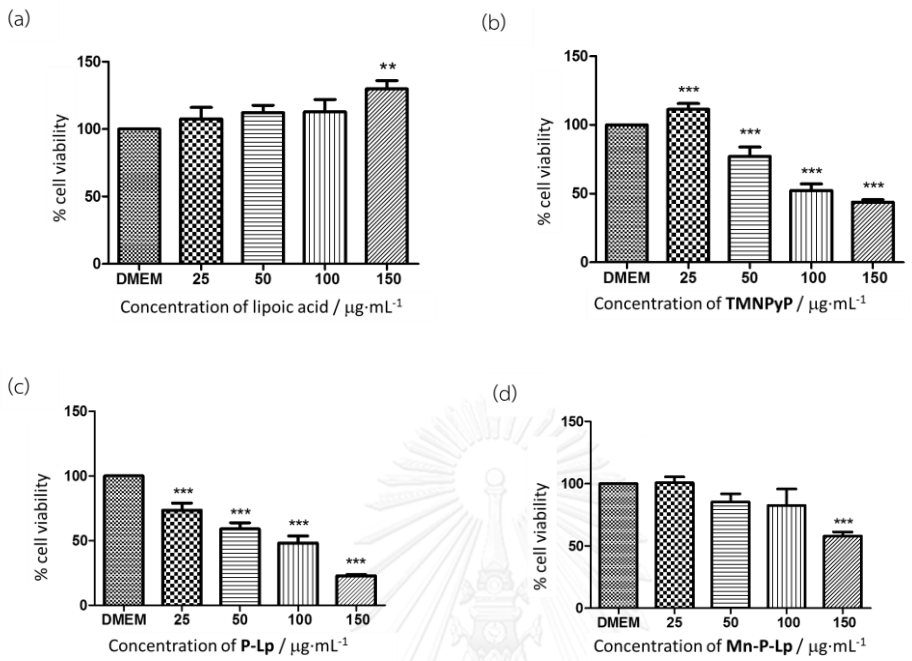

Figure 4–1: Cell viability upon the treatment of the HaCaT cells with (a) lipoic acid, (b) **TMNPyP**, (c) **P-Lp**, (d) **Mn-P-Lp** at 25, 50, 100, 150 µg·mL^{-1} ("***" indicates $p < 0.001$, "**" indicates $p < 0.01$ and "*" indicates $p < 0.05$).

Figure 4–1(a) shows that the cell viability of the HaCaT cells did not significantly change after being treated with lipoic acid at 25–100 µg·mL^{-1}, compared with the control group, while at the concentration of 150 µg·mL^{-1} of lipoic acid, enhancement of the cell viability became significant ($p < 0.01$). These results indicated that lipoic acid exhibited low cytotoxicity and slightly proliferation of the HaCaT cells at high concentration.

As shown in **Figure 4–1(b),** the concentration of **TMNPyP** at 25 µg·mL^{-1} exhibited significant increase in the cell viability ($p < 0.001$), compared with DMEM, while at the concentration of 50 µg·mL^{-1} significant decrease in the cell viability was detected. At the concentration of 100–150 µg·mL^{-1}, dramatical decrease in the cell viability was observed. Therefore, according to these results, **TMNPyP** exhibited

cytotoxicity with an half maximal inhibitory concentration (IC_{50}) value of 100–150 $\mu g \cdot mL^{-1}$.

As of **P-Lp**, the cell viability of the HaCaT cells was found to significantly decrease when being treated with **P-Lp** at the concentration of 25 $\mu g \cdot mL^{-1}$. The concentrations of 50, 100 and 150 $\mu g \cdot mL^{-1}$ caused drastic decrease in the cell viability of the HaCaT cells. These results indicated that **P-Lp** exhibited cytotoxicity with IC_{50} value of 50—100 $\mu g \cdot mL^{-1}$.

The cell viability of the HaCaT cells after being treated with **Mn-P-Lp** at 25, 50 and 100 $\mu g \cdot mL^{-1}$ did not significantly change, but obviously decreased when the concentration was 150 $\mu g \cdot mL^{-1}$, compared with those treated with DMEM, indicating that the IC_{50} of **Mn-P-Lp** was in the range of 25–150 $\mu g \cdot mL^{-1}$.

The effect of the introduction of the porphyrin unit on the cell viability of the HaCaT cells can be determined by the comparison of the results of lipoic acid and those of **P-Lp**. Lipoic acid exhibited the IC_{50} of >150 $\mu g \cdot mL^{-1}$, while **P-Lp** showed the IC_{50} of 50–100 $\mu g \cdot mL^{-1}$. These results indicated that the presence of the porphyrin unit adversely affect the cell viability of this type of cells. In addition, the effect of the introduction of the lipoic acid on the cell viability of the HaCaT cells can be determined by the comparison of the results of **TMNPyP** and those of **P-Lp**. **TMNPyP** exhibited the IC_{50} of 100–150 $\mu g \cdot mL^{-1}$, while **P-Lp** showed the IC_{50} of 50–100 $\mu g \cdot mL^{-1}$. These results indicated that the appearance of the lipoic acid slightly decrease the cell viability of this type of cells. Moreover, the effect of the introduction of the Mn-chelation of the porphyrin unit on the cell viability of the HaCaT cells can be determined by the comparison of the results of **P-Lp** and those of **Mn-P-Lp**. **P-Lp** exhibited the IC_{50} of 50–100 $\mu g \cdot mL^{-1}$, while **Mn-P-Lp** showed the IC_{50} of >150 $\mu g \cdot mL^{-1}$. These results indicated that the presence of the Mn-chelation of the porphyrin unit slightly improve the cell viability of this type of cells, which is consistent with the previous finding that Mn is an important metal for human health, being necessary for metabolism.[69]

In case of the HDFa cells, the cytotoxicity of lipoic acid, **TMNPyP**, **P-Lp** and **Mn-P-Lp** was determined by the cell viability assay as shown in **Figure 4–2**.

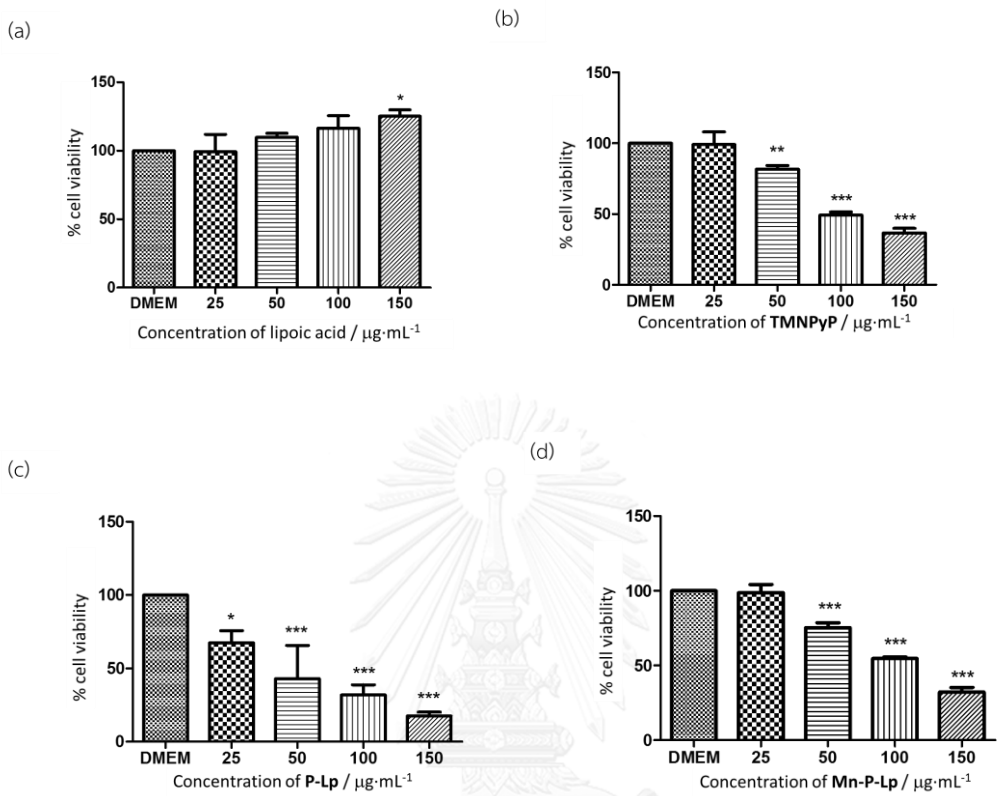

Figure 4–2: The cell viability upon the treatment of the HDFa cells with (a) lipoic acid, (b) **TMNPyP**, (c) **P-Lp**, (d) **Mn-P-Lp** at 25, 50, 100, 150 μg·mL^{-1} ("***" indicates $p < 0.001$, "**" indicates $p < 0.01$ and "*" indicates $p < 0.05$).

Figure 4–2(a) shows that the cell viability of the HDFa cells did not significantly change after being treated with lipoic acid at 25–100 μg·mL^{-1}, compared with the control group, while at the concentration of 150 μg·mL^{-1} of lipoic acid, enhancement of viable cell became significant ($p < 0.05$). These results indicated that lipoic acid exhibited low cytotoxicity and slightly proliferation of the HDFa cells at high concentration.

As shown in **Figure 4–2(b)**, the cell viability of the HDFa cells did not significantly change after being treated with **TMNPyP** at 25 μg·mL^{-1}, compared with DMEM, while at the concentration of 50 μg·mL^{-1} significant decrease in the cell viability

($p < 0.01$) was detected. At the concentration of 100–150 $\mu g \cdot mL^{-1}$, dramatical decrease in the cell viability was observed. These results indicated that **TMNPyP** exhibited cytotoxicity with the IC_{50} value of 50–100 $\mu g \cdot mL^{-1}$.

As of **P-Lp**, the cell viability of the HDFa cells was found to significantly decrease when being treated with **P-Lp** at the concentration of 25 $\mu g \cdot mL^{-1}$. The concentrations of 50, 100 and 150 $\mu g \cdot mL^{-1}$ caused drastic decrease in the cell viability of the HDFa cells. These results indicated that **P-Lp** exhibited cytotoxicity with the IC_{50} value of 25–50 $\mu g \cdot mL^{-1}$.

The cell viability of the HDFa cells after being treated with **Mn-P-Lp** at 25 $\mu g \cdot mL^{-1}$ did not significantly change, but obviously decreased when the concentration was 50, 100 and 150 $\mu g \cdot mL^{-1}$, compared with those treated with DMEM, indicating that the IC_{50} of **Mn-P-Lp** was in the range of 100–150 $\mu g \cdot mL^{-1}$.

The effect of the introduction of the porphyrin unit on the cell viability of the HDFa cells can be determined by the comparison of the results of lipoic acid and those of **P-Lp**. Lipoic acid exhibited the IC_{50} of >150 $\mu g \cdot mL^{-1}$, while **P-Lp** showed the IC_{50} of 25–50 $\mu g \cdot mL^{-1}$. These results indicated that the presence of the porphyrin unit adversely affect the cell viability of this type of cells. In addition, the effect of the appearance of the lipoic acid on the cell viability of the HDFa cells can be determined by the comparison of the results of **TMNPyP** and those of **P-Lp**. **TMNPyP** exhibited the IC_{50} of 50–100 $\mu g \cdot mL^{-1}$, while **P-Lp** showed the IC_{50} of 25–50 $\mu g \cdot mL^{-1}$. These results indicated that **P-Lp** has more cytotoxicity than **TMNPyP** in the HDFa cells. Consequently, the appearance of lipoic acid obviously decrease the cell viability of the HDFa cells. Moreover, the effect of the introduction of the Mn-chelation of the porphyrin unit on the cell viability of the HDFa cells can be determined by the comparison of the results of **P-Lp** and those of **Mn-P-Lp.** **P-Lp** exhibited the IC_{50} of 25–50 $\mu g \cdot mL^{-1}$, while **Mn-P-Lp** showed the IC_{50} of 100–150 $\mu g \cdot mL^{-1}$. These results indicated that the presence of the Mn-chelation of the porphyrin unit slightly increase the cell viability of this type of cells.[69]

According to above-mentioned IC_{50} results, the concentration of 25 and 50 μg·mL^{-1} of all compounds of interest was chosen for the ROS generation assay in both types of cells.

4.2.2 Reactive oxygen species (ROS) generation

The antioxidant activity of each compound was determined by the ROS generation assay,[70] using 2',7'-dichlorofluoreceine-diacetate (H_2DCF-DA). In this study, DMEM, lipoic acid, **TMNPyP**, **P-Lp** and **Mn-P-Lp** at concentration of 25 and 50 μg·mL^{-1} were added into cells for pre-treatment with the HaCaT and HDFa cells. Then, these cells were treated with H_2DCFDA in the dark and then with H_2O_2. Fluorescence was measured using a microplate reader at 485 nm and 528 nm. The %ROS generation was calculated by comparison to that of the control group after treated with H_2O_2.

4.2.2.1 ROS generation in the HaCaT cells

The %ROS generation observed for the HaCaT cells treated with lipoic acid at the concentration of 25 and 50 μg·mL^{-1}, and then with H_2O_2 for 10–60 min is shown in **Figure 4–3**.

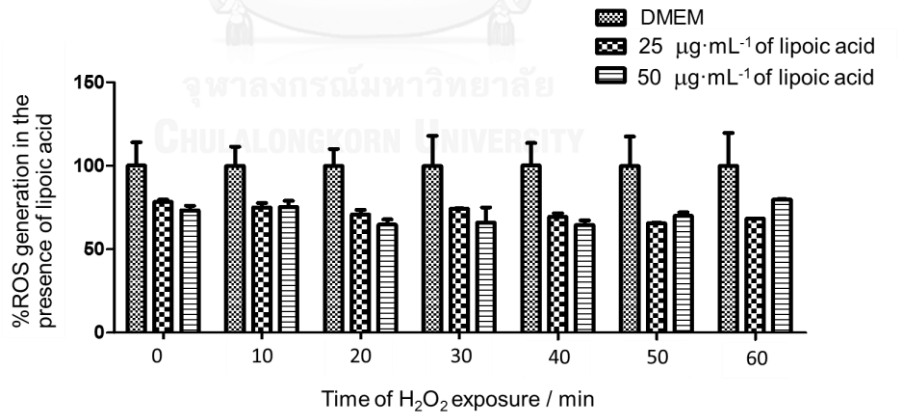

Figure 4–3: The ROS generation observed in the HaCaT cells upon the treatment with DMEM and lipoic acid at the concentration of 25 and 50 μg·mL^{-1} for 24 h, followed by the treatment with H_2O_2 for 0, 10, 20, 30, 40, 50 and 60 min.

For the case where the HaCaT cells were treated only with lipoic acid at concentration of 25 μg·mL^{-1} (at 0 min of the H_2O_2 exposure), decrease in the ROS

generation, compared with the control experiment, was observed. When the cells were treated with H_2O_2 for 10–60 min, the decrease in the ROS generation was not pronounced ($p > 0.05$). The same results were obtained when the concentration of 50 μg·mL^{-1}of lipoic acid was used. These results indicated that the ROS generation in the HaCaT cells was not dose-dependent, and lipoic acid seemed to exhibit antioxidative activity and dose-dependent has no effect in the ROS generation in the HaCaT cells.

The %ROS generation observed for the HaCaT cells treated with **TMNPyP** at the concentration of 25 and 50 μg·mL^{-1}, and then with H_2O_2 for 10–60 min is shown in **Figure 4–4**.

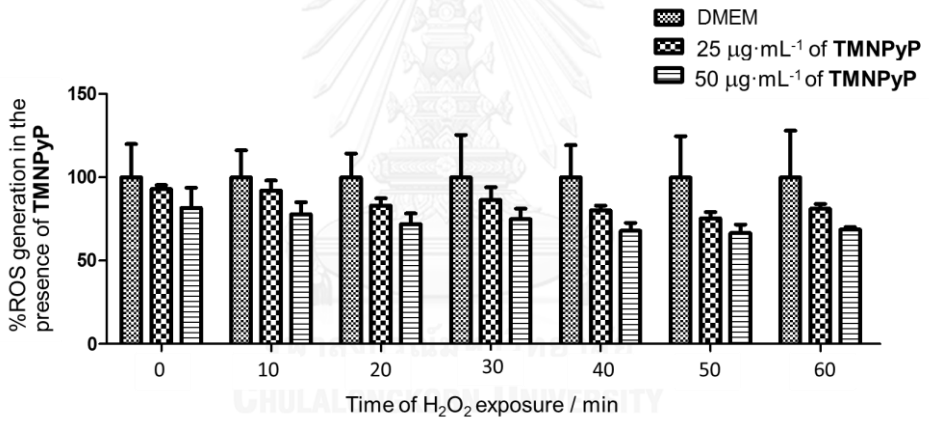

Figure 4–4: The ROS generation observed in the HaCaT cells upon the treatment with DMEM and **TMNPyP** at the concentration of 25 and 50 μg·mL^{-1} for 24 h, followed by the treatment with H_2O_2 for 0, 10, 20, 30, 40, 50 and 60 min.

For the case where the HaCaT cells were treated only with **TMNPyP** at concentration of 25 μg·mL^{-1} (at 0 min of the H_2O_2 exposure), decrease in the ROS generation, compared with the control experiment, was observed. When the cells were treated with H_2O_2 for 10–60 min, the decrease in ROS generation was not pronounced ($p > 0.05$). The same results were obtained when the concentration of 50 μg·mL^{-1} of **TMNPyP** was used. These results indicated that the ROS generation in

the HaCaT was not dose-dependent, and **TMNPyP** seemed to exhibit antioxidative activity without significant dose-dependency in the HaCaT cells.

The %ROS generation observed for the HaCaT cells treated with **P-Lp** at the concentration of 25 and 50 μg·mL^{-1}, and then with H_2O_2 for 10–60 min is shown in **Figure 4–5**.

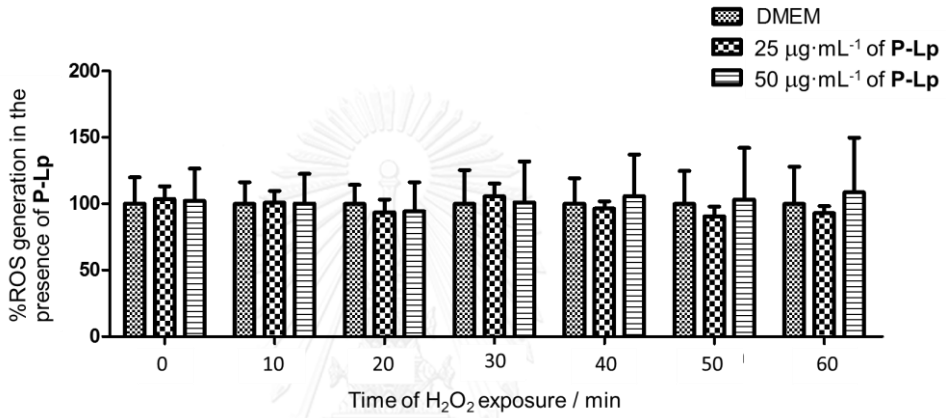

Figure 4–5: The ROS generation observed in the HaCaT cells upon the treatment with DMEM and **P-Lp** at the concentration of 25 and 50 μg·mL^{-1} for 24 h, followed by the treatment with H_2O_2 for 0, 10, 20, 30, 40, 50 and 60 min.

For the case where the HaCaT cells were treated only with **P-Lp** at concentration of 25 μg·mL^{-1} (at 0 min of the H_2O_2 exposure) as well as where the cells were treated with H_2O_2 for 10–60 min, no change in ROS generation, compared with the control experiment, was observed. The same results were obtained when the concentration of 50 μg·mL^{-1} of **P-Lp** was used. These results indicated that the ROS generation in the HaCaT was not affected by the presence of **P-Lp**, and no antioxidative activity of **P-Lp** exhibited in the HaCaT cells.

The %ROS generation observed for the HaCaT cells treated with **Mn-P-Lp** at the concentration of 25 and 50 μg·mL^{-1}, and then with H_2O_2 for 10–60 min is shown in **Figure 4–6**.

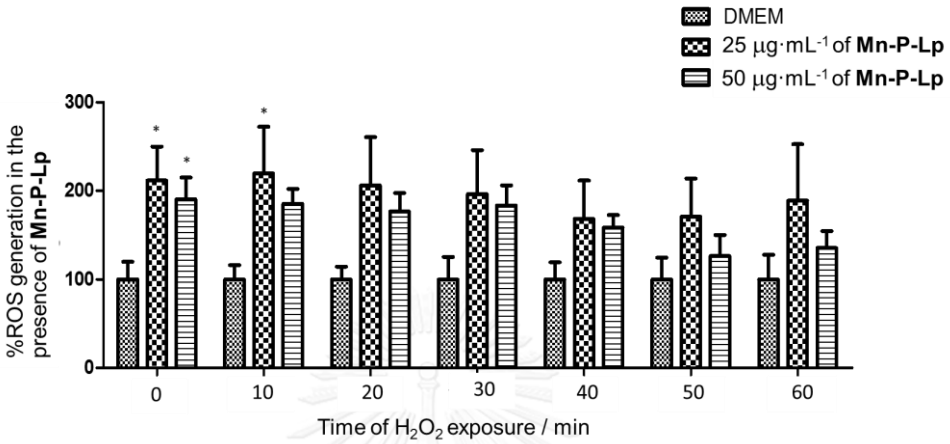

Figure 4–6: The ROS generation observed in the HaCaT cells upon the treatment with DMEM and **Mn-P-Lp** at the concentration of 25 and 50 μg·mL^{-1} for 24 h, followed by the treatment with H_2O_2 for 0, 10, 20, 30, 40, 50 and 60 min.

In the absence of H_2O_2 with the concentration of **Mn-P-Lp** of 25 μg·mL^{-1}, the significant increase in the ROS generation, compared with the control batch was observed. After the cells were treated with H_2O_2 for 10 and 20 min, The ROS generation was gradually decreased after 30 min. However, at 60 min of the H_2O_2 exposure, the %ROS generation observed in the cells was significantly decreased, but, however, to the level which is still higher than that observed for the control batch. These results indicated that the presence of **Mn-P-Lp** may induce the ROS generation in the HaCaT cells, but seemed to be able to scavenge ROS from an external source like H_2O_2 addition.[71] Similar results were obtained when 50 μg·mL^{-1} of **Mn-P-Lp** was used, indicating that ROS generation in this cell type caused by **Mn-P-Lp** was not dose-dependent.

The effect of the introduction of the porphyrin unit on the ROS generation of the HaCaT cells can be determined by the comparison of the results of lipoic acid and

those of **P-Lp**. Compared with the case of lipoic acid, the treatment of the cells with the concentration of 25 μg·mL^{-1} of **P-Lp** caused no difference in the ROS generation at 0–20 min of H_2O_2 exposure, but at 30–60 min, higher level of the ROS generation was observed. However, at the concentration of 50 μg·mL^{-1}, the treatment of the cells with both lipoic acid and **P-Lp** did not significantly different from each other in the ROS generation. These results indicated that the presence of porphyrin unit slightly induce the ROS generation (**Figure 4–7**).

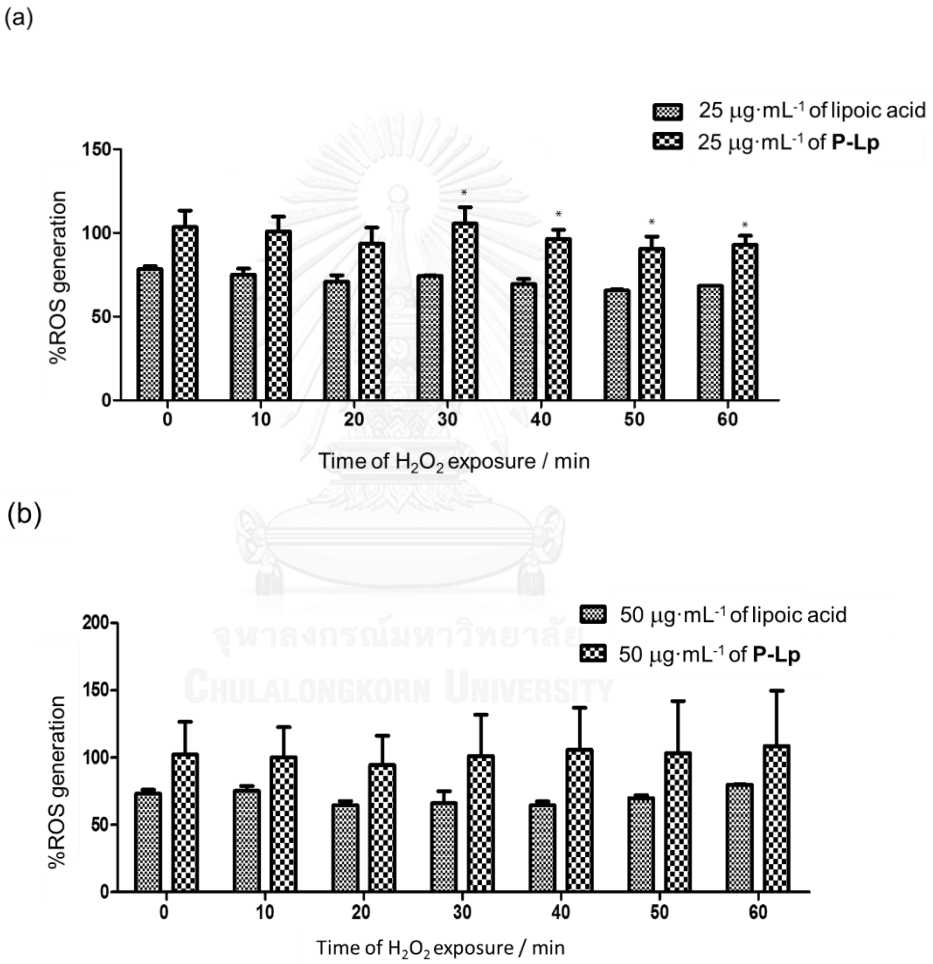

Figure 4–7: The ROS generation observed in the HaCaT cells upon the treatment with lipic acid and **P-Lp** at the concentration of (a) μg·mL^{-1} and (b) 50 μg·mL^{-1} for 24 h, followed by the treatment with H_2O_2 for 0, 10, 20, 30, 40, 50 and 60 min.

The effect of the introduction of lipoic acid on the ROS generation of the HaCaT cells can be determined by the comparison of the results of **TMNPyP** and **P-Lp**. Both before and after the exposure to H_2O_2, the treatment of the HaCaT cells with **TMNPyP** and **P-Lp** at the concentration of 25 and 50 μg·mL^{-1} caused no difference in the ROS generation. These results indicated that the attachment of a lipolyl unit on the porphyrin did not significantly affect the ROS generation in the HaCaT cells (**Figure 4–8**).

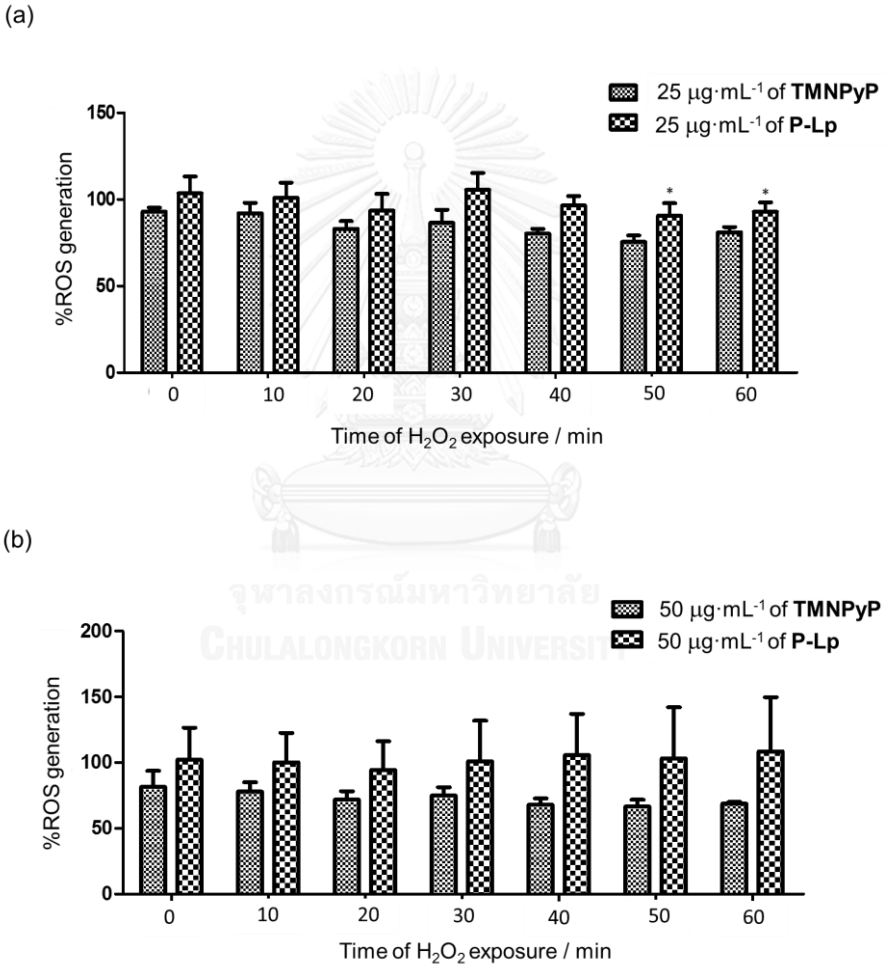

Figure 4–8: The ROS generation observed in the HaCaT cells upon the treatment with **TMNPyP** and **P-Lp** at the concentration of (a) 25 μg·mL^{-1} and (b) 50 μg·mL^{-1} for 24 h, followed by the treatment with H_2O_2 for 0, 10, 20, 30, 40, 50 and 60 min.

The effect of the introduction of the Mn-chelation of the porphyrin unit on the ROS generation of the HaCaT cells can be determined by the comparison of the results of **P-Lp** and those of **Mn-P-Lp**. After the exposure to H_2O_2 for 0–20 min, the treatment of the HaCaT cells with **Mn-P-Lp** at the concentration of 25 μg·mL^{-1} increased the ROS generation more than that with **P-Lp**, but at 30–60 min after the H_2O_2 exposure, the ROS generation level affected by the treatment of **Mn-P-Lp** was found to decrease to the level where no significant difference in the ROS generation was observed between these two cases. Similar results were obtained when 50 μg·mL^{-1} of **P-Lp** and **Mn-P-Lp** was used (**Figure 4–9**).

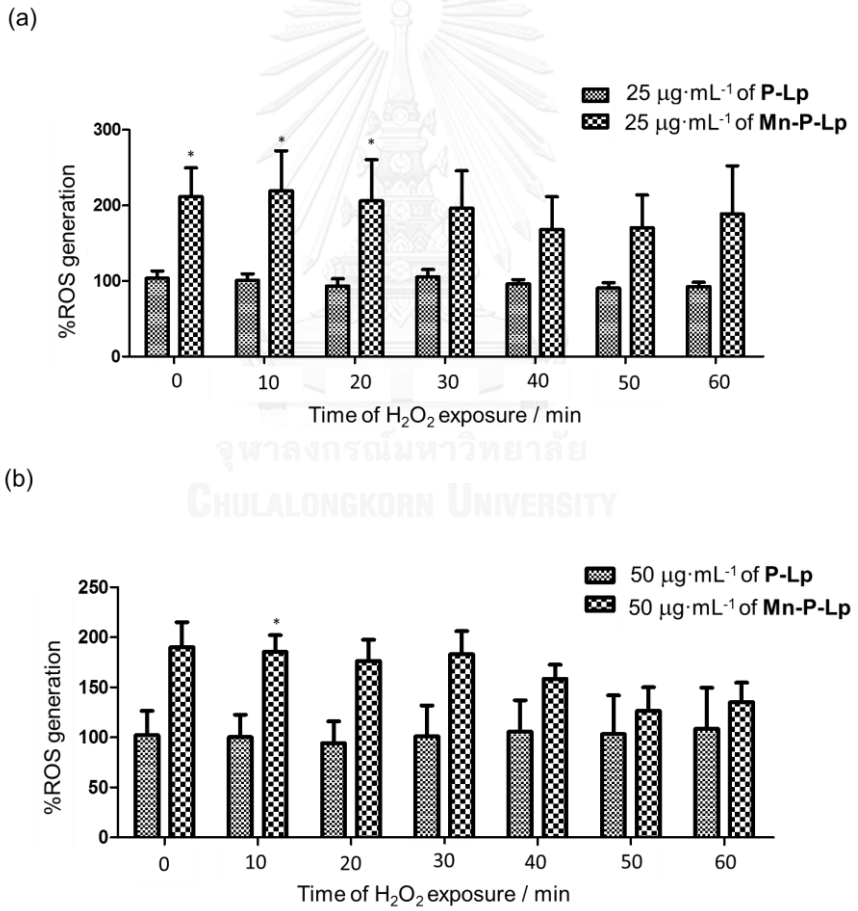

Figure 4–9: ROS generation observed in the HaCaT cells upon the treatment of **P-Lp** and **Mn-P-Lp** at the concentration of (a) 25 μg·mL^{-1} and (b) 50 μg·mL^{-1} for 24 h, followed by the treatment with H_2O_2 for 0, 10, 20, 30, 40, 50 and 60 min ("*" indicates $p < 0.05$).

Following a previous report,[72] where Mn(II)-porphyrin unit was conjugated with catalase to form a catalyst that could reduce superoxide anion radicals to H_2O_2 by the function of Mn^{2+} and could reduce H_2O_2 further to water under the catalysis of catalase. In the similar manner, the Mn(II)-porphyrin in **Mn-P-Lp** is expected to reduce the superoxide anion radicals and its lipoyl group is expected to convert the resulting H_2O_2 to water. Lipoic acid has an important role in inducing elevation of glutathione in the cell[73] that involves the conversion of H_2O_2 to water.[74] However, our results indicated that the Mn-chelation of the porphyrin unit caused the increase in the ROS generation in the HaCaT cells. This is likely to be because the rate of the H_2O_2 production from the reduction of the superoxide anion radicals by the Mn^{2+} in **Mn-P-LP** is higher than the conversion rate of the resulting H_2O_2 to water by dual function of lipoyl moiety in **Mn-P-Lp** and glutathione in the cells. Therefore, the accumulation of H_2O_2 in the HaCaT cells occurred, resulting in the increase of the ROS generation.

4.2.2.2 ROS generation in the HDFa cells

For the case where the HDFa cells were treated only with lipoic acid at concentration of 25 $\mu g \cdot mL^{-1}$ (at 0 min to 60 min of the H_2O_2 exposure), no change in the ROS generation, compared with the control experiment, was observed. When the concentration of 50 $\mu g \cdot mL^{-1}$ of lipoic acid was used, the %ROS generation seemed to decrease. There results indicated that lipoic acid seemed to exhibit antioxidative activity without significant dose-dependency in the HDFa cells (**Figure 4–10**).

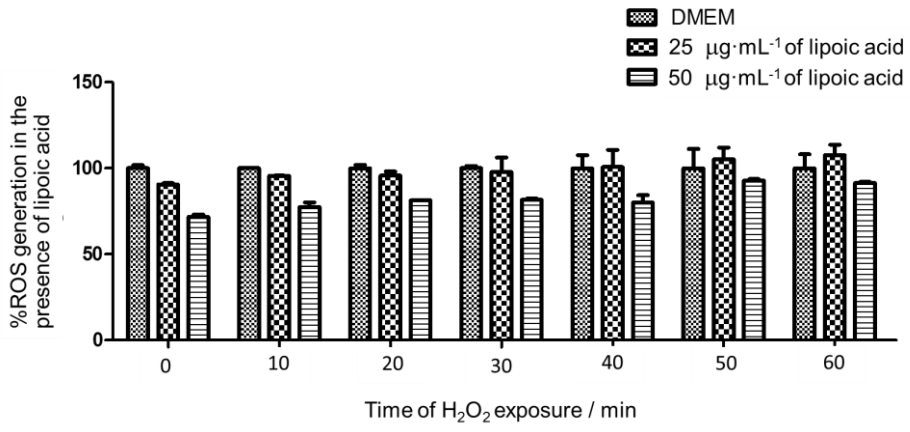

Figure 4–10: The ROS generation observed in the HDFa cells upon the treatment of DMEM and lipoic acid at the concentration of 25 and 50 μg·mL^{-1} for 24 h, followed by the treatment with H_2O_2 for 0, 10, 20, 30, 40, 50 and 60 min.

The %ROS generation observed for the HDFa cells treated with **TMNPyP** at the concentration of 25 and 50 μg·mL^{-1}, and then with H_2O_2 for 10–60 min is shown in **Figure 4–11**.

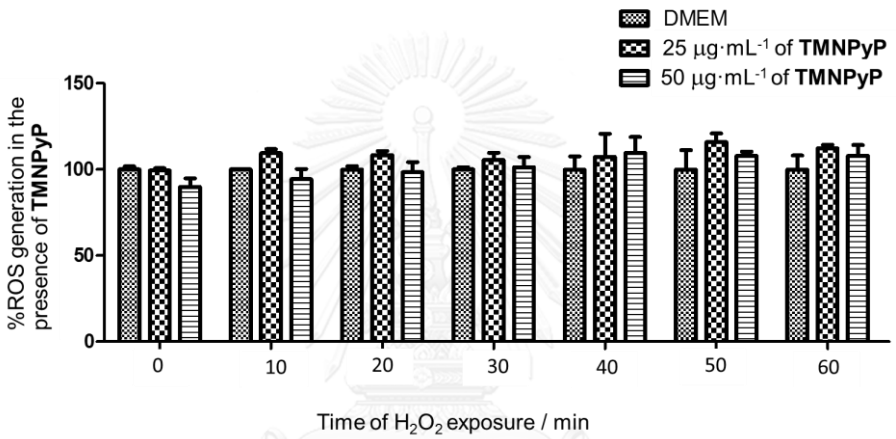

Figure 4–11: The ROS generation observed in the HDFa cells upon the treatment of DMEM and **TMNPyP** at the concentration of 25 and 50 μg·mL^{-1} for 24 h, followed by the treatment with H_2O_2 for 0, 10, 20, 30, 40, 50 and 60 min.

For the case where the HDFa cells were treated only with **TMNPyP** at concentration of 25 μg·mL^{-1} (at 0–60 min of the H_2O_2 exposure), no change in the ROS generation, compared with the control experiment, was observed. The same results were obtained when the concentration of 50 μg·mL^{-1} of **TMNPyP** was used. These results indicated that **TMNPyP** exhibited no antioxidative activity in the HDFa cells, and the ROS generation in the HDFa cells caused by **TMNPyP** was not dose-dependent.

The %ROS generation observed for the HDFa cells treated with **P-Lp** at the concentration of 25 and 50 μg·mL^{-1}, and then with H_2O_2 for 10–60 min is shown in **Figure 4–12**.

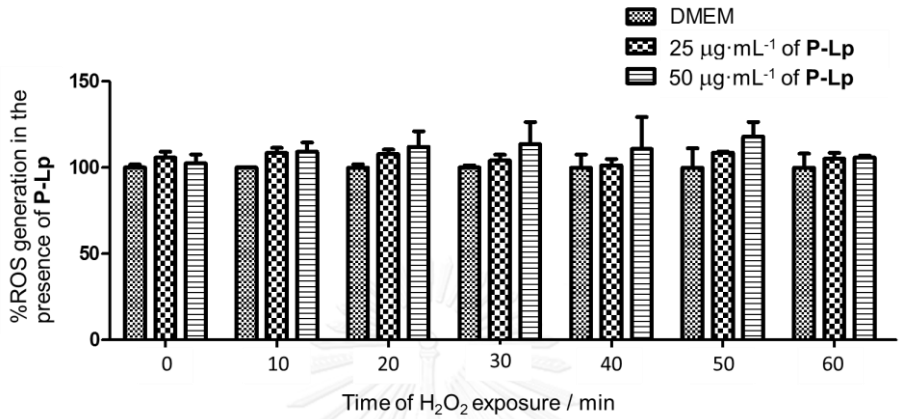

Figure 4–12: The ROS generation observed in the HDFa cells upon the treatment of DMEM and **P-Lp** at the concentration of 25 and 50 μg·mL^{-1} for 24 h, followed by the treatment with H_2O_2 for 0, 10, 20, 30, 40, 50 and 60 min.

For the case where the HDFa cells were treated only with **P-Lp** at concentration of 25 μg·mL^{-1} (at 0–60 min of the H_2O_2 exposure), no change in the ROS generation, compared with the control experiment, was observed. The same results were obtained when the concentration of 50 μg·mL^{-1} of **P-Lp** was used. These results indicated that **P-Lp** exhibited no antioxidative activity in the HDFa cells, and the ROS generation in the HDFa cells caused by **P-Lp** was not dose-dependent.

The %ROS generation observed for the HDFa cells treated with **Mn-P-Lp** at the concentration of 25 and 50 μg·mL^{-1}, and then with H_2O_2 for 10–60 min is shown in **Figure 4–13**.

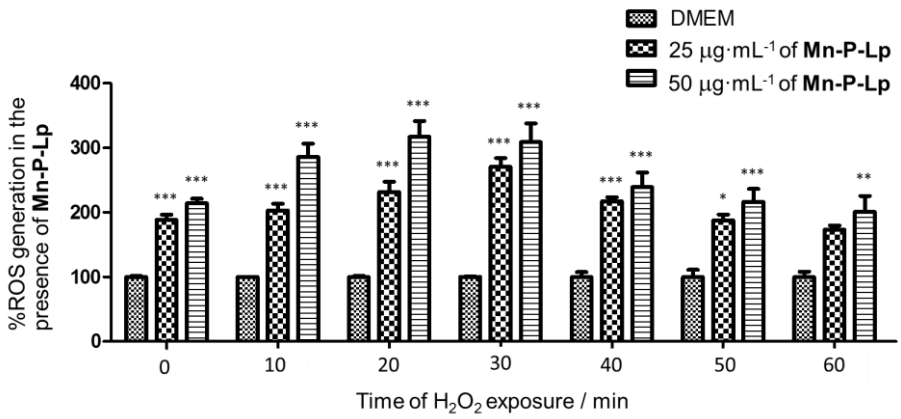

Figure 4–13: The ROS generation observed in the HDFa cells upon the treatment of DMEM and **Mn-P-Lp** at the concentration of 25 and 50 μg·mL^{-1} for 24 h, followed by the treatment with H_2O_2 for 0, 10, 20, 30, 40, 50 and 60 min ("***" indicates $p < 0.001$, "**" indicates $p < 0.01$ and "*" indicates $p < 0.05$).

In the absence of H_2O_2 with the concentration of **Mn-P-Lp** of 25 μg·mL^{-1}, the significant increase in the ROS generation, compared with the control batch, was observed. After the cells were treated with H_2O_2 for 10–30 min, the ROS generation obviously decreased at 40–60 min of the H_2O_2 exposure. However, at 60 min of the H_2O_2 exposure, the %ROS generation observed in the cells was significantly decreased, but, however, to the level which is still higher than that observed for the control batch. These results indicated that the presence of **Mn-P-Lp** may induce the ROS generation in the HDFa cells, but seemed to be able to scavenge ROS from the external source like H_2O_2 addition.[71] Similar results were obtained when 50 μg·mL^{-1} of **Mn-P-Lp** was used, indicating that ROS generation in this cell type caused by **Mn-P-Lp** was not dose-dependent.

The effect of the introduction of the porphyrin unit on the ROS generation of the HDFa cells can be determined by the comparison of the results of lipoic acid and those of **P-Lp**. Compared with the case of lipoic acid, the treatment of the cells with the concentration of 25 μg·mL^{-1} of **P-Lp** caused increase in the ROS generation at 0–10 min of H_2O_2 exposure, but at 20–60 min, no difference of the ROS generation was

observed. However, at the concentration of 50 μg·mL^{-1}, the treatment of the cells with both lipoic acid and **P-Lp** did not significantly different from each other in the ROS generation. These results indicated that the presence of porphyrin unit slightly induce the ROS generation (**Figure 4–14**).

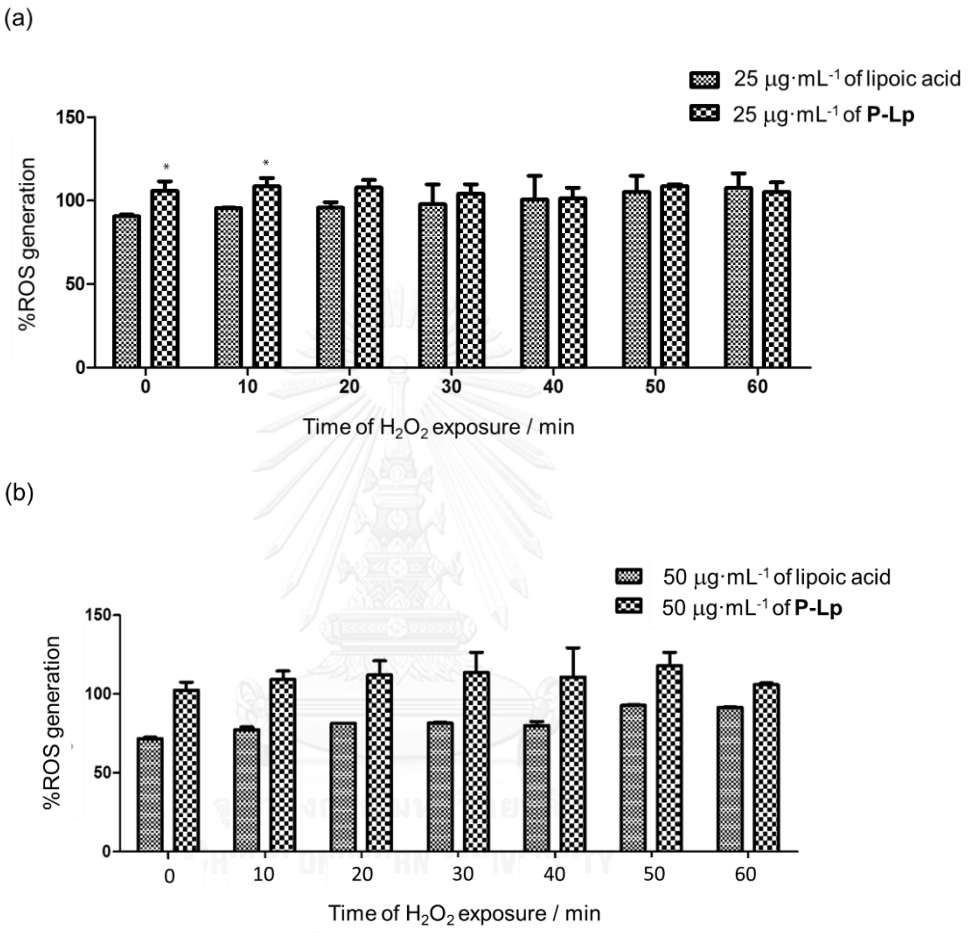

Figure 4–14: The ROS generation observed in the HDFa cells upon the treatment of lipoic acid and **P-Lp** at the concentration of (a) 25 μg·mL^{-1} and (b) 50 μg·mL^{-1} for 24 h, followed by the treatment with H_2O_2 for 0, 10, 20, 30, 40, 50 and 60 min ("*" indicates $p < 0.05$).

The effect of the introduction of lipoic acid on the ROS generation of the HaCaT cells can be determined by the comparison of the results of **TMNPyP** and **P-Lp**. Both before and after the exposure to H_2O_2, the treatment of the HDFa cells with **TMNPyP** and **P-Lp** at the concentration of 25 and 50 μg·mL^{-1} caused no difference in the ROS

generation. These results indicated that the attachment lipoyl unit on the porphyrin did not a significantly affect the ROS generation in the HDFa cells (**Figure 4–15**).

(a)

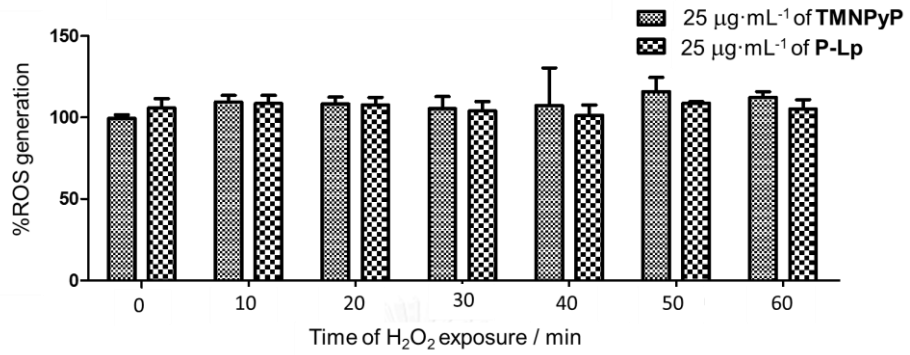

(b)

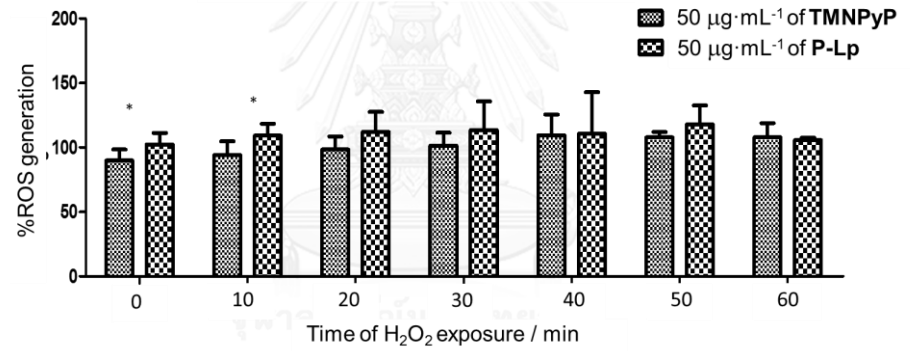

Figure 4–15: The ROS generation observed in the HDFa cells upon the treatment of **TMNPyP** and **P-Lp** at the concentration of (a) 25 μg·mL^{-1} and (b) 50 μg·mL^{-1} for 24 h, followed by the treatment with H_2O_2 for 0, 10, 20, 30, 40, 50 and 60 min.

The effect of the introduction of the Mn-chelation of the porphyrin unit on the ROS generation of the HDFa cells can be determined by the comparison of the results of **P-Lp** and those of **Mn-P-Lp**. After the exposure to H_2O_2 for 0–30 min, the treatment of the HDFa cells with **Mn-P-Lp** at the concentration of 25 μg·mL^{-1} increase the ROS generation more than that with **P-Lp**, but at 40–60 min after the H_2O_2 exposure, the ROS generation level affected by the treatment of **Mn-P-Lp** was found to decrease to the level where has significant difference in the ROS generation was observed between

these two cases. Similar results were obtained when 50 μg·mL^{-1} of **P-Lp** and **Mn-P-Lp** was used (**Figure 4–16**).

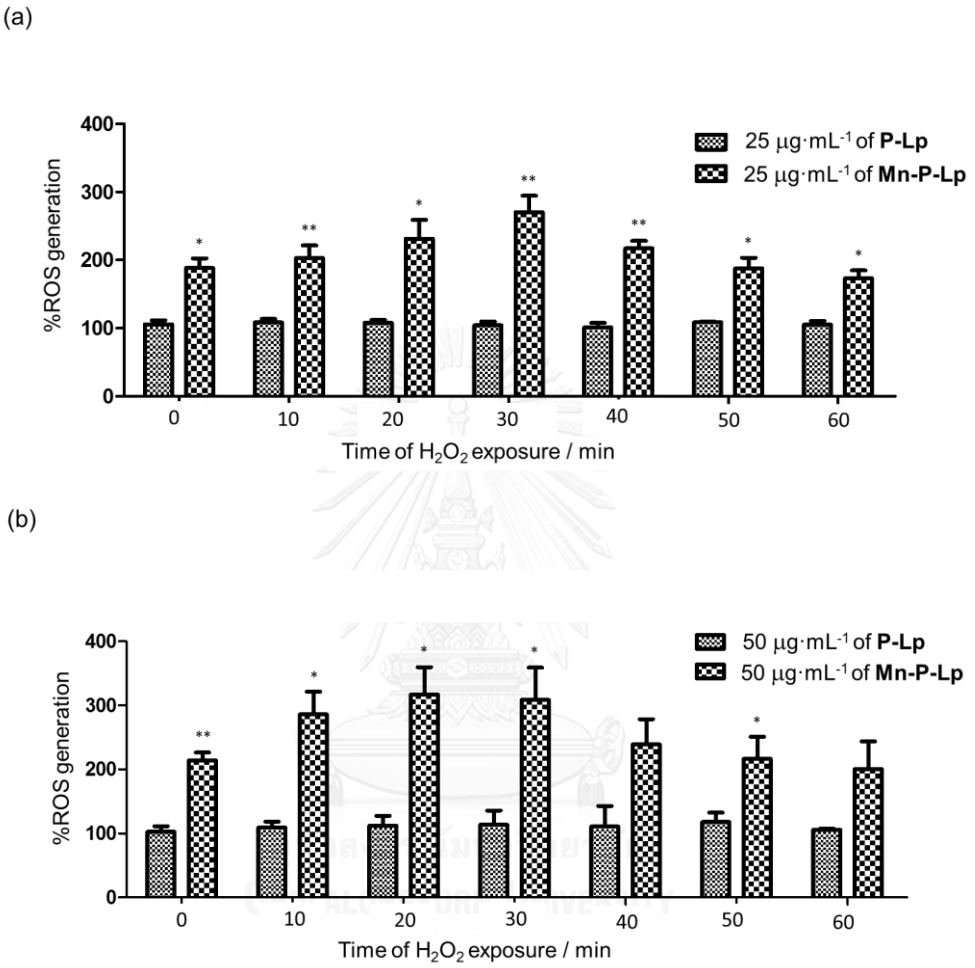

Figure 4–16: The ROS generation observed in the HDFa cells upon the treatment of **P-Lp** and **Mn-P-Lp** at the concentration of (a) 25 μg·mL^{-1} and (b) 50 μg·mL^{-1} for 24 h, followed by the treatment with H_2O_2 for 0, 10, 20, 30, 40, 50 and 60 min ("**" indicates $p < 0.01$ and "*" indicates $p < 0.05$).

These results indicated that the Mn-chelation of the porphyrin unit caused the increase in the ROS generation in the HaCaT cells, in the similar manner as mentioned for the HaCaT cells in Section 4.2.2.1.

4.2.3 Mitochondria-targeting evaluation

In this studies, the mitochondria targeting activity was determined by cell imaging using a LSM 800 confocal microscope. The HaCaT cells were chosen because this type of cells is human skin cells which has rapid cell division. Nuclei of the HaCaT cells were stained with Hoechst 33342 dye to indicate position of cells as seen in the blue region in **Figure 4–17**. After JC-1 was loaded into cells and allowed to diffuse into mitochondria. Normally, permeability of various compounds into the mitochondria affects to mitochondrial membrane potential ($\Delta\psi$M). At high $\Delta\psi$m, JC-1 spontaneously forms the *J*-aggregates with intense red fluorescence and at low $\Delta\psi$m, JC-1 remains in the monomeric form, which shows only green fluorescence.

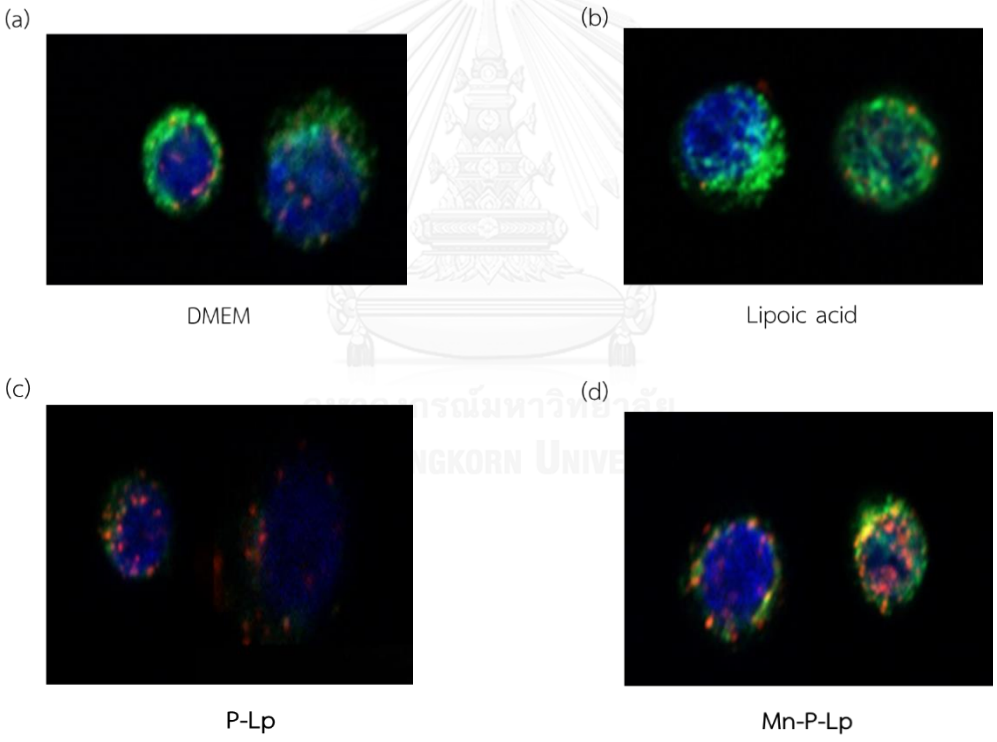

Figure 4–17: Images of the HaCaT cells treated by (A) DMEM, (B) lipoic acid, (C) **P-Lp**, (d) **Mn-P-Lp**.

The result demonstrated that the treated cells with only DMEM (control) mainly exhibited green fluorescence with red fluorescence at some parts, indicating

that DMEM was slightly accumulated in mitochondria **(Figure 4–17(a))**. For the cells treated with lipoic acid, the majority of the area exhibited green fluorescence, also indicating that lipoic acid was slightly accumulated in mitochondria (**Figure 4–17(b)**). In **Figure 4–17(c)**, it can be clearly seen that the cells treated with **P-Lp** showed more red fluorescence, compared with those treated with lipoic acid. This result indicated that **P-Lp** can be more accumulated in the mitochondria than lipoic acid, which is likely to be because of the presence of the porphyrin unit in **P-Lp**. This is attributed to an effect of positive charges on the porphyrin ring which can attach to negative charges of mitochondrial inner membrane which is consistent with the previous report[75]. **Figure 4–17(d)** shows that the cells treated with **Mn-P-Lp** mainly exhibited red fluorescence in similar extent to that observed in the cells treated with **P-Lp**. This result indicated that **Mn-P-Lp** can be accumulated in the mitochondria in the comparable level with **P-Lp** and, therefore, the Mn-chelation of the porphyrin unit did not significantly affect the mitochondria-targeting ability of **P-Lp**.

CHAPTER V
CONCLUSION

An asymmetric water-soluble porphyrin having pyridinium and lipoic acid-bared *meso*-substituents was successfully synthesized from amidation reaction between porphyrin unit and lipoic anhydride, followed by Mn-metallation with $MnCl_2{\cdot}4H_2O$. The resulting compounds were characterized by ^{1}H-NMR and ^{13}C-NMR spectroscopy, mass spectrometry, and UV-visible and fluorescence spectrophotometry. All compounds exhibited characteristic absorption peaks at around 418 to 469 nm, and emission ones at around 652 to 673 nm upon the excitation at their maximum absorption. In biological studies of the compounds of interest (lipoic acid, **TMNPyP**, **P-Lp** and **Mn-P-Lp**), the effects on the introduction of the porphyrin unit, and the presence of lipoic acid and Mn-chelation on the porphyrin unit on cell viability and antioxidant activity in HaCaT and HDFa cells were determined by cytotoxicity assay and the ROS generation assay, respectively. The results showed that the introduction of the porphyrin unit caused decrease in the IC_{50} value from > 150 $\mu g{\cdot}mL^{-1}$ when the cells was treated with lipoic acid to 25–100 $\mu g{\cdot}mL^{-1}$ when they were treated with **P-Lp**, while did not affect antioxidative activity in the both kinds of cells. The presence of lipoic acid and the Mn-chelation on the porphyrin unit resulted in increase in the cell viability, but no significant change in the antioxidative activity in those cells were observed. In mitochondria-targeting evaluation, the target porphyrin derivative exhibited accumulation specifically in the mitochondria. The results suggested that the specificity to mitochondria is attributed to the introduction of the pyridinium-containing porphyrin unit.

REFERENCES

1. Fulda, S.; Galluzzi, L.; Kroemer, G., "Targeting Mitochondria for Cancer Therapy" *Nat. Rev. Drug Discov.* **2010**, *9(6)*, 447–464.
2. Park, C. B.; Larsson, N. G., "Mitochondrial DNA Mutations in Disease and Aging" *J. Cell. Biol.* **2011**, *193(5)*, 809–8018.
3. (a) Harman, D. M. D. P. D., "Aging: A theory based on Free Radical and Radiation Chemistry" *J. Gerontol.* **1956**, 298–300; (b) Salviolia, S.; Bonafe, M.; Capria, M.; Montib, D.; Franceschia, C., "Mitochondria, Aging and Longevity-A New Perspective" *FEBS. Lett.* **2001**, *492*, 9–13.
4. Jang, Y. C.; Van Remmen, H., "The Mitochondrial Theory of Aging: Insight from Transgenic and Knockout Mouse Models" *Exp. Gerontol.* **2009**, *44(4)*, 256–260.
5. Lin, M. T.; Flint Beal, M., "The Oxidative Damage Theory of Aging" *Clin. Neurosci. Res.* **2003**, *2(5–6)*, 305–315.
6. Asuncion, J. G. D. L.; Millan, A.; Pla, R.; Bruseghini, L.; Esteras, A.; Pallardo, F. V.; Sastre, J.; Vina, J., "Mitochondrial Glutathione Oxidation Correlates with Age-associated Oxidative Damage to motochondrial DNA" *Res. Commun.* **1996**, *10*, 333–338.
7. Manaligod, M. J.; Milam, M.; Hill, S. A.; Sanders, T.; Skaggs, J.; Smith, R., "Age-related Mitochondrial DNA Mutations in the Human Larynx" *Laryngoscope* **2000**, *110*, 2123–2127.
8. Chandra, R.; Tiwari, M.; Kaur, P.; Sharma, M.; Jain, R.; Dass, S., "Metalloporphyrins-applications and Clinical Significance" *Indian J. Clin. Biochem.* **2000**, *15*, 183–199.
9. Huang, H.; Song, W.; Rieffel, J.; Lovell, J. F., "Emerging Aplications of Porphyrins in Photomedicine" *Front. Phys.* **2015**, *3*, 1–15.
10. Graca, D. M.; Vicente, H., "Porphyrins and the Photodynamic Therapy of Cancer" *Rev. Port. Quím.* **1996**, *3*, 47–57.

11. Sibrian-Vazquez, M.; Nesterova, V. I.; Jensen, J. T.; Graça, H. V., "Mitochondria Targeting by Guanidine- and Biguanidine-porphyrin Photosensitizers" *Bioconjug. Chem.* **2008**, *19*, 705–713.

12. Castano, A. P.; Demidova, T. N.; Hamblin, M. R., "Mechanisms in Photodynamic Therapy: Part One-photosensitizers, Photochemistry and Cellular Localization" *Photodiagnosis. hotodyn. Ther.* **2004**, *1(4)*, 279–293.

13. Lei, W.; Xie, J.; Hou, Y.; Jiang, G.; Zhang, H.; Wang, P.; Wang, X.; Zhang, B., "Mitochondria-targeting Properties and Photodynamic Activities of Porphyrin Derivatives Bearing Cationic Pendant" *J. Photochem. Photobiol. B* **2010**, *98(2)*, 167–171.

14. (a) Ibrahim, S. F.; Osman, K.; Das, S.; Othman, A. M.; Majid, N. A.; Rahman, M. P. A., "A Study of the Antioxidant Effect of Alpha Lipoic Acids on Sperm Quality" *Clinics* **2008**, *63(4)*, 545–550; (b) Packer, L.; Witt, H. E.; Tritschler, J. H., "Alpha-lipoic Acid as a Biological Antioxidant" *Free Radic. Bio. Med.* **1995**, *19(2)*, 227–250.

15. Golbidi, S.; Badran, M.; Laher, I., "Diabetes and Alpha Lipoic Acid" *Front. Pharmacol.* **2011**, *2*, 1–15.

16. McManus, M. J.; Murphy, M. P.; Franklin, J. L., "The Mitochondria-targeted Antioxidant MitoQ Prevents Loss of Spatial Memory Retention and Early Neuropathology in a Transgenic Mouse Model of Alzheimer's Disease" *J. Neurosci.* **2011**, *31(44)*, 15703–15715.

17. Figueiraa, F.; Pereiraa, M. R. P.; Silvaa, S.; Cavaleiroa, A. S. J.; Toméa, P. C. J., "Porphyrins and Phthalocyanines Decorated with Dendrimers: Synthesis and Biomedical Applications" *Curr. Org. Synth.* **2011**, *11*, 110–126.

18. Altmann, R., "Die Elementarorganismen Und Ihre Beziehungen Zu Den Zellen. Leipzig" *Veit & comp.* **1890**, *145*.

19. Ragoonanan, N. "Chemiosmotic Hypothesis" https://biochemist01.wordpress.com/tag/atp/ (retrieved 14 Sep 2016).

20. (a) Alberts, B.; Johnson, A.; Lewis, J. "The Transport of Proteins into Mitochondria and Chloroplasts" https://www.ncbi.nlm.nih.gov/books/NBK26828/ (retrieved 24 Sep 2016); (b) Zeth, K., "Structure and Evolution of Mitochondrial Outer

Membrane Proteins of Beta-barrel Topology" *Biochim. Biophys. Acta* **2010**, *1797(6–7)*, 1292–1299.

21. Harding, C. R.; Meissner, M., "The Inner Membrane Complex through Development of Toxoplasma Gondii and Plasmodium" *Cell. Microbiol.* **2014**, *16(5)*, 632–641.
22. Khan, S. M.; Smigrodzki, R. M.; Swerdlow, R. H., "Cell and Animal Models of mtDNA Biology: Progress and Prospects" *Am. J. Physiol. Cell Physiol.* **2007**, *292(2)*, 658–669.
23. Gilkerson, R.; Bravo, L.; Garcia, I.; Gaytan, N.; Herrera, A.; Maldonado, A.; Quintanilla, B., "The Mitochondrial Nucleoid: Integrating Mitochondrial DNA into Cellular Homeostasis" *Cold Spring Harb. Perspect. Biol.* **2013**, *5(5)*, 11080.
24. Perry, S. W.; Norman, J. P.; Barbieri, J.; Brown, E. B.; Gelbard, H. A., "Mitochondrial Membrane Potential Probes and the Proton Gradient: A Practical Usage Guide" *Biotechniques* **2011**, *50(2)*, 98–115.
25. Perelman, A.; Wachtel, C.; Cohen, M.; Haupt, S.; Shapiro, H.; Tzur, A., "JC-1: Alternative Excitation Wavelengths Facilitate Mitochondrial Membrane Potential Cytometry" *Cell Death. Dis.* **2012**, *3*, e430.
26. Lemasters, J. J.; Ramshesh, V. K., "Imaging of Mitochondrial Polarization and Depolarization with Cationic Fluorophores" *Methods cell Biol.* **2007**, *80*, 283–295.
27. Boncler, M.; Rozalski, M.; Krajewska, U.; Podsedek, A.; Watala, C., "Comparison of PrestoBlue and MTT Assays of Cellular Viability in the Assessment of Anti-proliferative Effects of Plant Extracts on Human Endothelial Cells" *J. Pharmacol. Toxicol. Methods* **2014**, *69(1)*, 9–16.
28. Rahman, K., "Studies on Free Radicals, Antioxidants, and Co-factors" *Clin. Interv. Aging* **2007**, *2(2)*, 219–236.
29. Pham-Huy, A. L.; He, H.; Pham-Huy, C., "Free Radicals, Antioxidants in Disease and Health" *Int. J. Biomed. sci.* **2008**, *4(2)*, 89–96.
30. Flora, J. S. S., "Structural, Chemical and Biological Aspects of Antioxidants for Strategies Against Metal and Metalloid Exposure. *Oxid. Med. Cell. Longev.* **2009**, *2(4)*, 191–206.

31. Lobo, V.; Patil, A.; Phatak, A.; Chandra, N., "Free Radicals, Antioxidants and Functional Foods: Impact on Human Health" *Pharmacogn. Rev.* **2010**, *4(8)*, 118–126.

32. "Reactive Oxygen Species (ROS) Detection Reagents" https://tools.thermofisher.com/content/sfs/manuals/mp36103.pdf (retrieved 10 Nov 2016).

33. Wojtala, A.; Bonora, M.; Malinska, D.; Pinton, P.; Duszynski, J.; Wieckowski, M. R., "Methods to Monitor ROS Production by Fluorescence Microscopy and Fluorometry" *Methods Enzymol.* **2014**, *542*, 243–262.

34. Moon, H. S., "Chemopreventive Effects of Alpha Lipoic Acid on Obesity-related Cancers" *Ann. Nutr. Metab.* **2016**, *68*, 137–144.

35. Castaneda-Arriaga, R.; Alvarez-Idaboy, J. R., "Lipoic Acid and Dihydrolipoic Acid. A Comprehensive Theoretical Study of their Antioxidant Activity Supported by Available Experimental Kinetic Data" *J. Chem. Inf. Model.* **2014**, *54(6)*, 1642–1652.

36. Harnett, J. J.; Auguet, M.; Viossat, I.; Dolo, C.; Bigga, D.; Chabrierb, P., "Novel Lipoic Acid Analogues that Inhibit Nitric Oxide Synthase" *Bioorg. Med. Chem. Lett.* **2002**, *12*, 1439–1442.

37. Liu, J., "The Effects and Mechanisms of Mitochondrial Nutrient Alpha-lipoic Acid on Improving Age-associated Mitochondrial and Cognitive Dysfunction: An Overview" *Neurochem. Res*. **2008**, *33(1)*, 194–203.

38. Swaran, J. S. F., "Structural, Chemical and Biological Aspects of Antioxidants for Strategies Against Metal and Metalloid Exposure" *Oxid. Med. Cell. Longev.* **2009**, *2(4)*, 191-206.

39. Chen, P.; Ma, Q. G.; Ji, C.; Zhang, J. Y.; Zhao, L. H.; Zhang, Y.; Jie, Y. Z., "Dietary Lipoic Acid Influences Antioxidant Capability and Oxidative Status of Broilers" *Int. J. Mol. Sci.* **2011**, *12(12)*, 8476–8488.

40. Shay, K. P.; Moreau, R. F.; Smith, E. J.; Smith, A. R.; Hagen, T. M., "Alpha-lipoic Acid as A Dietary Supplement: Molecular Mechanisms and Therapeutic Potential" *Biochim. Biophys. Acta* **2009**, *1790(10)*, 1149–1160.

41. Scherer, J., "Untersuchungen Liebigs" *Ann. Chem. Pharm.* **1841**, *40*, 1–64.

42. Moore, R. M., "The Biochemistry of Heme Synthesis in Porphyria and in the Porphyrinurias" *Clin. Dermatol.* **1998**, *16*, 203–223.

43. Moss, P. G., "Nomenclature of Tetrapyrroles" *Eur. J. Biochem.* **1988**, *178*, 277–328.

44. Makino, M.; Aihara, J., "Macrocyclic Aromaticity of Porphyrin Units in Fully Conjugated Oligoporphyrins" *J. Phys. Chem. A* **2012**, *116(30)*, 8074–8084.

45. Huang, X.; Nakanishi, K.; Berova, N., "Porphyrins and Metalloporphyrins: Versatile Circular Dichroic Reporter Groups for Structural Studies" *Chirality* **2000**, *12*, 237–255

46. Taies, J. A., "Spectrophotometric Determination of Trace Amounts of Uranium with 5,10,15,20–Tetra(4-sulfophenyl)porphyrin (TPPS4)" *IJST.* **2012**, *2(12)*.

47. Adler, A. D.; Longo, F. R.; Finarelli, J. D.; Goldmacher, J.; Assour, J.; Korsakoff, L., "A Simplified Synthesis for *Meso*-tetraphenylporphin" *J. Org. Chem.* **1967**, *32*, 476.

48. Lindsey, J. S.; Schreiman, I. C.; Hsu, H. C.; Keamey, P. C.; Marguerettaz, A. M. R.; Adler-Longo., "Synthesis of Tetraphenylporphyrins under Equilibrium Conditions" *J. Org. Chem.* 1**987**, *52*, 827–836.

49. Casas, C.; Saint-Jalmes, B.; Loup, C.; Lacey, C. J.; Meunier, B., "Synthesis of Cationic Metalloporphyrin Precursors Related to the Design of DNA Cleavers" *J. Org. Chem.* **1993**, *58(10)*, 2913–2917.

50. Banfi, S.; Caruso, E.; Buccafurni, L.; Murano, R.; Monti, E.; Gariboldi, M.; Papa, E.; Gramatica, P., "Comparison between 5,10,15,20-Tetraaryl- and 5,15-Diarylporphyrins as Photosensitizers : Synthesis, Photodynamic Activity, and Quantitative Structure-activity Relationship Modeling" *J. Med. Chem.* **2006**, *49*, 3293–3304.

51. Gelo-Pujic, M.; Desmurs, J. R.; Delaire, S.; Adao, A.; Tawil, D., "Synthesis of New Antioxidant Conjugates and their *in vitro* Hydrolysis with Stratum Corneum Enzymes" *Int. J. Cosmet. Sci.* **2008**, *30*, 195–204.

52. Ngen, E. J.; Rajaputra, P.; You, Y., "Evaluation of Delocalized Lipophilic Cationic Dyes as Delivery Vehicles for Photosensitizers to Mitochondria" *Bioorg. Med. Chem.* **2009**, *17(18)*, 6631–6340.

53. Lu, C.; Kim, B. M.; Chai, K. Y., "Design, Synthesis and Evaluation of PEGylated Lipoic Acid Derivatives with Functionality as Potent Anti-melanogenic Agents" *Eur. J. Med. Chem.* **2011**, *46(10)*, 5184–5188.

54. Bernini, R.; Crisante, F.; Merendino, N.; Molinari, R.; Soldatelli, M. C.; Velotti, F., "Synthesis of a Novel Ester of Hydroxytyrosol and Alpha-lipoic Acid Exhibiting an Antiproliferative Effect on Human Colon Cancer HT-29 Cells" *Eur. J. Med. Chem.* **2011**, *46(1)*, 439–446.

55. Biron, E.; Voyer, N., "Towards Sequence Selective DNA Binding: Design, Synthesis and DNA Binding Studies of Novel *Bis*-porphyrin Peptidic Nanostructures" *Org. Biomol. Chem.* **2008**, *6(14)*, 2507–2515.

56. Raffy, Q.; Ricoux, R.; Mahy, J.-P., "Synthesis of a New Estradiol–iron Metalloporphyrin Conjugate Used to Build Up a New Hybrid Biocatalyst for Selective Oxidations by the 'Trojan horse' Strategy" *Tetrahedron Lett.* **2008**, *49(11)*, 1865–1869.

57. Gomes, M. C.; Woranovicz-Barreira, S. M.; Faustino, M. A.; Fernandes, R.; Neves, M. G.; Tome, A. C.; Gomes, N. C.; Almeida, A.; Cavaleiro, J. A.; Cunha, A.; Tome, J. P., "Photodynamic Inactivation of Penicillium Chrysogenum Conidia by Cationic Porphyrins" *Photochem. Photobiol. Sci.* **2011**, *10(11)*, 1735–1743.

58. Liu, F.; Wang, M.; Wang, Z.; Zhang, X., "Polymerized Surface Micelles Formed under Mild Conditions" *Chem. Commun.* **2006**, *(15)*, 1610–1612.

59. Mbakidi, J. P.; Herke, K.; Alves, S.; Chaleix, V.; Granet, R.; Krausz, P.; Leroy-Lhez, S.; Ouk, T. S.; Sol, V., "Synthesis and Photobiocidal Properties of Cationic Porphyrin-grafted Paper" *Carbohydr. Polym.* **2013**, *91(1)*, 333–338.

60. Kawakami, H.; Ohse, T.; Kawano, M.; Nagaoka, S., "Superoxide Dismutase Activity of a Novel Macromolecular Manganese Porphyrin" *Polymer. Adv. Tech.* **1999**, *10*, 270–274.

61. Makpol, S.; Jam, F. A.; Khor, S. C.; Ismail, Z.; Mohd Yusof, Y. A.; Ngah, W. Z., "Comparative Effects of Biodynes, Tocotrienol-rich Fraction, and Tocopherol in Enhancing Collagen Synthesis and Inhibiting Collagen Degradation in Stress-induced Premature Senescence Model of Human Diploid Fibroblasts" *Oxid. Med. Cell. Longev.* **2013**, *2013*, 298574.

62. Tita, S. P. S.; Perussi, J. R., "The Effect of Porphyrins on Normal and Transformed Mouse Cell Lines in the Presence of Visible Light" *Braz. J. Med. Biol. Res.* **2001**, *34(10)*, 1331–1336.

63. Wu, D.; Yotnda, P., "Production and Eetection of Reactive Oxygen Species (ROS) in Cancers" *J. Vis. Exp.* **2011**, *(57)*.

64. Choi, I. Y.; Lee, S. J.; Ju, C.; Nam, W.; Hyoing-Chun, K.; Ko, K. H.; Won-Ki, K., "Protection by a Manganese Porphyrin of Endogenous Peroxynitrite-induced Death of Glial Cells *Via* Inhibition of Mitochondrial Transmembrane Potential Decrease" *GLIA.* **2000**, *31*, 155–164.

65. Chazotte, B., "Labeling Mitochondria with JC-1" *Cold Spring Harb. Protoc.* **2011**, *2011(9)*.

66. Asayama, S.; Mori, T.; Nagaoka, S.; Kawakami, H., "Chemical Modification of Manganese Porphyrins with Biomolecules for New Functional Antioxidants" *J. Biomater. Sci. Polym. Ed.* **2003**, *14(11)*, 1169–1179.

67. Montalbetti, C. A. G. N.; Falque, V., "Amide Bond Formation and Peptide Coupling" *Tetrahedron* **2005**, *61(46)*, 10827–10852.

68. "Cell Viability / Cytotoxicity" https://www.dojindo.com/ Protocol/ Cell_Proliferation_Protocol_Colorimetric.pdf (retrieved 6 Nov 2016).

69. Martinez-Finley, E. J.; Gavin, C. E.; Aschner, M.; Gunter, T. E., "Manganese Neurotoxicity and The Role of Reactive Oxygen Species" *Free Radic. Biol. Med.* **2013**, *62*, 65–75.

70. Ali, S.; Duhart, M. H.; Newport, D. G.; Lipe, W. G.; Slikker, W., "Manganese-induced Reactive Oxygen Species: Comparison Between Mn^{2+} and Mn^{3+}" *Neurodegeneration* **1995**, *4*, 329–334

71. Sharma, P.; Jha, A. B.; Dubey, R. S.; Pessarakli, M., "Reactive Oxygen Species, Oxidative Damage, and Antioxidative Defense Mechanism in Plants under Stressful Conditions" *J. Bot.* **2012**, *2012*, 1–26.

72. Asayama, S.; Mori, T.; Nagaoka, S.; Kawakami, H., "Chemical Modification of Manganese Porphyrins with Biomolecules for New Functional Antioxidants" *J. Biomater. Sci. Polym. Ed.* **2003**, *14(11)*, 1169–1179.

73. Moini, H.; Packer, L.; Saris, N.-E. L., "Antioxidant and Prooxidant Activities of α-Lipoic Acid and Dihydrolipoic Acid" *Toxicol. Appl. Pharmacol.* **2002**, *182(1)*, 84–90.

74. Castello, G.; Costantini, S.; Scala, S., "Targeting the Inflammation in HCV-associated Hepatocellular Carcinoma: A Role in the Prevention and Treatment" *J. Transl. Med.* **2010**, *8*, 109.

75. Batinic-Haberle, I.; Tovmasyan, A.; Spasojevic, I., "An Educational Overview of the Chemistry, Biochemistry and Therapeutic Aspects of Mn Porphyrins-From Superoxide Dismutation to H_2O_2-driven Pathways" *Redox. Biol.* **2015**, *5*, 43–65.

APPENDIX

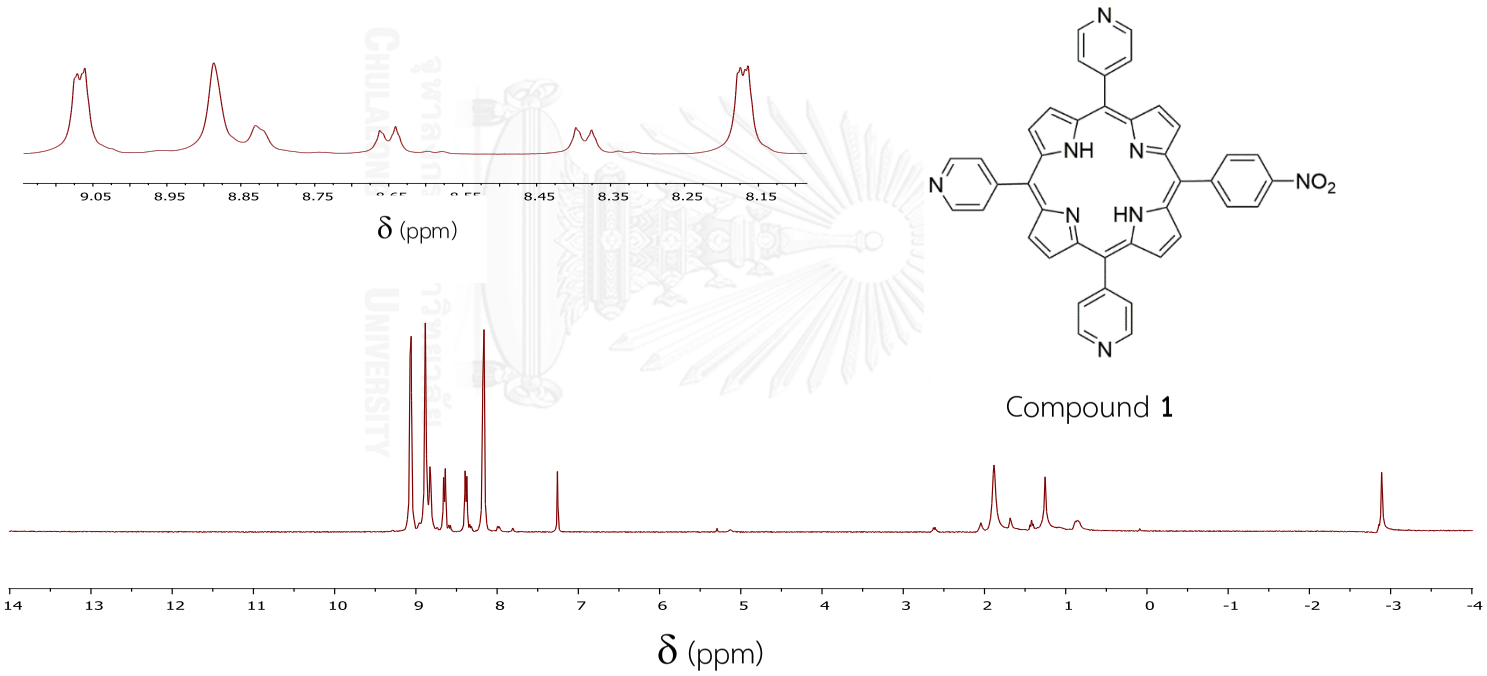

Figure A-1: ^{1}H-MNR spectrum of compound **1** in $CDCl_3$.

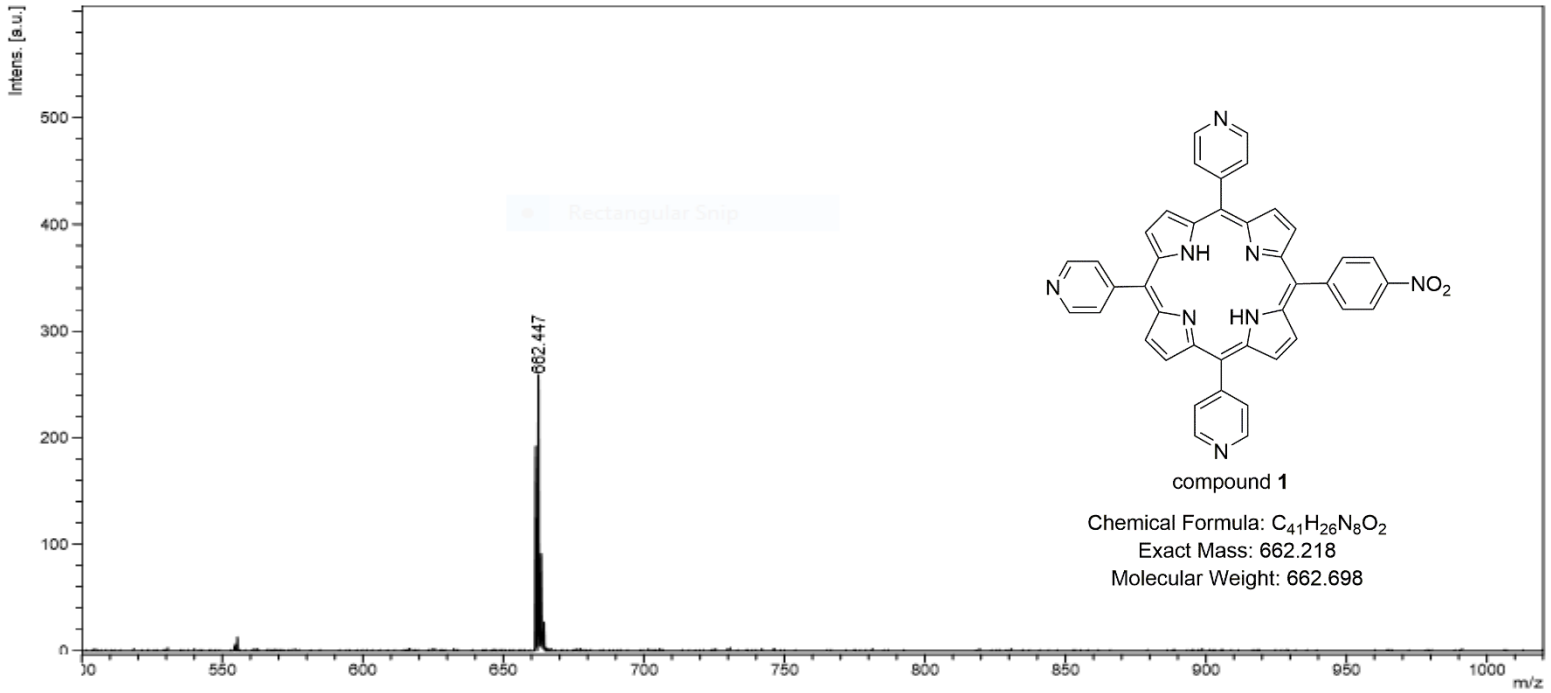

Figure A-2: MALDI-TOF mass spectrum of compound **1.**

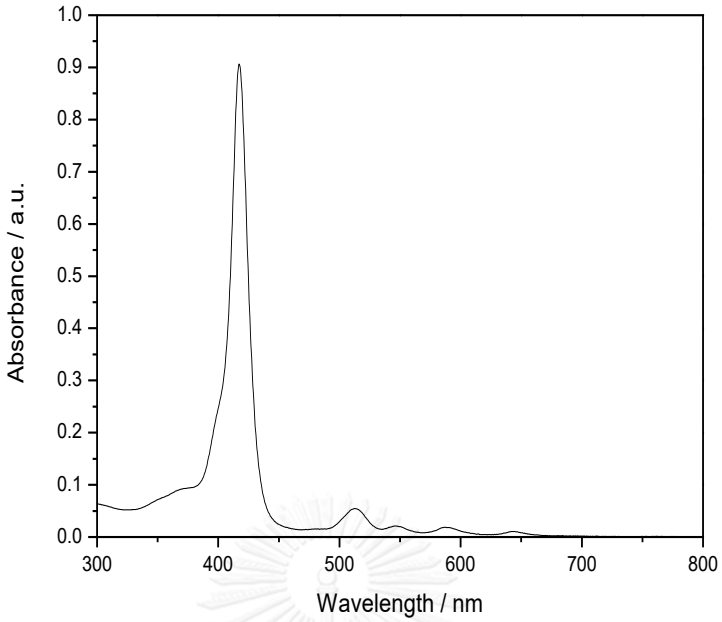

Figure A-3: Absorption spectrum of compound **1** in DMF.

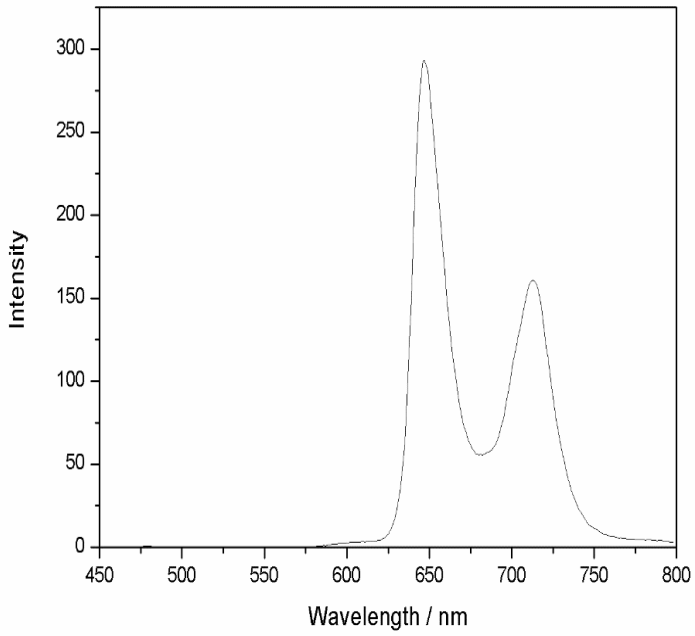

Figure A–4: Emission spectrum of compound **1** in DMF.

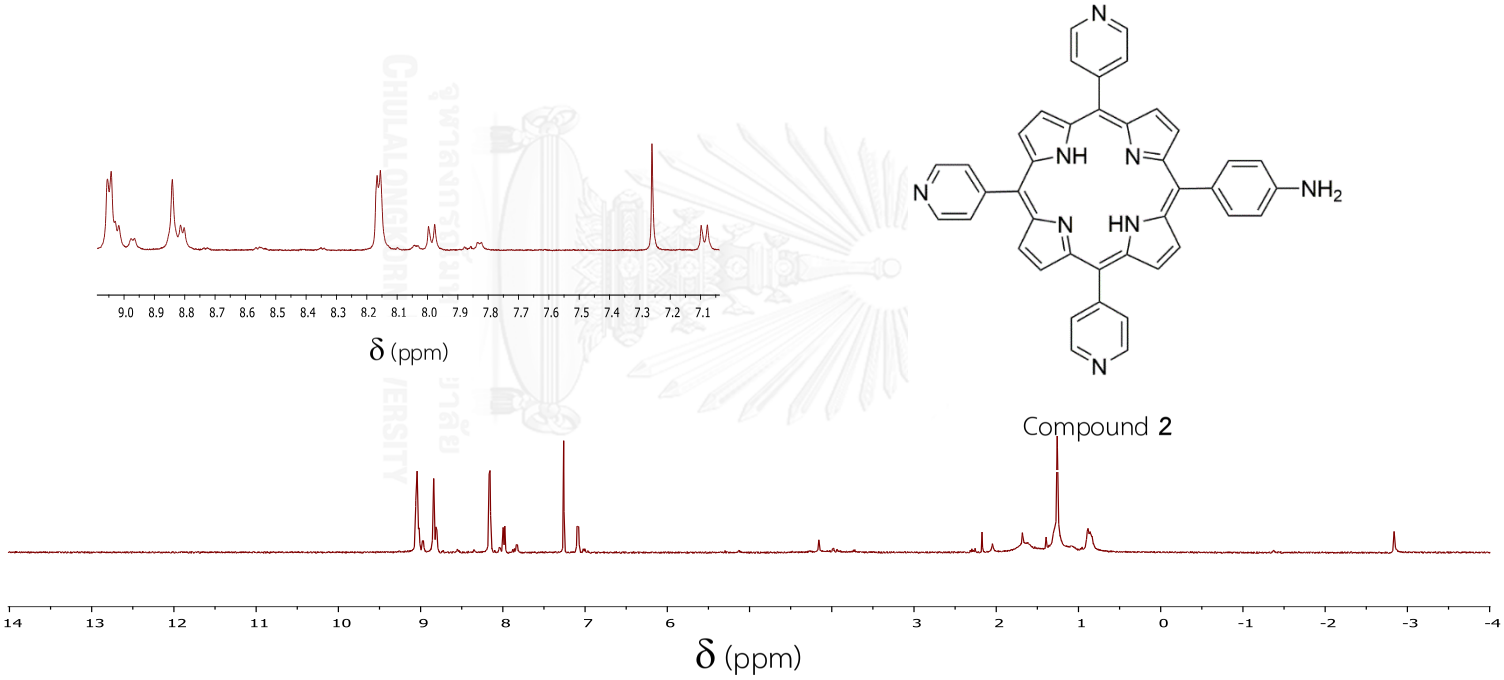

Figure A-5: ^{1}H-MNR spectrum of compound **2** in $CDCl_3$.

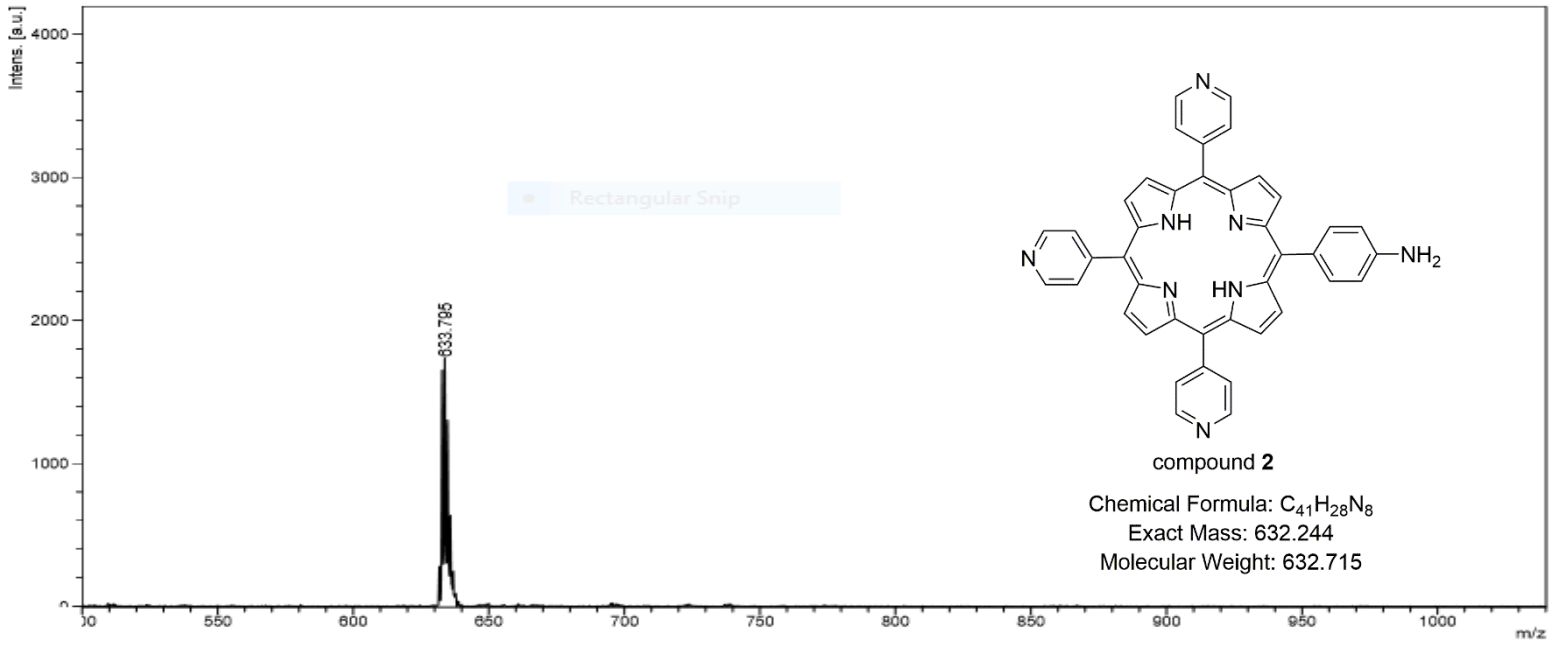

Figure A-6: MALDI-TOF-MS of compound **2**.

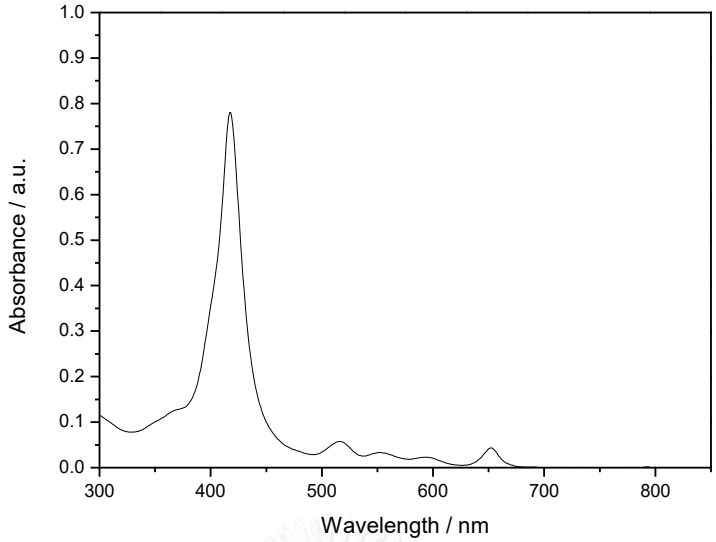

Figure A-7: Absorption spectrum of compound **2** in DMF.

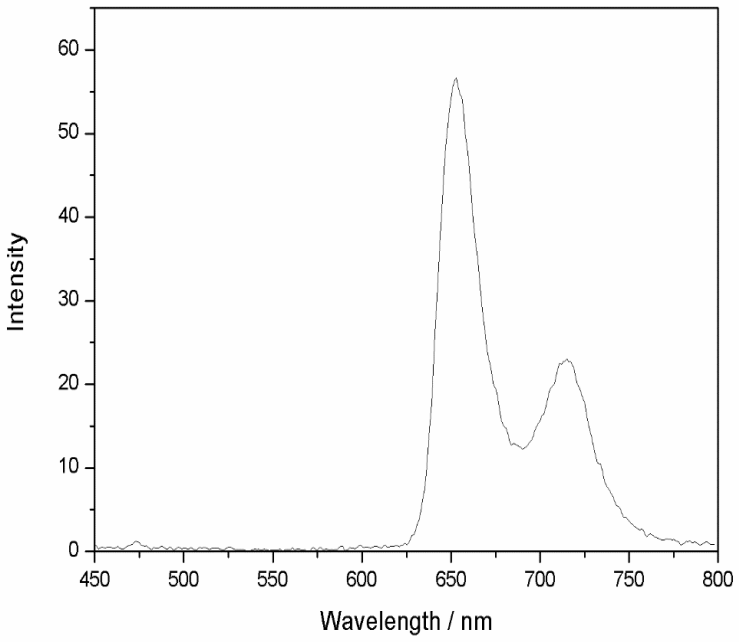

Figure A-8: Emission spectrum of compound **2** in DMF.

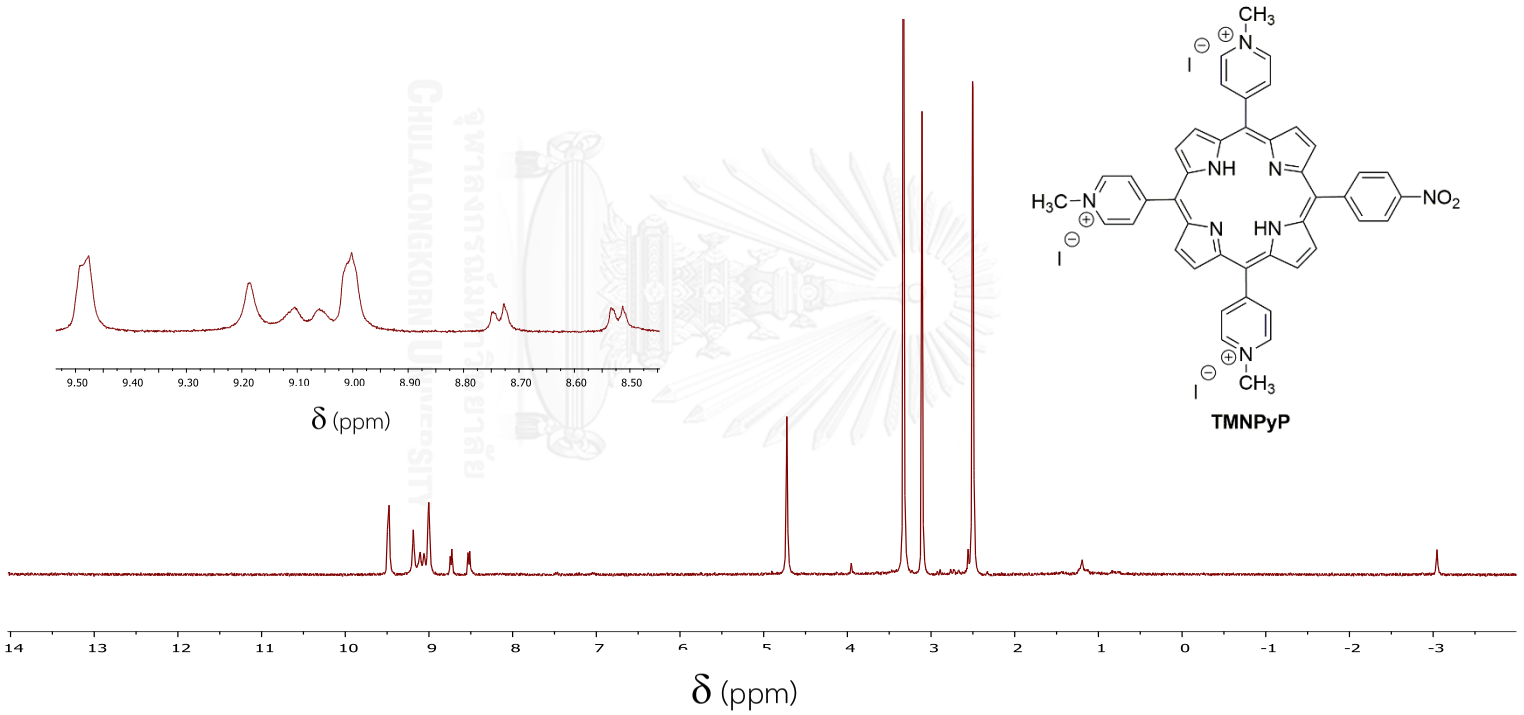

Figure A-9: ^{1}H-MNR spectrum of **TMNPyP** in DMSO-d_6.

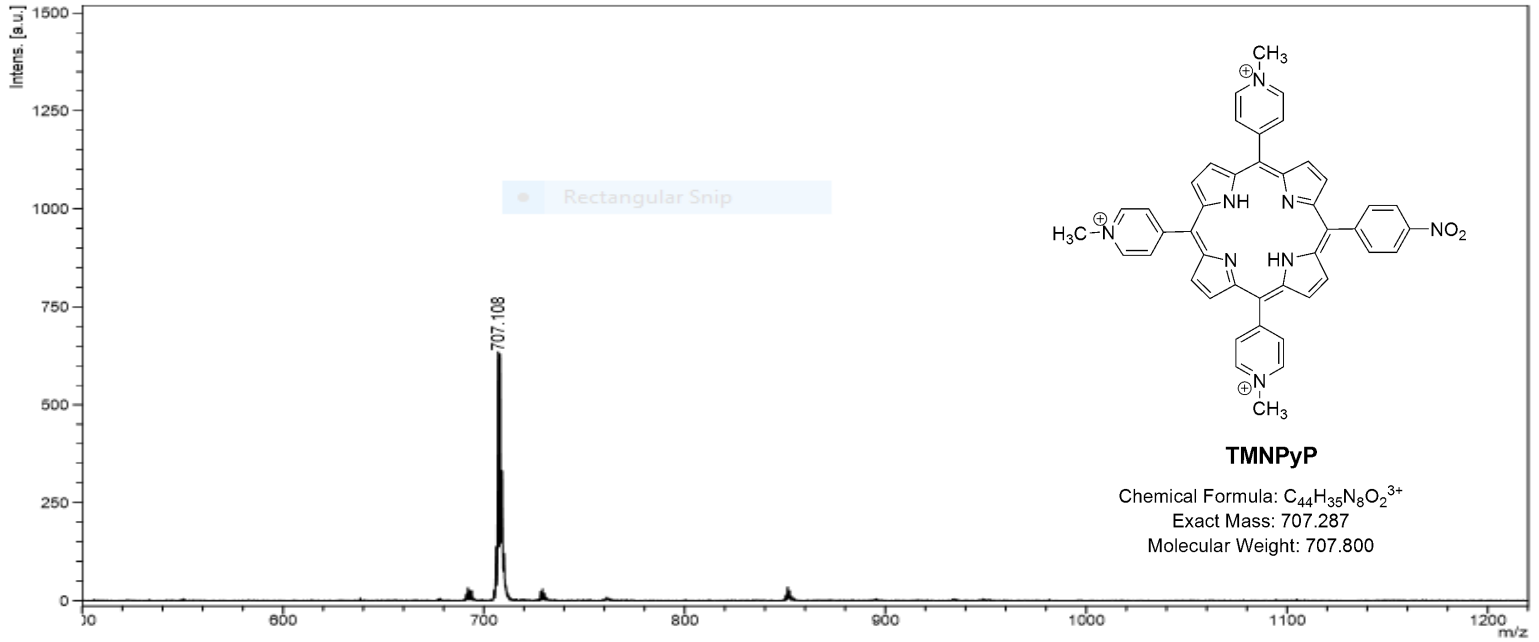

Figure A-10: MALDI-TOF mass spectrum of **TMNPyP**.

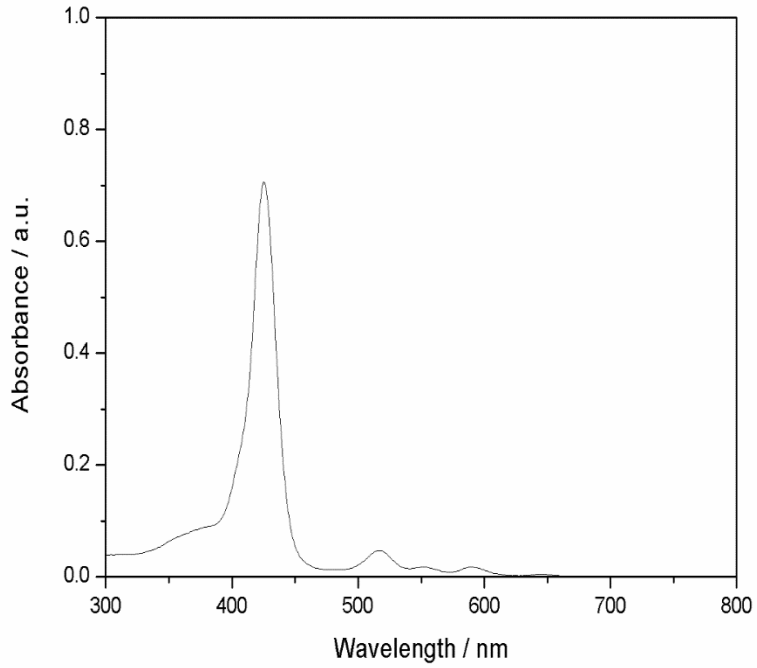

Figure A-11: Absorption spectrum of **TMPyP** in DMF.

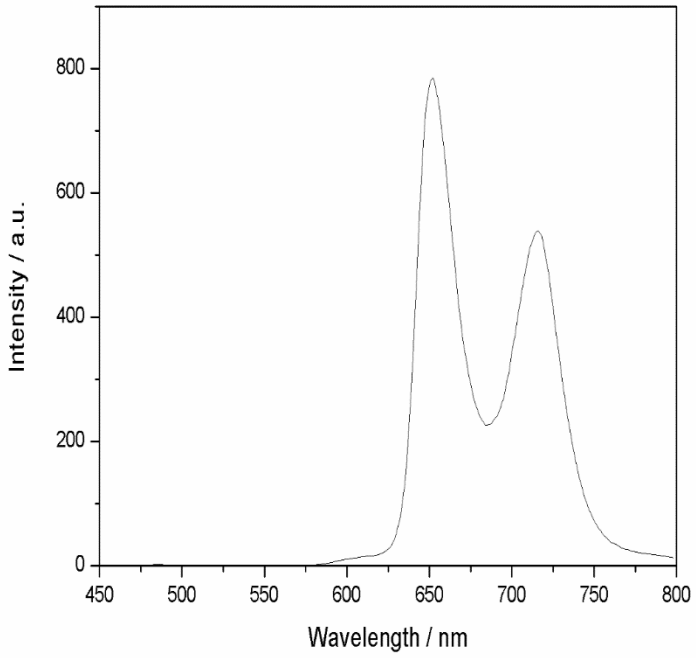

Figure A-12: Emission spectrum of **TMPyP** in DMF.

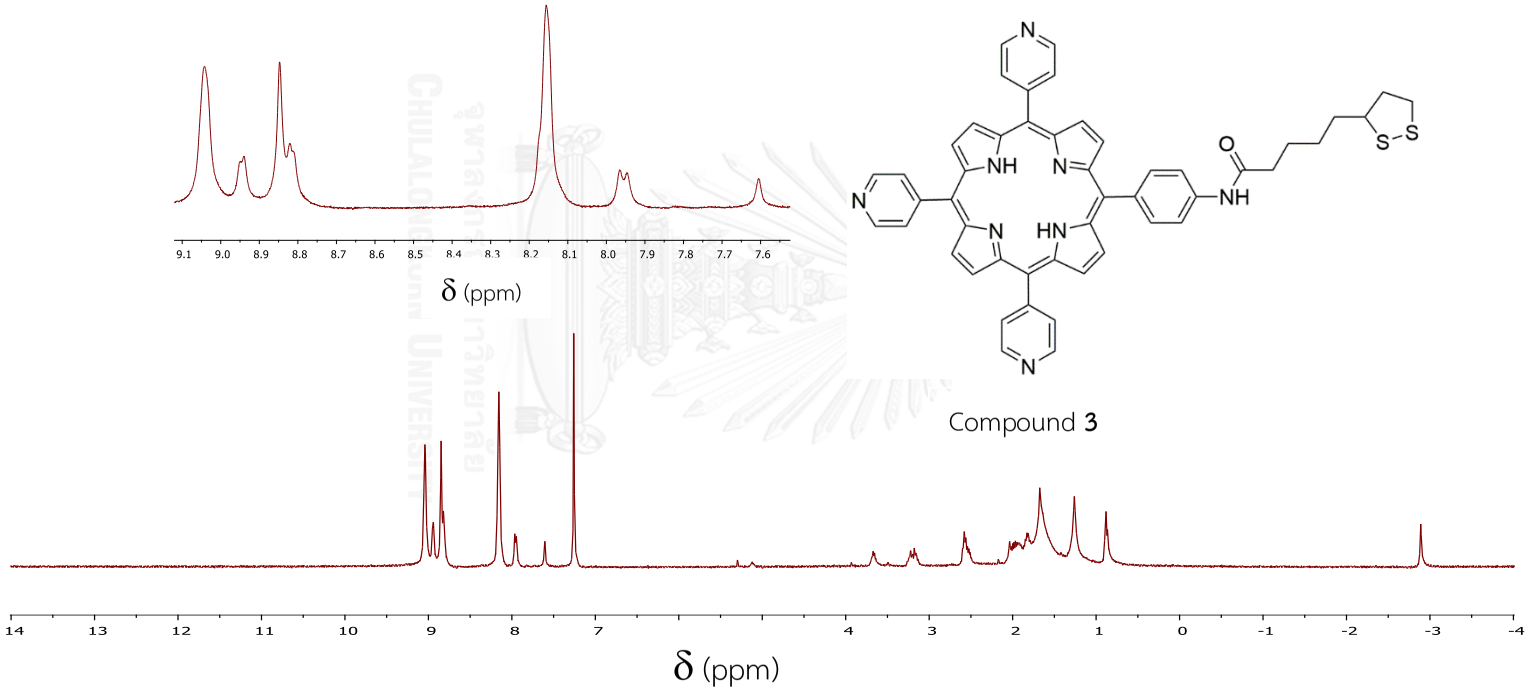

Figure A-13: ^{1}H-MNR spectrum of compound **3** in $CDCl_3$.

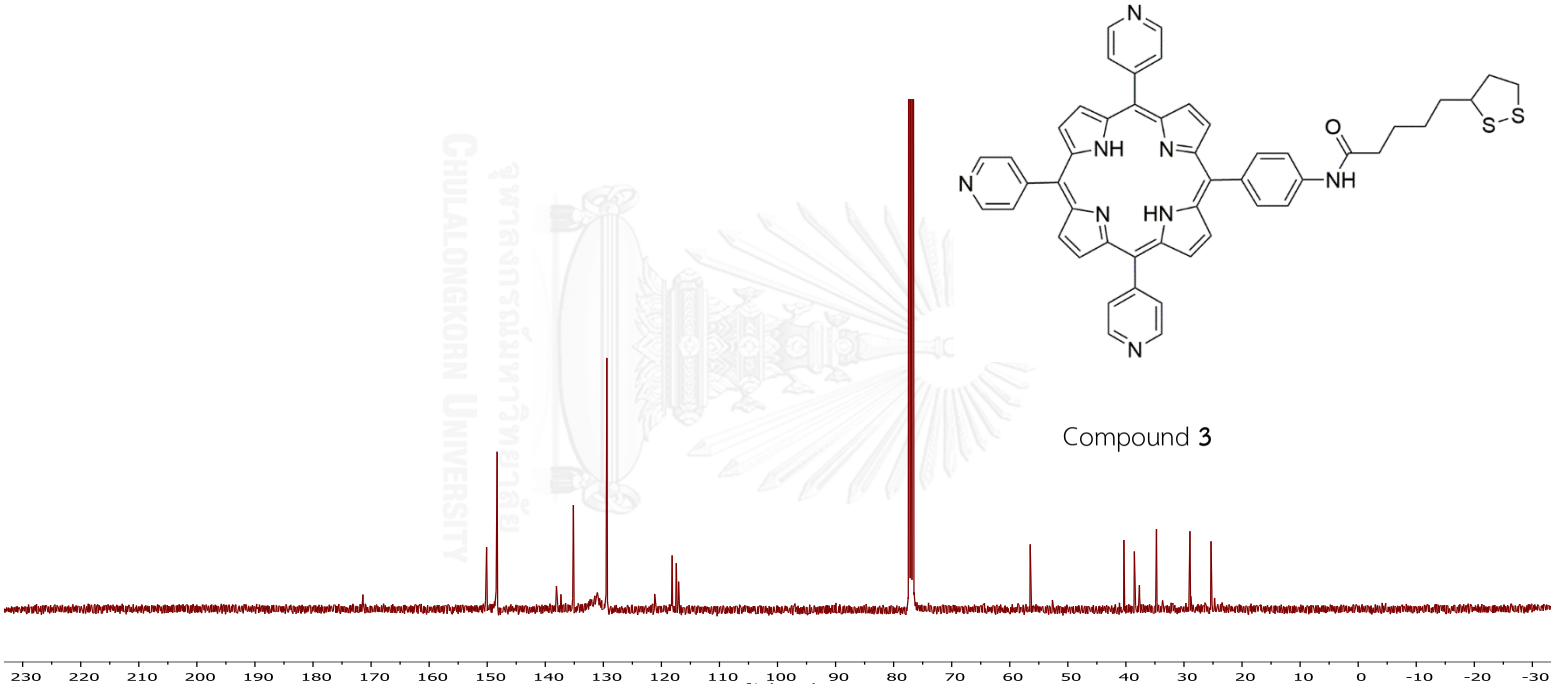

Figure A-14: ^{13}C-MNR spectrum of compound **3** in $CDCl_3$.

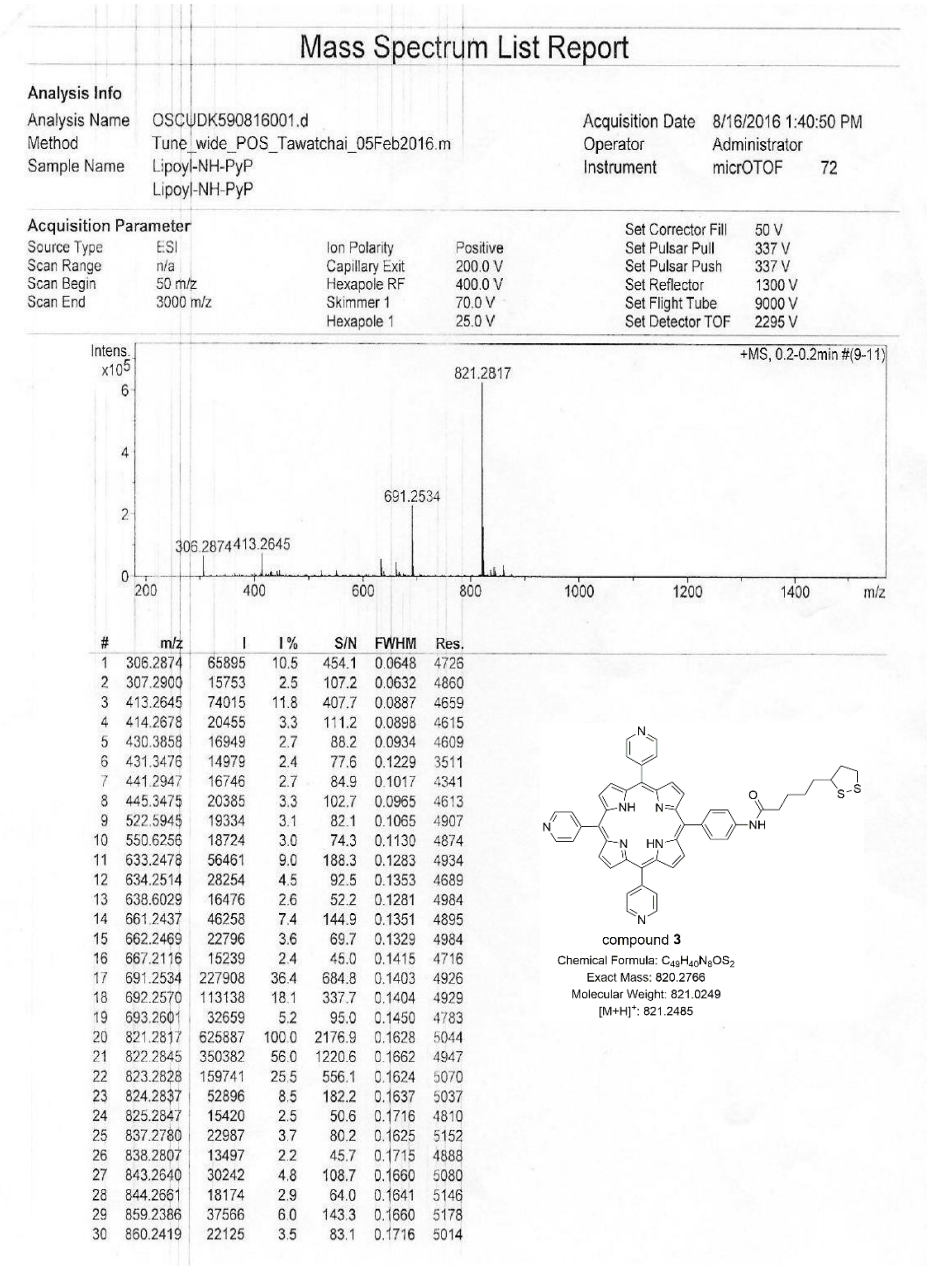

Mass Spectrum List Report

Analysis Info

Analysis Name	OSCUDK590816001.d	Acquisition Date	8/16/2016 1:40:50 PM
Method	Tune_wide_POS_Tawatchai_05Feb2016.m	Operator	Administrator
Sample Name	Lipoyl-NH-PyP Lipoyl-NH-PyP	Instrument	micrOTOF 72

Acquisition Parameter

Source Type	ESI	Ion Polarity	Positive	Set Corrector Fill	50 V
Scan Range	n/a	Capillary Exit	200.0 V	Set Pulsar Pull	337 V
Scan Begin	50 m/z	Hexapole RF	400.0 V	Set Pulsar Push	337 V
Scan End	3000 m/z	Skimmer 1	70.0 V	Set Reflector	1300 V
		Hexapole 1	25.0 V	Set Flight Tube	9000 V
				Set Detector TOF	2295 V

#	m/z	I	I %	S/N	FWHM	Res.
1	306.2874	65895	10.5	454.1	0.0648	4726
2	307.2900	15753	2.5	107.2	0.0632	4860
3	413.2645	74015	11.8	407.7	0.0887	4659
4	414.2678	20455	3.3	111.2	0.0898	4615
5	430.3858	16949	2.7	88.2	0.0934	4609
6	431.3476	14979	2.4	77.6	0.1229	3511
7	441.2947	16746	2.7	84.9	0.1017	4341
8	445.3475	20385	3.3	102.7	0.0965	4613
9	522.5945	19334	3.1	82.1	0.1065	4907
10	550.6256	18724	3.0	74.3	0.1130	4874
11	633.2478	56461	9.0	188.3	0.1283	4934
12	634.2514	28254	4.5	92.5	0.1353	4689
13	638.6029	16476	2.6	52.2	0.1281	4984
14	661.2437	46258	7.4	144.9	0.1351	4895
15	662.2469	22796	3.6	69.7	0.1329	4984
16	667.2116	15239	2.4	45.0	0.1415	4716
17	691.2534	227908	36.4	684.8	0.1403	4926
18	692.2570	113138	18.1	337.7	0.1404	4929
19	693.2601	32659	5.2	95.0	0.1450	4783
20	821.2817	625887	100.0	2176.9	0.1628	5044
21	822.2845	350382	56.0	1220.6	0.1662	4947
22	823.2828	159741	25.5	556.1	0.1624	5070
23	824.2837	52896	8.5	182.2	0.1637	5037
24	825.2847	15420	2.5	50.6	0.1716	4810
25	837.2780	22987	3.7	80.2	0.1625	5152
26	838.2807	13497	2.2	45.7	0.1715	4888
27	843.2640	30242	4.8	108.7	0.1660	5080
28	844.2661	18174	2.9	64.0	0.1641	5146
29	859.2386	37566	6.0	143.3	0.1660	5178
30	860.2419	22125	3.5	83.1	0.1716	5014

compound **3**

Chemical Formula: $C_{49}H_{40}N_8OS_2$

Exact Mass: 820.2766

Molecular Weight: 821.0249

$[M+H]^+$: 821.2485

Figure A-14: HR-ESI mass spectrum of compound **3**.

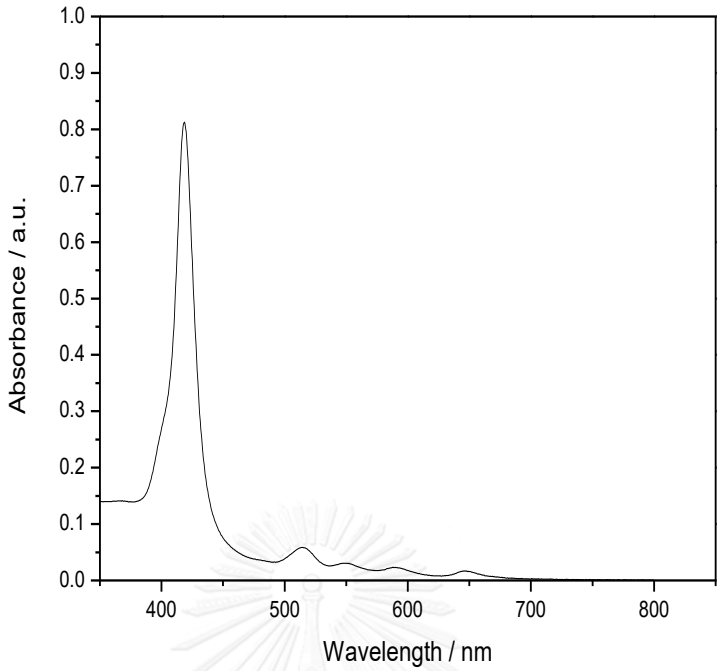

Figure A-16: Absorption spectrum of compound **3** in DMF.

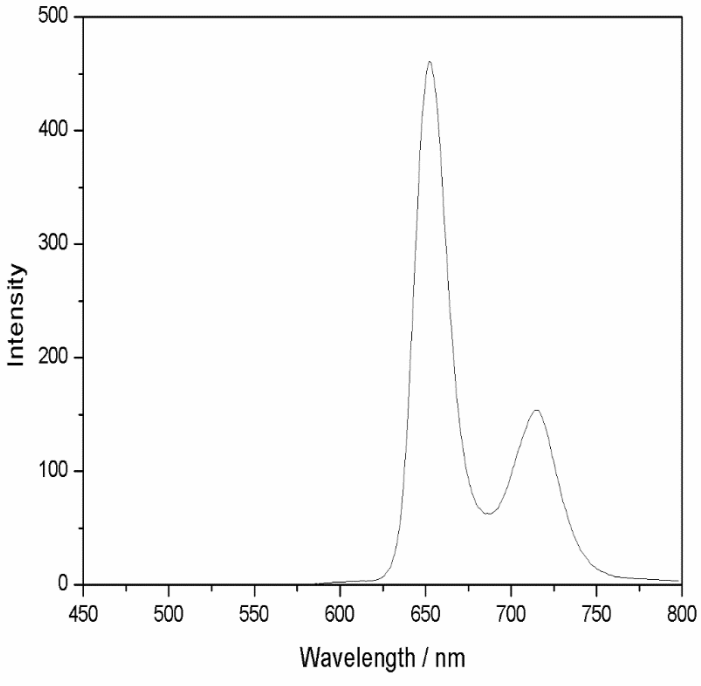

Figure A-17: Emission spectrum of compound **3** in DMF.

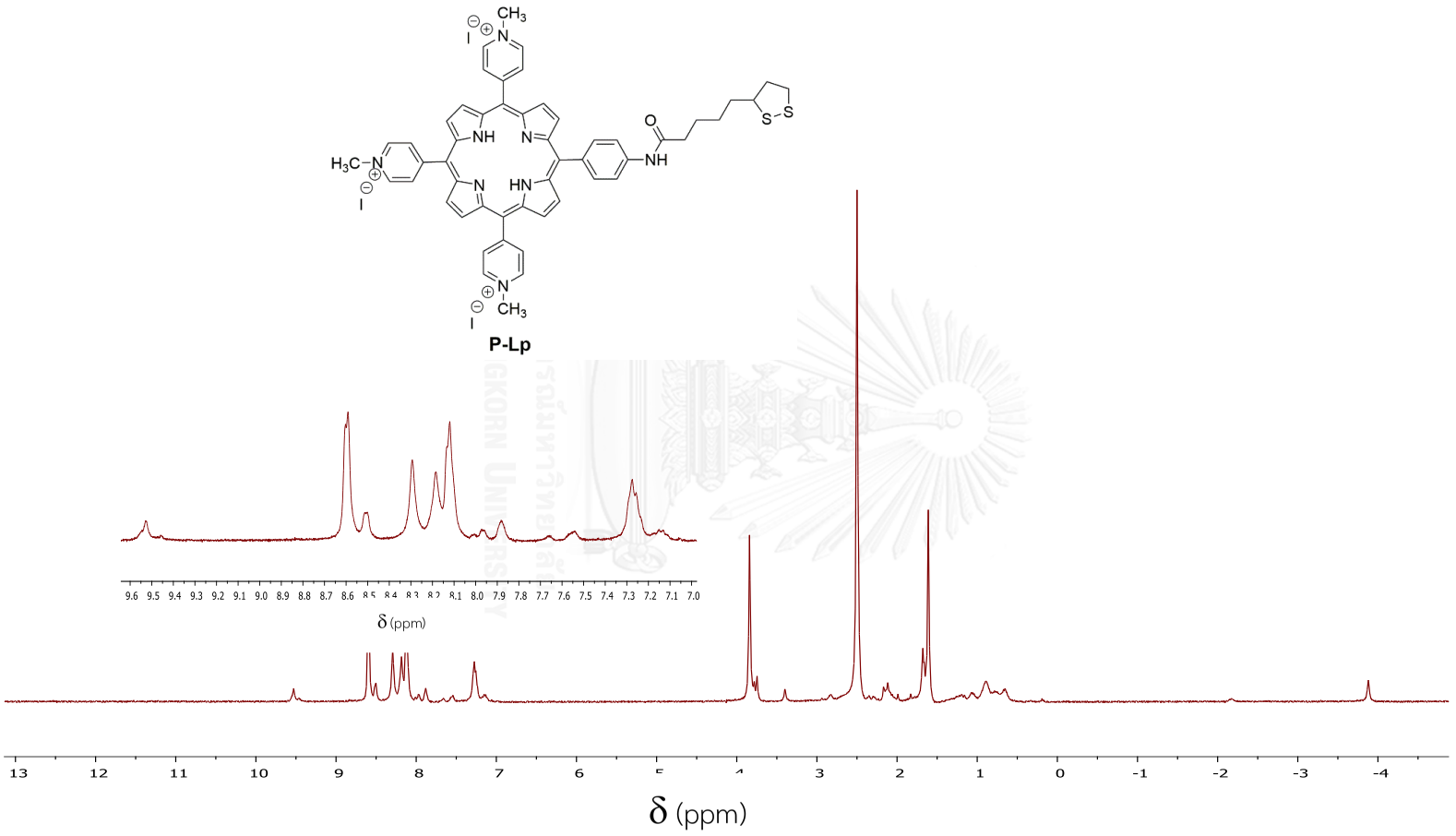

Figure A-18: ^{1}H-NMR spectrum of **P-Lp** in DMSO-d_6.

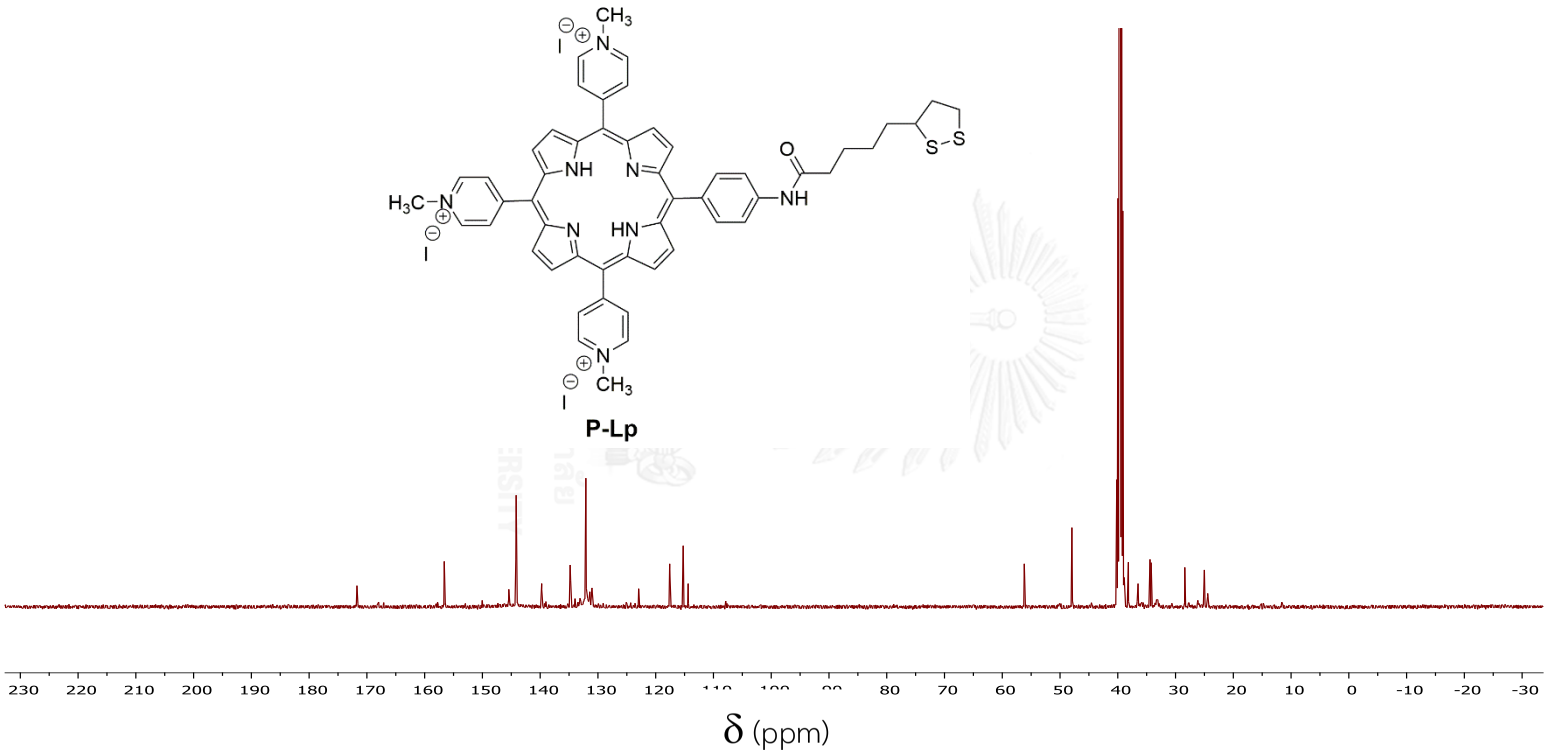

Figure A-19: ^{13}C-NMR spectrum of **P-Lp** in DMSO-d_6.

Mass Spectrum List Report

Analysis Info

Analysis Name	OSCUDK591108001.d	Acquisition Date	11/8/2016 11:59:09 AM
Method	Tune_wide_POS_Tawatchai_05Feb2016.m	Operator	Administrator
Sample Name	P-LP	Instrument	micrOTOF 72
	P-LP		

Acquisition Parameter

Source Type	ESI	Ion Polarity	Positive	Set Corrector Fill	50 V
Scan Range	n/a	Capillary Exit	250.0 V	Set Pulsar Pull	337 V
Scan Begin	50 m/z	Hexapole RF	400.0 V	Set Pulsar Push	337 V
Scan End	3000 m/z	Skimmer 1	70.0 V	Set Reflector	1300 V
		Hexapole 1	25.0 V	Set Flight Tube	9000 V
				Set Detector TOF	2295 V

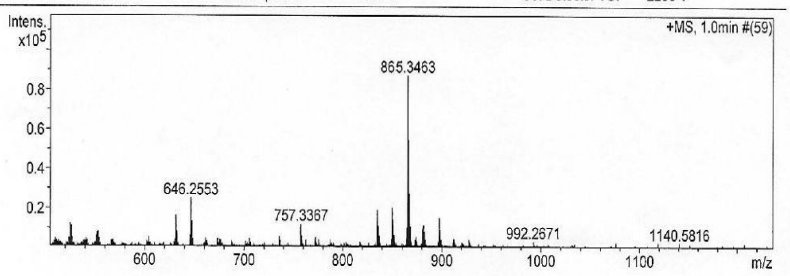

#	m/z	I	I %	S/N	FWHM	Res.
1	323.1249	15821	18.2	31.0	0.0585	5520
2	330.1273	12649	14.5	24.5	0.0812	4064
3	330.6404	40094	46.0	79.1	0.0597	5536
4	331.1371	31145	35.7	61.3	0.0654	5067
5	331.6438	10754	12.3	20.7	0.0655	5060
6	344.1269	23169	26.6	45.1	0.0673	5113
7	351.1413	22248	25.5	43.5	0.0622	5642
8	351.6419	11272	12.9	21.7	0.0577	6090
9	358.1385	15663	18.0	30.5	0.0715	5006
10	386.1816	42979	49.3	86.6	0.0676	5710
11	386.6829	23809	27.3	47.6	0.0620	6236
12	393.1789	10524	12.1	20.7	0.1014	3877
13	395.1486	12833	14.7	25.5	0.0923	4281
14	425.1614	15289	17.5	31.1	0.0734	5791
15	525.1781	12326	14.1	26.8	0.0990	5303
16	526.1834	11222	12.9	24.3	0.0939	5605
17	631.2359	16389	18.8	38.5	0.1101	5736
18	646.2553	25030	28.7	59.8	0.1032	6265
19	647.2614	13654	15.7	32.3	0.1041	6220
20	757.3367	11929	13.7	29.7	0.1136	6665
21	835.3034	19273	22.1	48.1	0.1447	5772
22	836.2974	11563	13.3	28.5	0.1435	5827
23	850.3243	20280	23.3	50.6	0.1461	5819
24	851.3187	14528	16.7	36.0	0.1386	6143
25	865.3463	87163	100.0	220.3	0.1409	6143
26	866.3489	54451	62.5	137.2	0.1417	6114
27	867.3442	27485	31.5	68.8	0.1585	5471
28	868.3379	10930	12.5	26.8	0.1522	5706
29	881.3593	11714	13.4	28.7	0.1588	5551
30	897.3347	15205	17.4	37.5	0.1313	6834

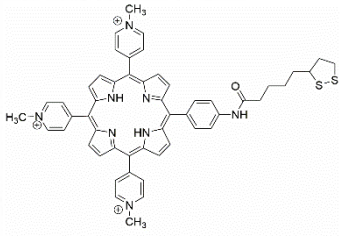

P-Lp

Chemical Formula: $C_{52}H_{48}N_8OS_2^{3+}$

Exact Mass: 865.3454

Molecular Weight: 866.1374

Figure A-20: HR-ESI mass spectrum of **P-Lp**.

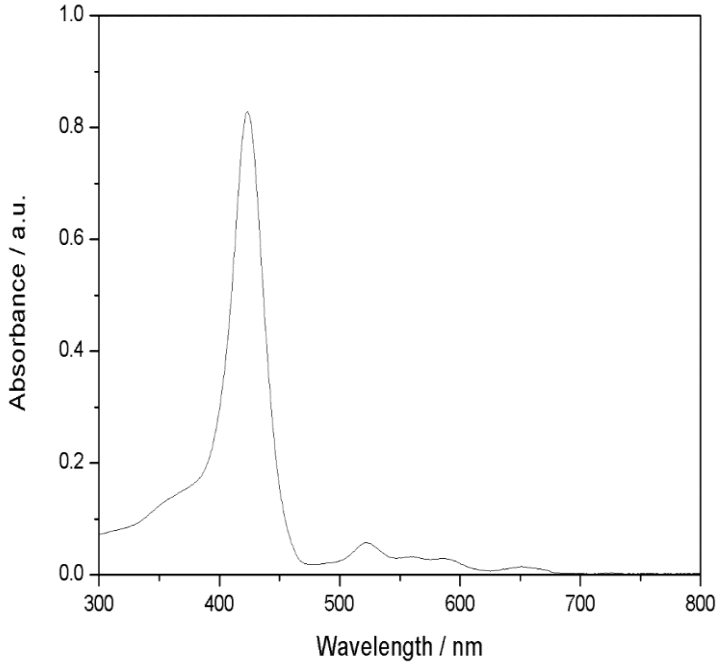

Figure A-21: Absorption spectrum of **P-Lp** in H_2O.

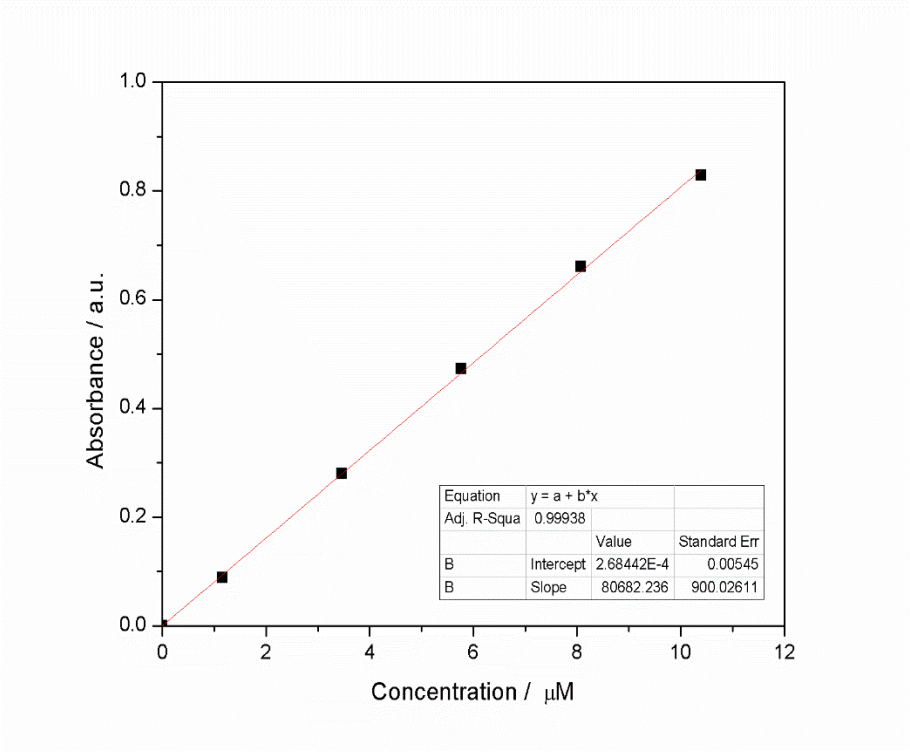

Figure A-22: Calibration curve for quantitative determination of **P-Lp** in H_2O (λ_{abs} = 428 nm).

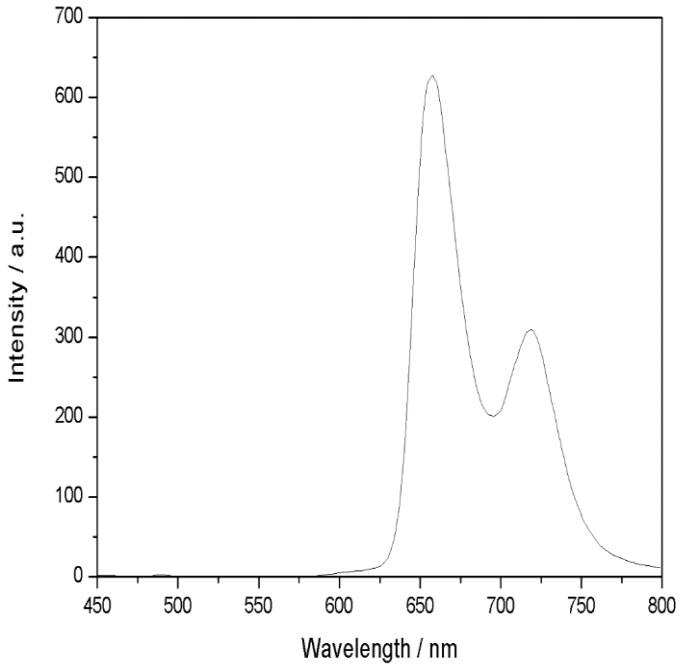

Figure A-23: Emission spectrum of **P-Lp** in H_2O.

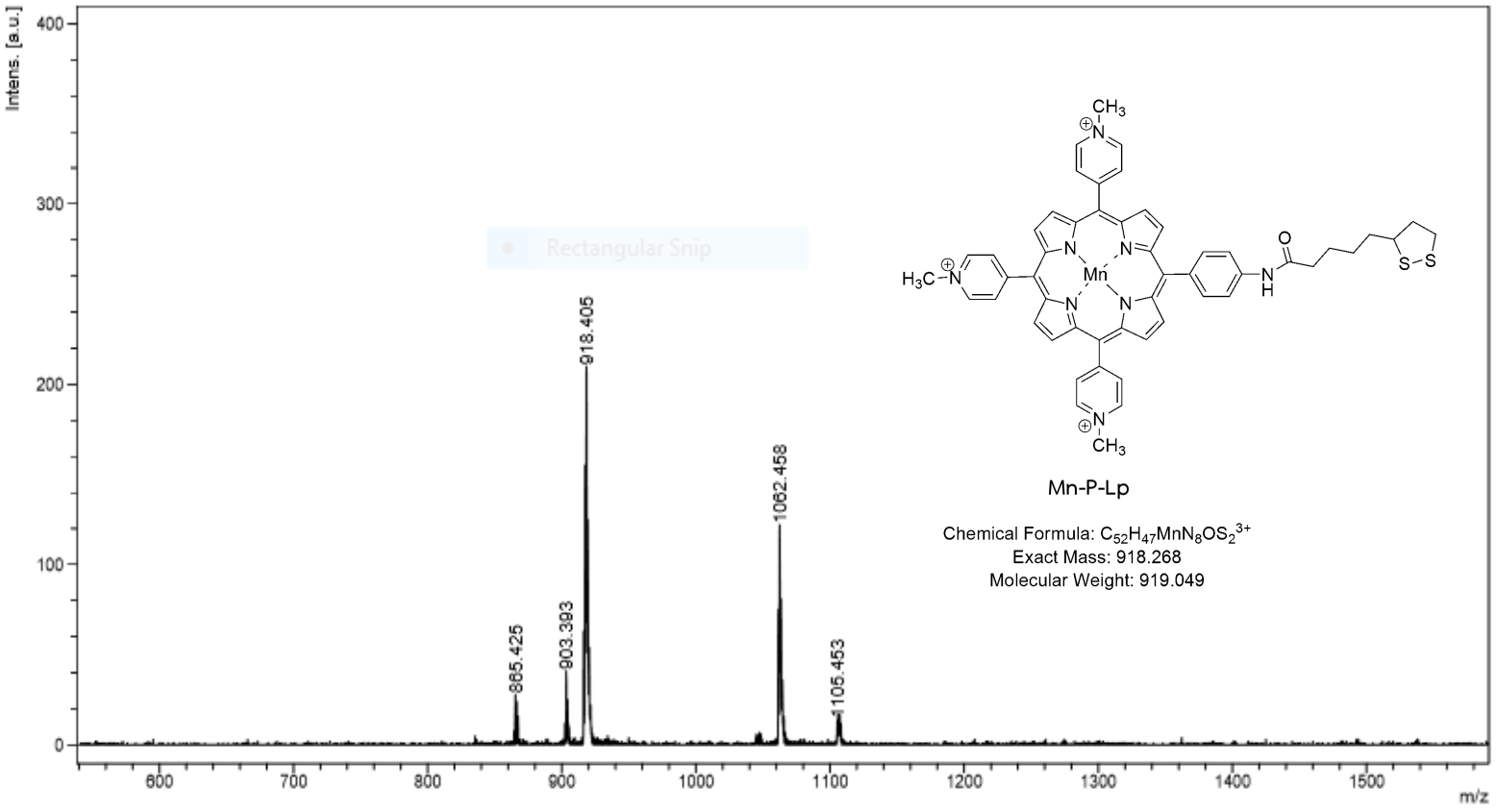

Figure A-24: MALDI-TOF mass spectrum of **Mn-P-Lp**.

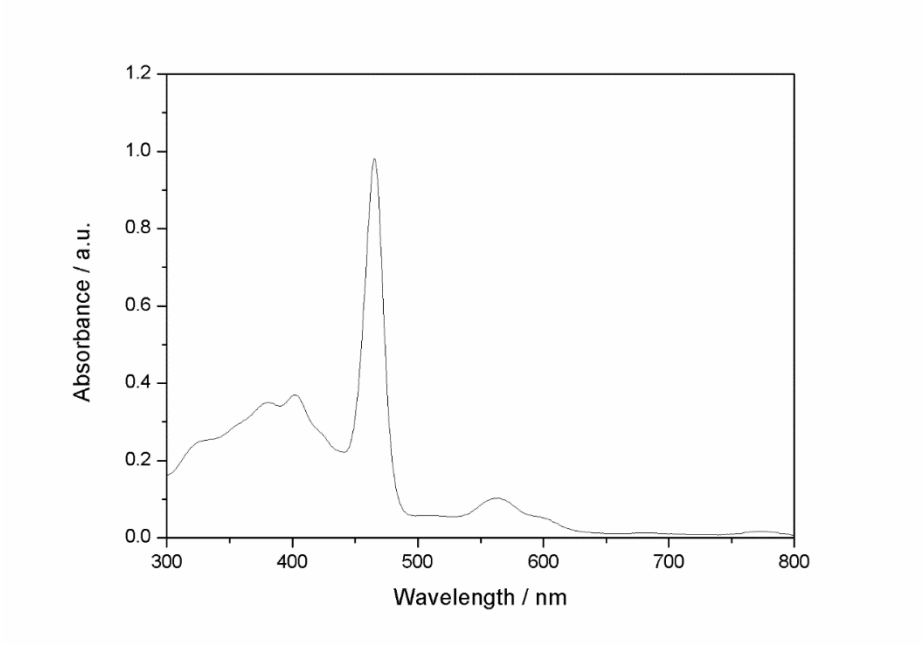

Figure A-25: Absorption spectrum of **Mn-P-Lp** in H_2O.

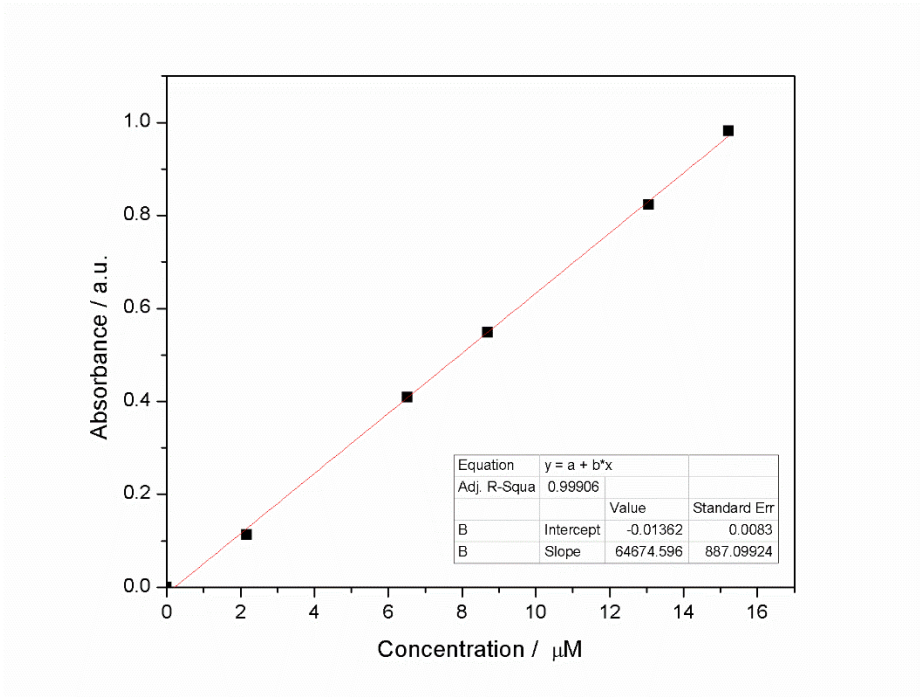

Figure A-26: Calibration curve for quantitative determination of **Mn-P-Lp** in H_2O (λ_{abs} = 469 nm).

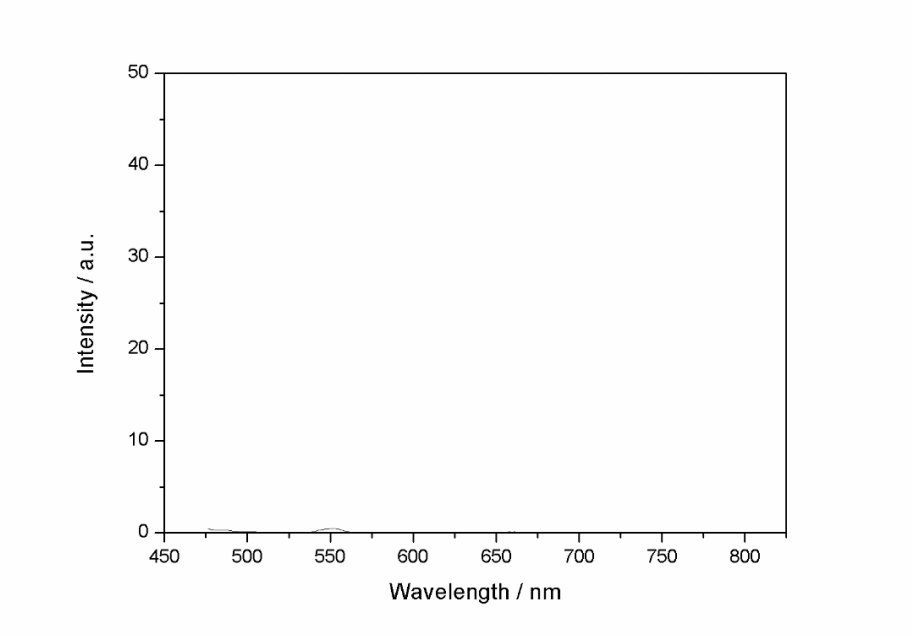

Figure A-27: Emission spectrum of **Mn-P-Lp** in H_2O.

VITA

Miss Duangkamon Kaewwichit was born on April 30, 1990 in Songkhla, Thailand. She got a Bachelor Degree of Chemistry from Faculty of Science at Prince of Songkla University, Songkhla in 2012. Then, she was admitted into a Master Degree in the major of Chemistry, Faculty of Science, Chulalongkorn University, Bangkok in 2012 and completed the program in 2016.